ACS NANO

www.acsnano.org

REVIEW

MXene-Based Micro-Supercapacitors: Ink Rheology, Microelectrode Design and Integrated System

Haichao Huang and Weiqing Yang*

Cite This: *ACS Nano* 2024, 18, 4651−4682

Read Online

ACCESS | Metrics & More | Article Recommendations

ABSTRACT: MXenes have shown great potential for micro-supercapacitors (MSCs) due to the high metallic conductivity, tunable interlayer spacing and intercalation pseudocapacitance. In particular, the negative surface charge and high hydrophilicity of MXenes make them suitable for various solution processing strategies. Nevertheless, a comprehensive review of solution processing of MXene MSCs has not been conducted. In this review, we present a comprehensive summary of the state-of-the-art of MXene MSCs in terms of ink rheology, microelectrode design and integrated system. The ink formulation and rheological behavior of MXenes for different solution processing strategies, which are essential for high quality printed/coated films, are presented. The effects of MXene and its compounds, 3D electrode structure, and asymmetric design on the electrochemical properties of MXene MSCs are discussed in detail. Equally important, we summarize the integrated system and intelligent applications of MXene MSCs and present the current challenges and prospects for the development of high-performance MXene MSCs.

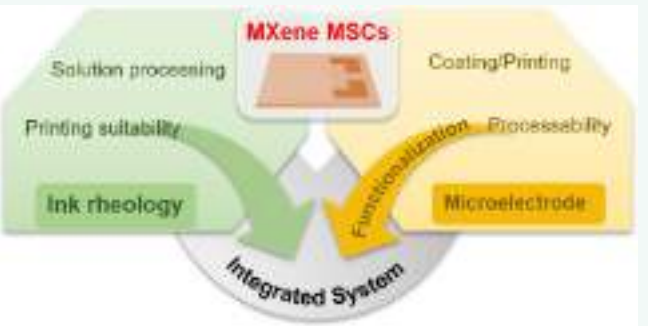

KEYWORDS: *MXene, micro-supercapacitors, ink, rheology, solution processing, printing, microelectrode, integrated system, applications*

1. INTRODUCTION

With the increasing demand for portable and multifunctional electronic devices, energy storage devices tend to be miniaturized, lightweight, and integratable.[1−6] Microbatteries (MBs) and micro-supercapacitors (MSCs) are two complementary microenergy storage devices that have received wide attention.[7−10] Although MBs are popular microenergy devices due to their high energy density (1 mWh cm^{-2}), their limited cycle life (up to 500 to 10,000 cycles) means that they require frequent maintenance and replacement, and low power density (<5 mW cm^{-2}) limits their application at high currents.[11−14] In contrast, MSCs possess excellent cycle life (>100,000 cycles) and high power density (>10 mW cm^{-2}), making them more promising for a wide range of applications.[12,15] However, their relatively low energy density (<0.1 mWh cm^{-2}) often limits their application in integrated microelectronic systems. Therefore, the option of electrode materials with high conductivity and large charge storage capacity is crucial for high-performance micro-supercapacitors.

Recently, two-dimensional (2D) nanomaterials, including graphene, MoS_2, h-BN, WS_2, and MXenes,[16−19] show excellent performance in the field of supercapacitors due to their high specific surface area and unique physicochemical properties, which have attracted great interest of researchers.[20−22] Among them, transition metal carbides, nitrides, and/or carbonitrides (MXenes), with the formula $M_{n+1}X_nT_z$ (n = 1, 2, or 3), where M represents an early transition metal, X stands for carbon and/or nitrogen, and T refers to various terminations, are particularly noteworthy.[23,24] MXene often offers high metallic conductivity, excellent hydrophilicity, adjustable interlayer spacing and high charge storage capacity, which gives it outstanding advantages in the field of energy storage.[25−27] To date, nearly 30 different MXenes have been synthesized successfully.[27−29] As a typical pseudocapacitive material, the excellent electrochemical properties of MXenes can be attributed to several factors: (i) the free electrons present in

Received: October 19, 2023
Revised: January 13, 2024
Accepted: January 17, 2024
Published: February 2, 2024

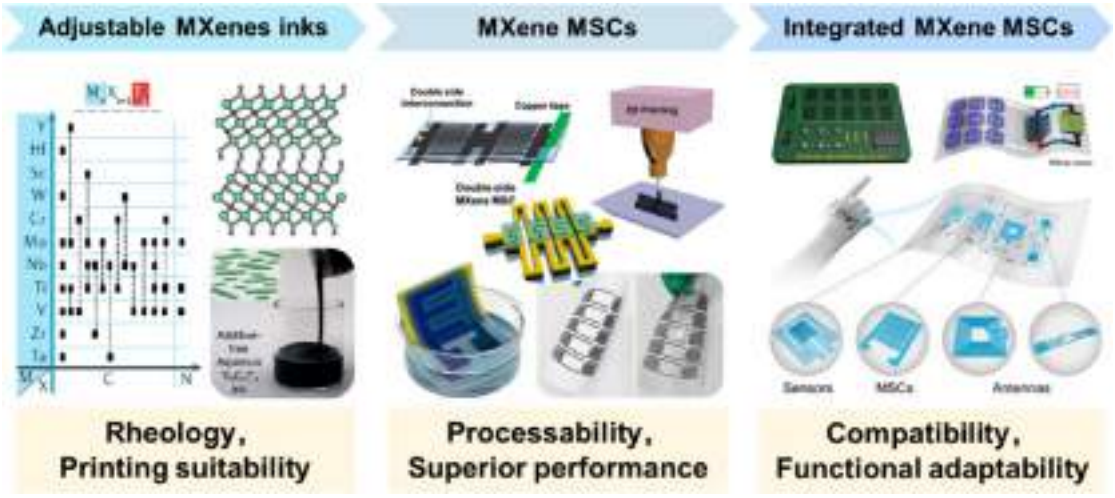

Figure 1. Outline illustration of the review for MXene-based MSCs. Adjustable MXene inks. From left to right: Reprinted with permission from ref [28]. Copyright 2022 Springer Nature. Reprinted with permission from ref [66]. Copyright 2021 John Wiley and Sons. In-plane MXene MSCs. From top to bottom: Reprinted with permission from ref [24]. Copyright 2020 John Wiley and Sons. Reprinted with permission from ref [68]. Copyright 2019 John Wiley and Sons. Reprinted with permission under a Creative Commons CC BY License from ref [67]. Copyright 2019 John Wiley and Sons. Reprinted with permission under a Creative Commons CC BY License from ref [69]. Copyright 2022 American Chemical Society. Reprinted with permission from ref [143]. Copyright 2018 Elsevier. MXene integrated system. From top to bottom: Reprinted with permission from ref [70]. Copyright 2020 Elsevier. Reprinted with permission from ref [57]. Copyright 2021 John Wiley and Sons. Reprinted with permission under a Creative Commons CC BY License from ref [60]. Copyright 2022 Springer Nature.

the main chain allow MXenes to exhibit metallic conductivity, enabling fast electron transport; (ii) the two-dimensional nature of MXenes promotes high electrochemical activity, leading to efficient ion transport; (iii) the abundant surface termination groups result in excellent hydrophilicity and serve as active centers for rapid redox reactions; and (iv) the interlayer spacing of MXenes can be adjusted by intercalation of H^+, Li^+, Na^+, K^+, Zn^{2+}, Al^{3+}, or other molecules, allowing for more electrolyte ions to be stored.[30−36] Overall, the outstanding advantages of MXenes enable them to exhibit excellent electrochemical performance, making them highly suitable for micro-supercapacitors. These properties have attracted a great deal of attention from researchers, and the use of MXene-based conductive inks for energy storage devices shows great promise for future practical applications.

In addition to the exceptional electrochemical properties of MXenes, their excellent hydrophilicity and high negative charge (with a zeta potential of around −38 mV) generated by surface functional groups (−O, −F, and/or −OH) further enhance their application as inks for printing and coating electrodes.[37−39] MXenes can form stable colloidal dispersions in aqueous and organic solvents, making them highly suitable for microelectrode manufacturing.[21,38] However, one of the major challenges is tuning the rheology of MXene inks to match microelectrode fabrication techniques. Rheological properties, such as viscosity and surface tension, have a significant impact on available printing techniques, reproducibility of the printing process, and print quality.[40−42] These properties are crucial factors in developing MXene inks for specific microelectrode manufacturing methods. Additionally, matching the surface energy between MXene inks and substrates is essential for the wettability and printability of electrodes. Poor wetting behavior of the printed pattern, resulting in a nonuniform distribution of the active material and pattern cracking, can occur due to inappropriate matching of surface energy.[43,44] Therefore, a thorough understanding of the rheological behavior of MXene inks, from ink formulation through microelectrode fabrication, is necessary to develop high-performance MXene-based microelectrodes.

The stable dispersion of MXene in various solvents allows for its direct use in solution processing techniques such as coating, printing, and filtration.[21,39,45] Currently, research is mainly focused on enhancing the electrochemical performance and energy storage mechanism of MXene MSCs through methods such as composite materials,[46−48] intercalation,[33,49−51] 3D structures,[52−54] and asymmetric electrode design.[55,56] However, integrating MSCs into functional microelectronic devices is also a key driving force for the industrialization of MSCs. It requires compatible manufacturing and functional matching between MXene MSCs and other functional devices. Currently, MXene MSCs have been successfully integrated with nanogenerators, solar cells, sensors, filter circuits, and more.[56−65] During the integration process, a rational design of series-parallel integration between MSCs and matching of parameters such as voltage, current, and power between MSCs and other components is essential.

Over the past few years, MXene MSCs have become a highly competitive research area, but a systematic summary of MXene rheology, microelectrode processing, and integrated multifunctional device is still relatively lacking. With this in mind, we have structured this review as follows (Figure 1): we first discuss how to convert MXenes into inks, focusing on the rheology of MXene inks and their printability. We then describe the electrode construction associated with MXene MSCs, mainly based on pure and composite MXene, 2D and 3D MXene microelectrodes, and symmetric and asymmetric structures. In the third part, we discuss the integration of MXene MSCs with other functional devices. Finally, we present our views on the current state and future directions of this interesting field.

https://doi.org/10.1021/acsnano.3c10246
ACS Nano 2024, 18, 4651−4682

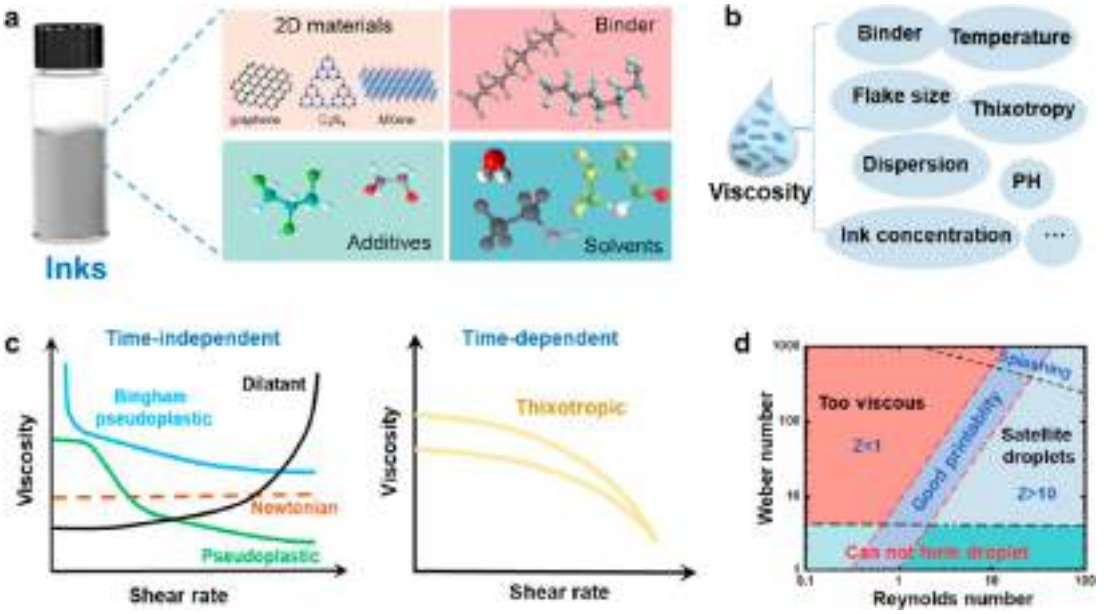

Figure 2. Rheology of two-dimensional nanomaterial inks. (a) Main components of printing inks, including electrode materials, additives, binders and solvents. (b) Factors influencing the rheology (mainly viscosity) of 2D material inks, such as binder, nanosheet size, solution concentration, *etc.* (c) Relation between viscosity and shear rate of the ink fluids. (d) Effect of Reynolds number and Weber number related to printing performance. Reprinted with permission from ref [40]. Copyright 2021 AIP Publishing.

2. MXENE INKS FOR SOLUTION PROCESSING

2.1. Commonality of 2D Functional Inks. Currently, many technologies have been utilized in the manufacture of MSCs, including vacuum filtration, laser patterning, and coating and printing technology.[11,71−75] Among them, coating and printing technology shows great promise in enabling large-scale production of planar MSCs due to its simplicity, efficiency, and cost-effectiveness. Furthermore, two-dimensional (2D) nanomaterials have been identified as potential electrode inks for printed MSCs due to their unique properties, such as high surface area and electrical conductivity.[76−78] It is crucial to investigate the rheological and printing performance of these inks to achieve high-performance MSCs.

2D functional ink typically comprises active materials (2D), binders, additives, and solvents (Figure 2a).[40] Among these components, the 2D materials are the primary ingredient of the ink, which can include graphene, MXene, MoS_2 and BN, with particle sizes ranging from nanometers to microns to suit varied printing technologies.[22,79] For instance, screen printing utilizes a larger mesh, allowing for particle sizes of up to 100 μm. On the contrary, most inkjet printing requires material particle diameters below 200 nm to avoid nozzle clogging.[80] Binders are mainly used to ensure the fluidity and stability of the ink, including water-soluble and thermoplastic adhesives, but often reduce the conductivity and electrochemical activity of the materials. So, binder-free ink is an effective way to improve the electrode electrochemical performance, such as MXene aqueous/organic ink.[71,81] In addition, additives are also an important component of printable ink, which can effectively adjust the viscosity and printing adaptability of the ink. At the same time, it can also improve the electrical conductivity of the printed electrodes by adding highly conductive materials, such as acetylene black, carbon black, and super P.[82] Last but not least, the choice of solvent is critical to the ink formulation, which can disperse electrode materials, adjust ink viscosity, and enhance printing adaptability. For example, MXene dispersed in solvents with varying polarities exhibits markedly different rheological behaviors.[38,66,83]

The properties of ink, which play a crucial role in determining the consistency and reproducibility of printing results, are influenced by the composition of ink and the synergistic effect between its components.[84] Viscosity (η) is the most commonly used rheological parameter, which is calculated by the ratio of shear stress (τ) to shear rate (γ) and is used to describe the frictional force in ink systems. Generally, as shown in Figure 2b, the viscosity of ink is mainly affected by factors such as solid content, nanoplate size, thixotropy, pH, and temperature and shows significant differences.[34,37,66] For example, the viscosity of MXene inks with different concentrations can differ by 3 orders of magnitude.[83] The flow behavior of liquids can be characterized by the relationship between viscosity and shear rate (Figure 2c), which can be classified into two categories: Newtonian fluids, where η and γ are linearly related, and non-Newtonian fluids, where η and γ are nonlinearly related.[43,84,85] Almost all particulate inks are non-Newtonian fluids that exhibit shear-thinning behavior, namely, pseudoplasticity or thixotropy. Fluids with these properties can flow through printer nozzles under stress, recover their high viscosity, and maintain an ideal pattern after printing by dissipating stress outside of the nozzle.[86,87] The main difference between pseudoplastic and thixotropic fluids is their recovery time.[20,44] Pseudoplastic fluids almost instantly return to their gel state after stress disappears, making them time-independent. In contrast, thixotropic fluids require some time to restore their original viscosity after stress removal, making them time-dependent. Pseudoplastic and thixotropic fluids are well-suited for various printing and coating techniques, including spraying, screen printing, inkjet printing, and 3D printing.[68,88,89]

The formation of ink droplets is also important to the printing process and can be described with dimensionless groups of physical constants, including the Reynolds number (Re), Weber number (We), and Ohnesorge number (Oh).[41]

https://doi.org/10.1021/acsnano.3c10246
ACS Nano 2024, 18, 4651−4682

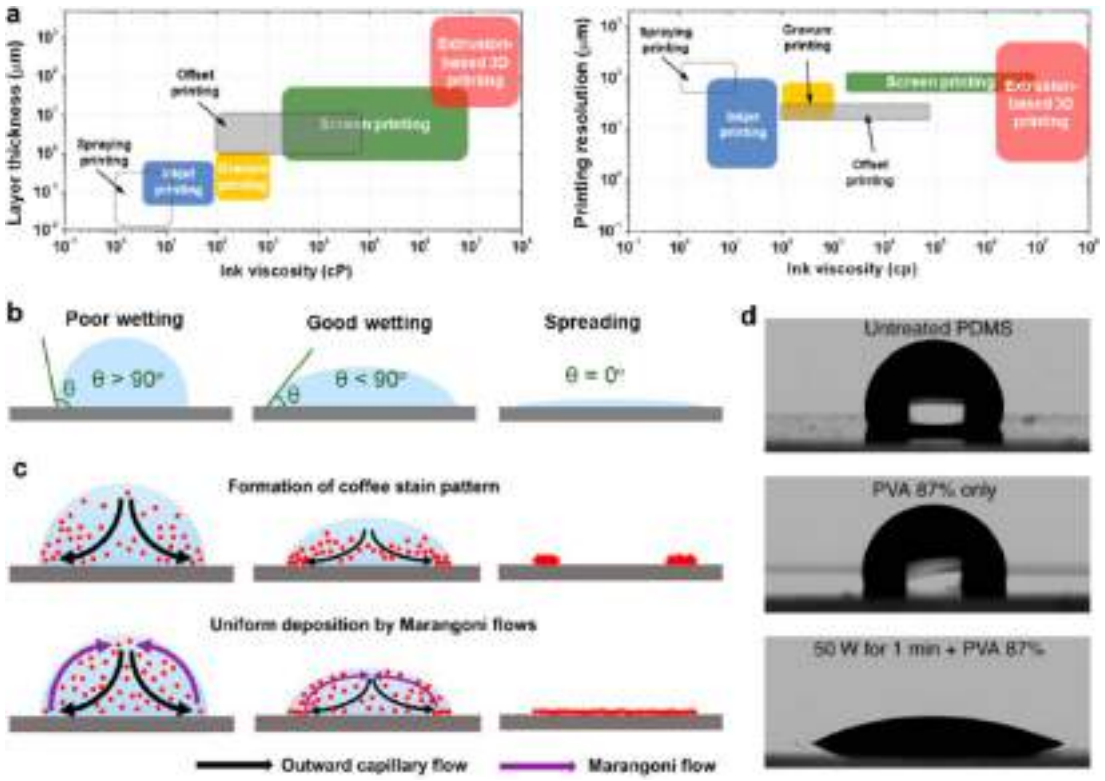

Figure 3. Print suitability of different printing methods. (a) Comparison of the features for different printing methods, including applicable ink viscosity, the deposition layer thickness and printing resolution. Reprinted with permission from ref [84]. Copyright 2020 John Wiley and Sons. (b) Wettability of droplet on the substrate. A small contact angle (<90°) indicates good wettability, while a large contact angle (>90°) indicates poor wettability. (c) Droplet drying process: coffee ring effect (top) and Marangoni flow inhibition coffee ring (bottom). Reprinted with permission from ref [43]. Copyright 2020 American Chemical Society. (d) Surface treatment to adjust the hydrophilicity of the substrate for enhanced wettability. Reprinted with permission under a Creative Commons CC BY License from ref [92]. Copyright 2017 Springer Nature.

$$Re = \frac{v\rho a}{\eta} \tag{1}$$

$$We = \frac{v^2\rho a}{\sigma} \tag{2}$$

$$Oh = \frac{\sqrt{We}}{Re} = \frac{\eta}{\sqrt{\sigma\rho a}} \tag{3}$$

Here, ρ is density, v is velocity, a is characteristic length, η is viscosity, and σ is surface tension of the ink. Moreover, the formation of small droplets is determined by the inverse Ohnesorge number Z ($Z = 1/Oh$). The inverse Ohnesorge number Z plays a significant role in determining whether small droplets will form or satellite droplets and splashing will occur (Figure 2d).[40,41] These issues adversely affect print quality and must be avoided by properly controlling these variables.

Different printing methods have significantly different requirements for ink rheology, which in turn affects the resulting print resolutions (Figure 3a).[84] Also, ink requirements for different printing technologies and printing parameters are summarized in Table 1. For instance, low-concentration dispersions are necessary for inkjet and spray coating, whereas viscous pastes are required for extrusion-based 3D printing and screen printing.[89,90] In general, the required ink viscosity follows this order: spray coating/inkjet printing (low) < gravure/flexo printing (medium) < screen printing/3D printing (high).[89,91] Printing resolution is influenced by various factors, including the printing process, physical properties of ink (such as rheology and wetting), substrate surface characteristics, and postprocessing conditions. Therefore, it requires an analysis based on the specific printing process to determine the print resolution.

Table 1. Comparison of Different Printing Technologies

Technology	Speed (m/min)	Viscosity (cP)	Resolution (μm)	Thickness (μm)
Spray	~20	1–10	50–200	5–100
Inkjet printing	~1	1–100	10–50	0.5–5
Screen printing	~70	100–10^7	30–100	10–100
3D printing	~4	10^6–10^8	10–100	>50
Gravure	~1000	100–1000	10–50	10–100

Further, once the ink is printed, the subsequent ink spreading and drying determine the quality and resolution of the printed pattern.[43,92] The diffusion of ink on a solid surface is dependent on the ink's wetting properties, which can be explained by the Young's equation (wetting equation):[45]

$$\gamma_{s-g} = \gamma_{s-l} + \gamma_{l-g} \times \cos\theta \tag{4}$$

where γ_{s-g}, γ_{s-l}, and γ_{l-g} represent the interfacial tensions between solid–gas, solid–liquid, and liquid–gas, respectively, and θ is the contact angle. As shown in Figure 3b, a smaller contact angle indicates good wetting properties, where the ink can spread on the solid surface and achieve continuous

https://doi.org/10.1021/acsnano.3c10246
ACS Nano 2024, 18, 4651–4682

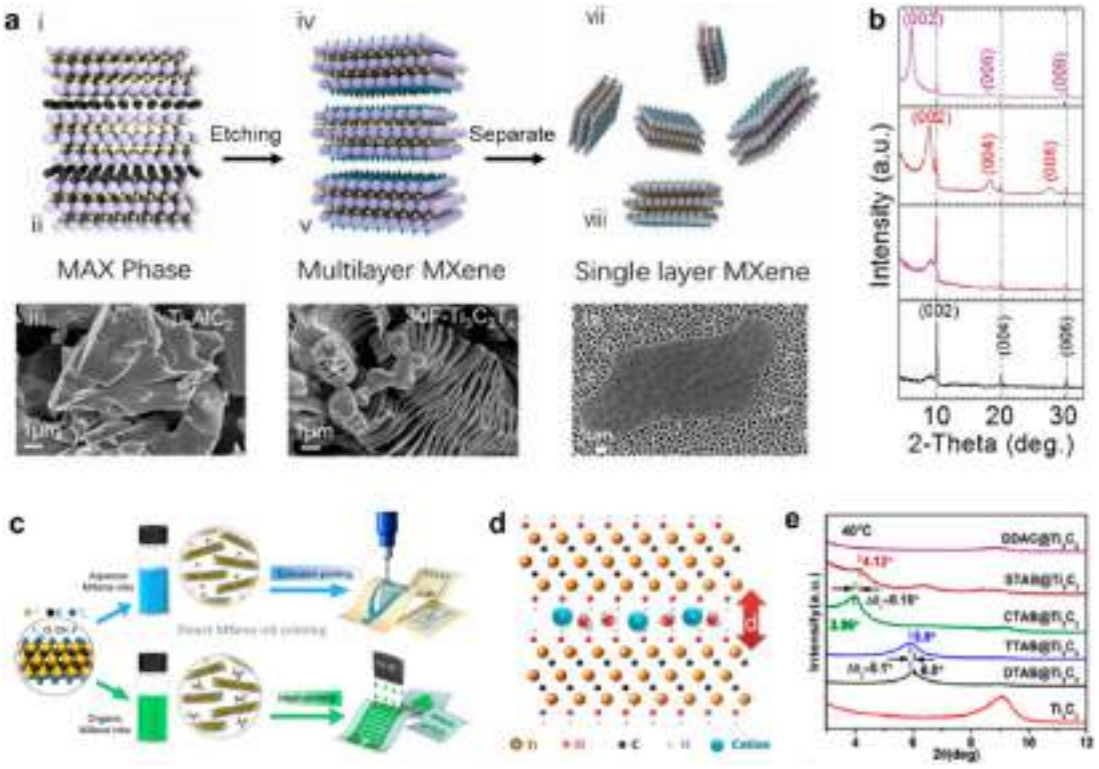

Figure 4. Formulation of MXene ink. (a) Selective etching process of MXene: from MAX phase to multilayer MXene and single-layer MXene. Reprinted with permission under a Creative Commons CC BY License from ref [99]. Copyright 2021 Taylor & Francis. (b) X-ray diffraction (XRD) spectra of MAX (Ti_3SiC_2) and MXene (Ti_3C_2). From bottom to top, Ti_3SiC_2, Ti_3SiC_2 treatment with 50 wt % HF (50HF-Ti_3SiC_2) and HF/H_2O_2 (Ti_3C_2(HF/H_2O_2)), TMAOH intercalated Ti_3C_2(HF/H_2O_2) (TMAOH-Ti_3C_2). Reprinted with permission from ref [113]. Copyright 2018 John Wiley and Sons. (c) Schematic of direct MXene ink printing. $Ti_3C_2T_x$ organic inks for inkjet printing and $Ti_3C_2T_x$ aqueous inks for extrusion printing on flexible substrates. Reprinted with permission under a Creative Commons CC BY License from ref [42]. Copyright 2019 Springer Nature. (d) Schematic illustration of cation intercalation between $Ti_3C_2T_x$ layers, which increases the interlayer spacing *d*. Reprinted with permission from ref [51]. Copyright 2013 American Association for the Advancement of Science. (e) Pillared structure design to expand the interlayer spacing of MXene. Intercalation XRD of hydrophobic alkyl cationic surfactants with different lengths [dodecyltrimethylammonium bromide (DTAB), tetradecyltrimethylammonium bromide (TTAB), cetyltrimethylammonium bromide (CTAB), stearyltrimethylammonium bromide (STAB) and dioctadecyl dimethylammonium chloride (DDAC)] at 40 °C. Reprinted with permission from ref [118]. Copyright 2017 American Chemical Society.

deposition through maintaining contact.[44] A larger contact angle may cause the ink to contract into beads, resulting in discontinuous deposition and poor print quality. To achieve proper wetting, the ink's surface tension should be lower than the surface energy of the substrate (at least 7−10 mN m^{-1}). For substrates such as polyethylene terephthalate (PET), polycarbonate (PC), and silicon/silica, with surface energies of 48, 40, and 36 mN m^{-1}, respectively, the ink's surface tension should be less than 30 mN m^{-1}.[9,40,44] Also, surface treatment of the substrate is an effective method for improving wetting properties.[92,93] For example, PDMS has a low surface energy of only 21.6 mN/m, which makes it challenging to find a matching ink with good wetting properties. Ces et al. improved the surface wetting properties of PDMS by modifying its surface with plasma treatment combined with poly(vinyl alcohol) deposition, as illustrated in Figure 3d.[92] Likewise, plasma etching and chemical treatment of the substrate surface is effective in enhancing wettability.[94] This is mainly achieved by increasing hydrophilic surface functional groups.

For inks with low viscosity, such as those used in inkjet printing and spray coating, an unwanted effect known as the "coffee ring" may occur during the ink drying process.[41] This effect causes the deposited material to dry and aggregate at the droplet's periphery, resulting in a concave center area, and can decrease the resolution of inkjet printed patterns. To explain the "coffee ring" effect, Deegan et al. put forth a widely accepted theory.[95] As depicted in Figure 3c, when a droplet is deposited onto a substrate, the interface edge between the droplet and substrate (also known as the contact line) typically experiences the highest rate of evaporation during the drying process. This evaporation induces an outward convective flow from the droplet center to the edge, replenishing the evaporated solvent. This flow leads to material mainly depositing at the edge of the droplet, while the center receives very little material deposition.[5,41,95] Effective strategies to suppress the coffee ring effect include using a cooled substrate, increasing environmental humidity, adjusting the pH of the droplet, and reducing the droplet size.[41,43] Another effective method is the Marangoni flow, which involves mixing solvents with different surface tensions to generate a flow opposing the direction of capillary flow, redistributing the material back to the center of the droplet and achieving uniform deposition (Figure 3c).[96−98]

2.2. Formulation of MXene Ink. MXenes are typically obtained by selectively removing the "A" atomic layer from the MAX phase (shown in Figure 4a), where A is an element from the 13th or 14th main group in the periodic table, such as Al or Ga.[23,99] Due to the presence of strong M-A-M chemical bonds,

https://doi.org/10.1021/acsnano.3c10246
ACS Nano 2024, 18, 4651−4682

Table 2. Rheologies and Electrical Conductivities of Different MXene Inks

Solvent type	Concentration (mg mL^{-1})	Viscosity (cP)	Surface tension (mN m^{-1})	Conductivity	Application	Ref
Water	30	10	68.8	0.15 Ω cm^{-1}	MSCs	131
Water	60	10^4	—	6900 S cm^{-1}	Flexible wireless electronics	60
Water	18	5	76.5	9.8 Ω cm^{-1}	MSCs	132
Water	30	32	58.6	215 S cm^{-1}	MSCS	133
Water	5	1	73	119 S cm^{-1}	MSCs	134
NMP/DMSO	12.5	14/13	40.8 (NMP) 43.5 (DMSO)	2770 S cm^{-1}	MSCs	42
Ethanol	0.7	19.71	22.1	—	MSCs	42
DMSO	2.25	3.4	40	1080 S cm^{-1}	Electromagnetic shielding	135
DMSO	2	2.4	23	—	Photonics	5

it is difficult to obtain MXene through mechanical shearing methods like graphene. Instead, MXene is typically obtained by stripping the MAX precursor using chemical etching methods.[100−103] Since the report in 2011, where MXene ($Ti_3C_2T_x$) was obtained by selectively etching Ti_3AlC_2 with hydrogen fluoride (HF),[104] over 30 discrete stoichiometric forms of MXenes have been synthesized.[28] It is expected that more thermodynamically stable MXene structures will be discovered in the future.

The synthesis methods of MXene can be mainly divided into two categories: (a) selective etching of the MAX phase, including HF etching,[104,105] fluorine-containing etching,[103,106] alkali etching,[107] molten salt etching,[108,109] and supercritical etching;[110] and (b) bottom-up synthesis methods, such as chemical vapor deposition (CVD).[111,112] Among them, the most widely used method is chemical etching using hydrofluoric acid or in situ generated HF, which often yields MXene with hydrophilic terminations such as −OH, −O, and −F.[27] For multilayer MXene obtained by HF etching, it is necessary to insert large organic molecules (such as TMAOH, DMSO, urea, hydrazine, *etc.*) between the layers and then undergo ultrasound treatment to obtain single or few-layer MXenes.[103,113,114] The (002) peak of MXene with organic molecule intercalation shows a significant shift to the left, indicating an increase in layer spacing (Figure 4b).[113] The MILD method, based on in situ generated HF using lithium fluoride (LiF) and hydrochloric acid (HCl), allows MXene to be directly layered by ultrasonic or manual shaking due to the larger interlayer spacing brought by lithium ion intercalation.[103]

The adjustable surface chemistry of MXenes give them excellent affinity for both organic and inorganic solvents.[21,38] The abundant surface functional groups of MXenes impart negative zeta potential and hydrophilic surfaces, enabling stable dispersion of MXenes in water and some common polar solvents (such as dimethyl sulfoxide (DMSO), dimethylformamide (DMF), tetrahydrofuran (THF), and acetonitrile (ACN)) without the need for any surfactants or additives.[38,39,66,115] This is crucial for the formulation and application of MXene inks. For example, Zhang et al. successfully formulated additive-free aqueous and organic MXene inks for extrusion printing and inkjet printing (Figure 4c).[42] These high-concentration MXene inks exhibit long-term colloidal stability and achieve high printing resolution and spatial uniformity.

On the other hand, the physicochemical properties of MXene are highly dependent on the size of the two-dimensional nanosheets.[45,116,117] Typically, single or few-layered MXene dispersions can be obtained via centrifugation, but they commonly exhibit considerable lateral size disparity. In order to address this issue, Maleski et al. employed density gradient centrifugation to separate MXenes of different flake sizes (ranging from 0.1 to 5 μm) and investigate their relationship with physical and electrochemical properties.[116] The conductivity of smaller MXene flakes was significantly lower than that of larger flakes due to an increase in intersheet contact resistance and defect density. Similarly, the optical properties are linearly correlated with their flake size, with the absorption in the visible range decreasing as the sheet size decreases. In contrast, MXene films composed of ∼1.0 μm flakes showed greater capacitance than those composed of ∼4.4 μm flakes, mainly due to an increase in active sites resulting from defects. Thus, to achieve the desired performance, it is necessary to strike a balance between sheet size and properties, such as conductivity and active site density in MXenes.[63,66,88]

Furthermore, the interlayer spacing of MXene can be tuned by ion and molecule intercalation.[51,119] In 2013, Lukatskaya et al. discovered that various cations, including Na^+, K^+, NH^{4+}, Mg^{2+}, and Al^{3+}, could spontaneously or electrochemically intercalate into the interlayers of MXene, leading to an increase in *c* lattice parameter (Figure 4d).[51] Building on this discovery, researchers have developed a variety of intercalated MXene structures.[33,118,120,121] For instance, Luo et al. prepared a pillared Ti_3C_2 MXene (CTAB-Sn(IV)@Ti_3C_2) via a cetyltrimethylammonium bromide (CTAB) prepillaring and Sn^{4+} pillaring method, which increased the interlayer spacing of MXene by 177% (from 0.977 nm to 2.708 nm) (Figure 4e), thus greatly enhancing its charge storage capacity.[118] Similarly, Li et al. augmented the density of MXene active sites through cation intercalation and surface modification, resulting in a 3-fold increase in the pseudocapacitance of MXene, with a high energy density of 27.4 Wh kg^{-1}.[122] These structures demonstrate that stable MXene inks with improved ion-accessible active sites can be obtained via intercalation, which is of paramount importance for the preparation of high-performance MXene inks.

The stability of the ink is equally important. However, oxygen dissolved in water plays a crucial role in the chemical degradation process of MXene flakes, with oxidation starting at the edges of the MXene flakes and progressing toward the entire basal surface.[23] Therefore, removing dissolved oxygen from water with nitrogen or argon is an effective method to inhibit the oxidation of MXene. In addition, a low-temperature environment can significantly reduce the rate of oxidation caused by H_2O. Currently, MXene inks are mainly placed in sealed vials, energized with argon gas, and stored at low temperatures, which can enhance their stability to more than one month.[123] However, this still does not fully satisfy the need for long-term storage.[45] Instead, storing MXenes in organic

https://doi.org/10.1021/acsnano.3c10246
ACS Nano 2024, 18, 4651−4682

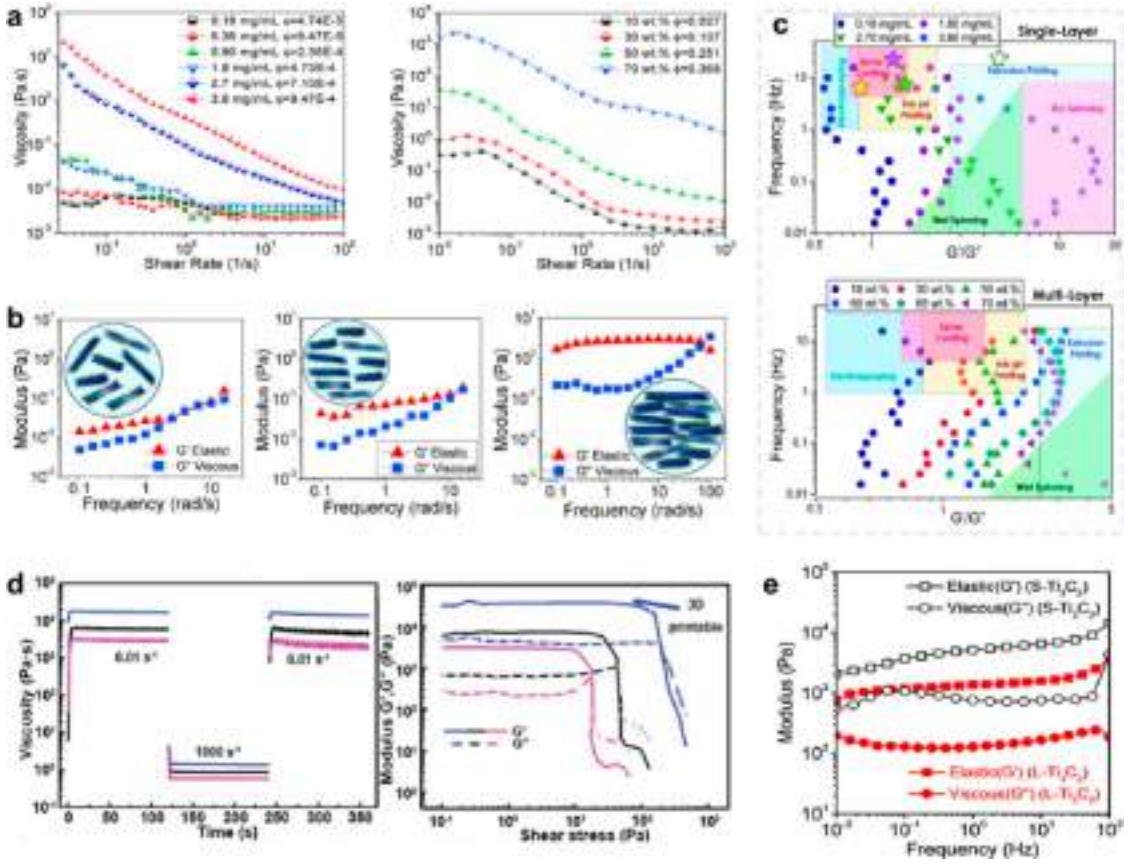

Figure 5. Rheological properties of MXene aqueous ink. (a) Viscosity versus shear rate for different concentrations of MXene suspensions, the left and right graphs show single- and multilayer MXene flakes, respectively. Reprinted with permission from ref [83]. Copyright 2018 American Chemical Society. (b) Viscoelasticity of single-layer MXene flake suspensions with different concentrations. Reprinted with permission from ref [83]. Copyright 2018 American Chemical Society. (c) Frequency relationship between the ratio of elastic modulus (G') and viscous modulus (G'') of single-layer and multilayer $Ti_3C_2T_x$ MXene aqueous suspensions. Reprinted with permission from ref [83]. Copyright 2018 American Chemical Society. (d) Left: viscosity variation of MXene aqueous inks with time at low (0.01 s^{-1}) and high shear rates (1000 s^{-1}); Right: variation of viscoelastic modulus (G' and G'') versus shear stress, and viscoelastic characteristics of high-concentration MXene ink for 3D printing technology. Reprinted with permission under a Creative Commons CC BY License from ref [37]. Copyright 2021 Springer Nature. (e) Viscoelastic behavior of large-Ti_3C_2 with a concentration of 26.5 mg mL^{-1} and small-Ti_3C_2 with a concentration of 150 mg mL^{-1}. Reprinted with permission under a Creative Commons CC BY License from ref [126]. Copyright 2020 American Chemical Society.

solvents seems to be a better option due to the stabilizing solvation effect of organic solvents.[124] The results showed that the well-suspended MXene dispersion system in organic solvents remained stable for several months. Antioxidants, such as sodium L-ascorbate, are also an effective means of inhibition. It can hinder the reaction between MXene edge sites and water molecules, inhibiting the oxidation of MXene flakes in water for more than 3 weeks.[125] The long-time stability of MXene is also an important limiting factor for its industrialization, and there is still a need for cleaner, more efficient and cheaper oxidation inhibition solutions.

2.3. Rheology of MXene Inks. The rheological behaviors of MXene inks is dependent on various aspects, such as single-layer and multilayer MXene sheets, ink concentration, MXene sheet size and different dispersants.[42,83,126,127] First, regarding MXene aqueous dispersion, the unique dispersibility of MXenes enables them to remain stably dispersed within a wide concentration range.[39] Different concentrations of MXene ink exhibit distinct rheological behaviors, significantly affecting reproducibility in existing printing techniques and the quality of printed patterns (Table 2). Akuzum et al. investigated the rheological properties of MXenes by performing shear experiments on single-layer and multilayer MXene suspensions at different concentrations (Figure 5a).[83] Both suspensions exhibited significant shear-thinning behavior at different concentrations, with viscosity increasing markedly with concentration. At a high shear rate (γ = 100 s^{-1}), the viscosities of different concentrations of single-layer dispersion were similar, while the viscosity of multilayered $Ti_3C_2T_x$ particles still varied by 3 orders of magnitude between the highest (70 wt %) and lowest (10 wt %) concentrations. Moreover, the viscosity of multilayer MXene suspensions was 2 orders of magnitude higher than that of single-layer MXene suspensions at the highest concentration.

The ratio of elastic modulus (G') to viscous modulus (G'') is another important parameter for determining the rheology of ink.[127,128] For example, spray coating typically requires high processing rates and high viscous modulus, while extrusion printing requires high elastic modulus to maintain the shape of the pattern.[43,84] Single-layer MXene ink exhibits viscoelastic properties at different concentrations (Figure 5b).[83] At low MXene concentrations (0.36 mg mL^{-1}), significant elastic behavior (G') can be observed, which is beneficial for thin film processing methods such as spin coating and spray coating, as

https://doi.org/10.1021/acsnano.3c10246
ACS Nano 2024, 18, 4651−4682

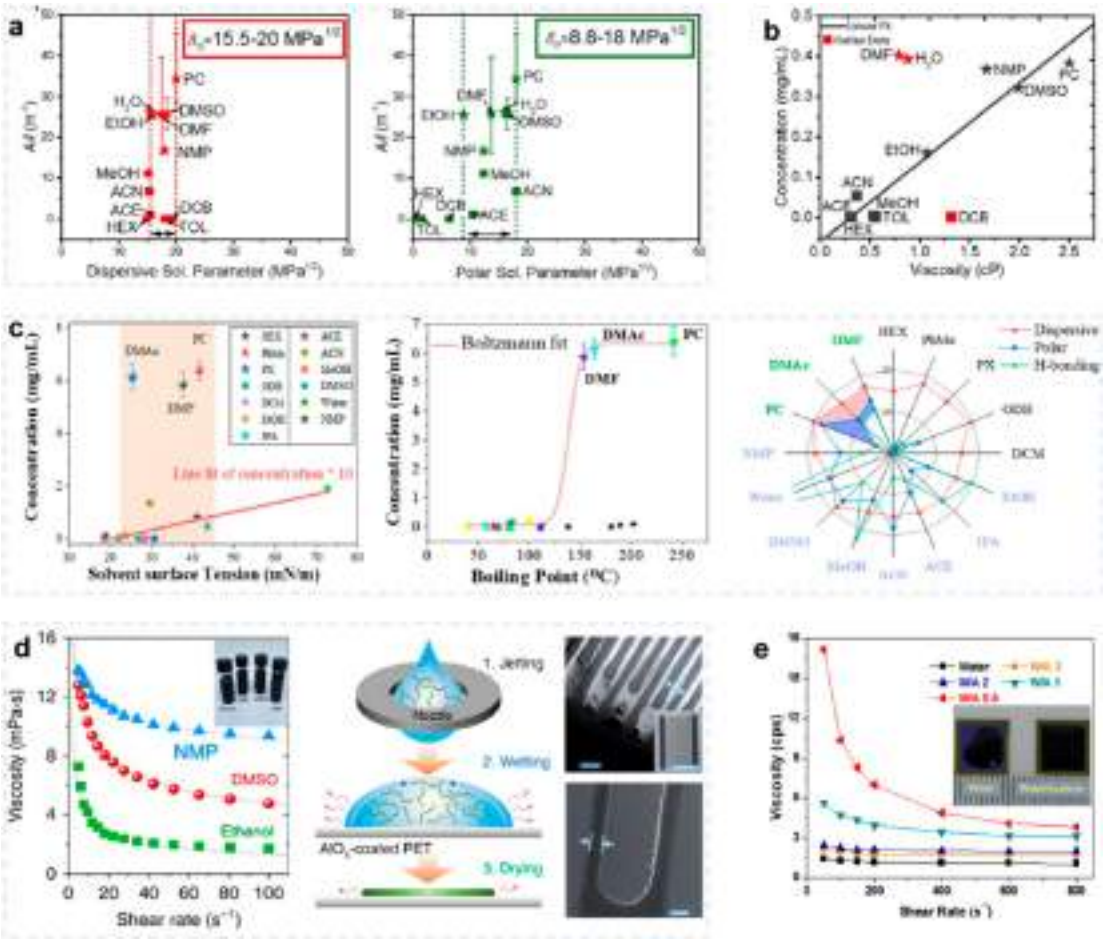

Figure 6. Rheological properties of MXene organic ink. (a) Relationships between $Ti_3C_2T_x$/solvent absorbance per cell path length (A/l) supported by a solvent and its Hansen solubility parameters: dispersive and polar, respectively. Reprinted with permission from ref [38]. Copyright 2017 American Chemical Society. (b) Concentration relationship of MXene solutions with different viscosity solvents. Reprinted with permission from ref (38). Copyright 2017 American Chemical Society. (c) Dispersibility of surface-modified MXene in different solvents, including the fitting of concentration to solvent surface tension and boiling point, and the relationship between the solubility of $Ti_3C_2T_x$ and the Hansen solubility parameter of the solvent. Reprinted with permission from ref [124]. Copyright 2021 American Chemical Society. (d) Relationship between the viscosity versus shear rate of different MXene organic inks. This additive-free MXene ink has good wettability to the substrate and can be used directly for printing. Reprinted with permission under a Creative Commons CC BY License from ref [42]. Copyright 2019 Springer Nature. (e) Rheological behavior of mixed organic/aqueous MXene dispersions. The addition of acetone significantly increased the viscosity of MXene solution. Reprinted with permission from ref [93]. Copyright 2022 American Chemical Society.

it helps to eliminate disturbances during processing.[129] When the MXene concentration increases to 0.9 mg/mL, an interpenetrating volume percolation network begins to form in the system, exhibiting soft-solid behavior at low frequencies and fluid-like behavior at high frequencies (power-law scaling), indicating that $Ti_3C_2T_x$ sheets interact with each other through electrostatic forces at far distances, which may be applicable to techniques such as inkjet printing.[5,46] At higher concentrations, G' increases significantly and becomes more independent of frequency, and the intersection point with G'' also shifts to higher frequencies, indicating an increase in long-range order of the percolation network and the emergence of behavior similar to that of a soft gel, which is usually beneficial for wet spinning.[130] Similarly, multilayer $Ti_3C_2T_x$ ink also exhibits significant viscoelastic behavior.[83] At low concentrations, G'' dominates, but with increasing concentration, G' becomes greater than G'', indicating gel transitions and percolation. This also indicates that by changing the concentration of multilayer $Ti_3C_2T_x$, its rheology can be effectively adjusted, making it suitable for a wide range of applications, such as electrospinning, spray coating, inkjet printing, wet spinning, and extrusion printing (Figure 5c).[83]

However, it is worth noting that the highest G' value of single-layer MXene obtained above is not sufficient for extrusion-based 3D printing.[89] Further increasing the concentration of single-layer MXene ink (>10 mg) can increase the viscosity and elasticity of the system, obtaining viscoelasticity and yield stress suitable for 3D printing (Figure 5d).[37,54] Yang et al. found that the viscosity of single-layer MXene dispersion with higher aspect ratio (15 mg mL^{-1}) is of the same order of magnitude as that of high-concentration multilayer MXene dispersion (2.33 g mL^{-1}, 70 wt %), indicating that MXene flakes with higher aspect ratio can be effectively used to adjust rheology.[68] Meanwhile, the elastic modulus and yield stress of ink with a concentration of 50 mg mL^{-1} were increased to 36,507 and 206 Pa, respectively, making it feasible for 3D printing. Subsequent work by Zhang et al. revealed that adjusting the aspect ratio and concentration of MXene flakes

https://doi.org/10.1021/acsnano.3c10246
ACS Nano 2024, 18, 4651−4682

can induce their self-assembly into a liquid crystal (LC) phase that is suitable for wet spinning.[126] For example, the aqueous ink of large MXene flakes (referred to as L-$Ti_3C_2T_x$; average flake size of ~3.1 μm) can form LC at a concentration as low as 26.5 mg/mL, while smaller MXene (S-$Ti_3C_2T_x$; ~310 nm) flakes require much higher concentrations (~150 mg mL^{-1}). Additionally, the S-$Ti_3C_2T_x$ ink must be more concentrated than the L-$Ti_3C_2T_x$ ink to obtain the same viscosity and G'/G'' ratio. As shown in Figure 5e, the rheological behavior of MXene ink is closely related to the liquid crystal phase, as there is a significant change in the relationship between G'/G'' and oscillatory shear frequency.[126] Specifically, as the concentration increases, the rheological behavior gradually shifts from liquid-like to solid-like. Fan et al. also demonstrated that nitrogen-doped $Ti_3C_2T_x$ MXene dispersion with a concentration as high as 300 mg mL^{-1} can transition from solid-like to liquid-like behavior under shear stress exceeding 170 Pa, which is favorable for ink extrusion.[136] In the same year, Orangi et al. prepared high-concentration single-layer MXene dispersion (290 mg mL^{-1}) through a superabsorbent polymer bead, and the yield stress obtained from the Herschel−Bulkley model was 24 Pa.[54] They also observed that the G' value remained consistently higher than G'' across different frequency ranges, indicating significant viscoelastic behavior of the ink at rest.

In the previous section, the rheological behavior of MXene in aqueous solutions was discussed. However, for many printing processes, it is necessary to disperse MXene in organic solvents in order to improve substrate compatibility. In 2017, Maleski et al. reported on the dispersion of MXene in common organic solvents and studied the correlation between solvent physicochemical properties and dispersion stability.[38] The results showed that good solvents for MXene must have high polarity and provide strong nonspecific dispersion interactions, while their ability to form hydrogen bonds is not necessarily important (Figure 6a). Solvents with a surface tension between 35 and 42 mN m^{-1} and a polar/dispersive component ratio between 0.61 and 0.87 were found to have good dispersibility, including *N*,*N*-dimethylformamide, *N*-methyl-2-pyrrolidone, dimethyl sulfoxide, propylene carbonate, and ethanol.[45] This suggests that the rheological behavior of the MXene dispersion, including surface tension and viscosity, can be adjusted by changing the solvent, as shown in Figure 6b. In addition, by modifying the surface chemistry of MXene, hydrophilic MXene can be converted into hydrophobic MXene, resulting in organic MXene dispersions. For example, Zhang et al. used tetrabutylammonium hydroxide (TBAOH) as an intercalating agent and surface modifier to achieve high concentration dispersion of MXene in organic solvents (PC, DMAc and DMF) (Figure 6c).[124] At the same time, the solvents used have high boiling points and suitable Hansen solubility parameters, which is consistent with previous reports.[38]

MXene demonstrates similar rheological properties in organic solvents as it does in aqueous dispersions, but there has been relatively little research conducted on this topic.[42,85,137] Zhang et al. developed an organic $Ti_3C_2T_x$ ink formulation for inkjet printing and were able to achieve good printing results for microdevices.[42] $Ti_3C_2T_x$ exhibited shear-thinning behavior in dimethyl sulfoxide (DMSO), *N*-methyl-2-pyrrolidone (NMP), and ethanol, with corresponding Ohnesorge numbers (Z) of approximately 2.5 and 2.2 for DMSO and NMP, respectively, falling within the optimal range for stable jetting ($1 < Z < 14$). Additionally, PET coated with AlO_x (surface tension is ~66 mN m^{-1}) was used as the printing substrate to achieve good substrate wetting, resulting in high printing resolution and no coffee-ring effect after drying. Similarly, we adjusted the surface tension and viscosity of the MXene ink by using a mixture of water and acetone to achieve good wetting on a silicon substrate, obtaining a uniform MXene-SiO_2 electrode through drop casting.[93]

During the MXene electrode deposition process, there is a significant difference in the rheological properties of MXene ink applicable to different processing techniques. In addition to viscosity, other parameters such as the resolution of printing methods, film conductivity, film thickness, and film transparency also need to be further considered.[44,45,79] However, there remains a significant amount of research yet to be completed regarding the rheological behavior of MXene dispersions, including the rheological properties of MXene in organic dispersions and mixed solvents. Such insights are of great importance to inform and guide future solution-processing of MXene and MXene compositions.

3. MXENE-BASED MICRO-SUPERCAPACITORS

Two-dimensional MXenes possess numerous outstanding intrinsic physicochemical properties, such as metallic conductivity, high redox activity, and abundant surface functional groups, rendering them highly promising for application in the field of micro-supercapacitors.[28,29] The unique conductive transition metal carbide layer in MXenes enables efficient electron transport, and intercalation between layers can store more electrolyte ions (such as H^+, Li^+, Na^+, Zn^{2+} and Al^{3+}) or molecules.[51,85,122] Moreover, the edges of the MXene layer can provide high electrochemical activity.[27] The rich surface functional groups not only endow MXenes with hydrophilicity but also serve as active centers for fast redox reactions.[138] They also have a strong impact on the Fermi level, thus altering their electronic and electrochemical properties.[28,102] Additionally, the flexible and mechanical properties of the two-dimensional crystal structure provide robust mechanical strength for flexible MSCs. These prominent advantages make MXene-based micro-supercapacitors exhibit excellent electrochemical performance, arousing increasing attention from researchers.

The hydrophilic surface functional groups and negative zeta potential of MXene endow it with stable dispersion in polar solvents, which is highly favorable for constructing micro-supercapacitors through solution processing, including coating and printing processes, such as spray/spin-coating, 3D transfer, ink writing, patterned coating, screen printing and others (Figure 7).[42,74,85,139,140]

3.1. MXene MSCs Based on Pure MXenes. At present, researchers have achieved submillimeter MXene-based micro-supercapacitors using various techniques, which can be classified into two categories: (i) coating the MXene material on the surface of the substrate and directly forming MXene patterns through laser scribing and other techniques;[34,72,93,141] and (ii) transferring MXene ink to different patterns using various printing technologies.[66,74,142,143]

Laser scribing technology is an economical, efficient, and direct method that can create custom patterns in one step on a wide range of substrates, with excellent flexibility in burnable materials and electrode depth.[144,145] In 2016, Peng et al. used laser scribing technology to fabricate solid-state all-MXene MSCs (Figure 8a), directly using two layers of $Ti_3C_2T_x$ MXene with two different flake sizes as a current collector and active material, showing an areal capacitance of 27 mF cm^{-2}.[88]

https://doi.org/10.1021/acsnano.3c10246
ACS Nano 2024, 18, 4651−4682

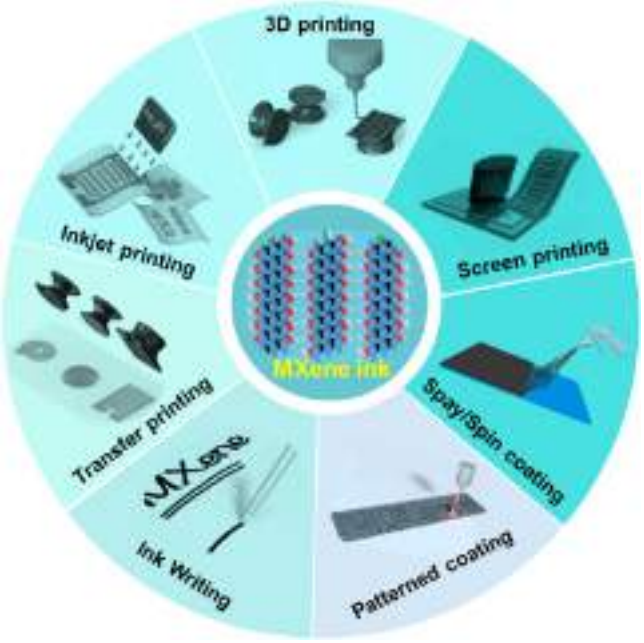

Figure 7. Methods for fabricating MXene-based micro-supercapacitors through solution processes, including coating and printing techniques such as spray/spin coating, 3D transfer, ink writing, pattern coating, screen printing, *etc.* Reprinted with permission under a Creative Commons CC BY License from ref [42]. Copyright 2019 Springer Nature. Reprinted with permission from ref (74). Copyright 2018 John Wiley and Sons. Reprinted with permission from ref [85]. Copyright 2020 John Wiley and Sons. Reprinted with permission from ref [139]. Copyright 2019 John Wiley and Sons.

Similarly, Kurra et al. fabricated paper-based MXene micro-supercapacitors via laser processing, even depicting MXene film electrodes up to 120 μm thick (Figure 8b).[146] However, patterned electrodes obtained by laser processing methods often have uneven and rough edges because the local heat generated by optical fiber and CO_2 lasers cannot dissipate quickly through the substrate. In addition, the laser also accelerates the conversion of MXene to titanium dioxide.

Considering this, Huang et al. utilized UV cold laser to process MXene microelectrodes, effectively reducing the damage to the edges of MXene during the laser processing (Figure 8c).[147] Subsequently, they employed a UV laser etching strategy to construct MXene-SiO_2 electrodes, effectively suppressing the hydrogen evolution reaction during the electrochemical process.[93] The resulting pure MXene-based MSCs achieved an expanded voltage window of up to 1.2 V (Figure 8d) and a high energy density of 71 mWh cm^{-3}. Similarly, femtosecond lasers have an ultrashort pulse duration, and their laser-affected area along the laser-etched edge is limited to approximately 800 nm transverse distance, minimizing the effect on the active material electrode area.[34] The MXene interdigital electrodes, obtained via femtosecond laser etching, exhibit ultranarrow gaps (10 μm) and retain the majority of their electrochemical activity. These electrodes demonstrate excellent electrochemical performance and can attain a high working voltage of 7.2 V through a series-parallel design (Figure 8e).

Automated scalpel patterning and vacuum filtration are also alternative methods for manufacturing MXene MSCs.[72,148−150] Salles et al. utilized dip-coating method to produce optically transparent Ti_3C_2 MXene films (10−100 nm) and subsequently employed a one-step automated scalpel engraving to fabricate transparent MXene MSCs (as shown in Figure 8f).[148] These devices exhibited outstanding electrochemical storage capabilities at high scan rates and superior optoelectronic properties. But this method produced a relatively low gap resolution (0.1−0.2 mm), and the finger widths and lengths were relatively large (0.8−1 mm and 1−10 mm, respectively). In addition, vacuum filtration is also a commonly used method, which can directly obtain free-standing MXene electrodes with controllable and uniform thickness. For instance, Huang et al. employed a gentle water freezing-and-thawing (FAT) approach to enhance the delamination yield of multilayer-MXene, followed by interdigital mask-assisted vacuum filtration to fabricate MXene MSCs (Figure 8g).[151] The MSCs show an areal and volumetric capacitance of 23.6 mF cm^{-2} and 591 F cm^{-3}, respectively, along with a high energy density of 29.6 mWh cm^{-3}. It should be noted that the limitations of the filtration method are that the electrode processing is limited by the size of the filtration equipment and the filtration speed. As well, it is also necessary to transfer MXene films to the target substrate for further processing, which makes it difficult to achieve large-scale production of MXene MSCs.[11,45]

Printing technology is another crucial process for the fabrication of patterned MXene films, which is of great significance for the large-scale production of MXene MSCs. Various techniques such as inkjet printing, screen printing, transfer printing, and 3D printing have been employed.[66,74,90,142] For instance, stamping technology has been adopted to fabricate MXene-based MSCs, achieving a high areal capacitance of 61 mF cm^{-2} and energy density of 0.76 μWh cm^{-2} (Figure 9a).[74] This method boasts of lower production cost and time, but the resolution is relatively low. Inkjet and extrusion printing are also promising methods for the large-scale production of MXene MSCs, but they require MXene ink with higher rheological properties. Zhang et al. demonstrated a high electronic conductivity of 2770 S cm^{-1} by printing circuits with additive-free MXene ink, which remained stable at 1093 S cm^{-1} even after 1000 bending cycles. As the printing layers increased, the areal capacitance improved to 43 mF cm^{-2} with a high energy density of 0.32 μWh cm^{-2} at a power density of 11.4 μW cm^{-2} (Figure 9b).[42] Additionally, Uzun et al. demonstrated the thermal inkjet printing of additive-free aqueous MXene inks onto textiles and further enhanced the performance of MXene MSCs (294 mF cm^{-2} and 4.46 μWh cm^{-2}) by controlling the $Ti_3C_2T_x$ flake size (Figure 9c).[66]

Furthermore, screen printing has been widely utilized in the manufacture of MXene MSCs. Zheng et al. employed a high-viscosity MXene ink (with an apparent viscosity of 3548 Pa·s, ∼10 wt % mass loading) for screen printing, which yielded an ultrahigh areal capacitance of 1.1 F cm^{-2} and an energy density of 13.8 μWh cm^{-2} (Figure 9d).[57] Additionally, they were able to connect a series of 100 MXene MSCs to output a high voltage of 60 V. To improve the utilization of MXene materials, Abdolhosseinzadeh et al. developed a strategy to turn trash into treasure by directly using the viscosity-controlled MXene sediment as aqueous inks for screen printing of MXene MSCs (Figure 9e).[142] These MSCs achieved a high areal capacitance of 158 mF cm^{-2} and energy density of 1.64 μWh cm^{-2}. The "turning trash into treasure" strategy effectively increases the utilization of MXene materials,

https://doi.org/10.1021/acsnano.3c10246
ACS Nano 2024, 18, 4651−4682

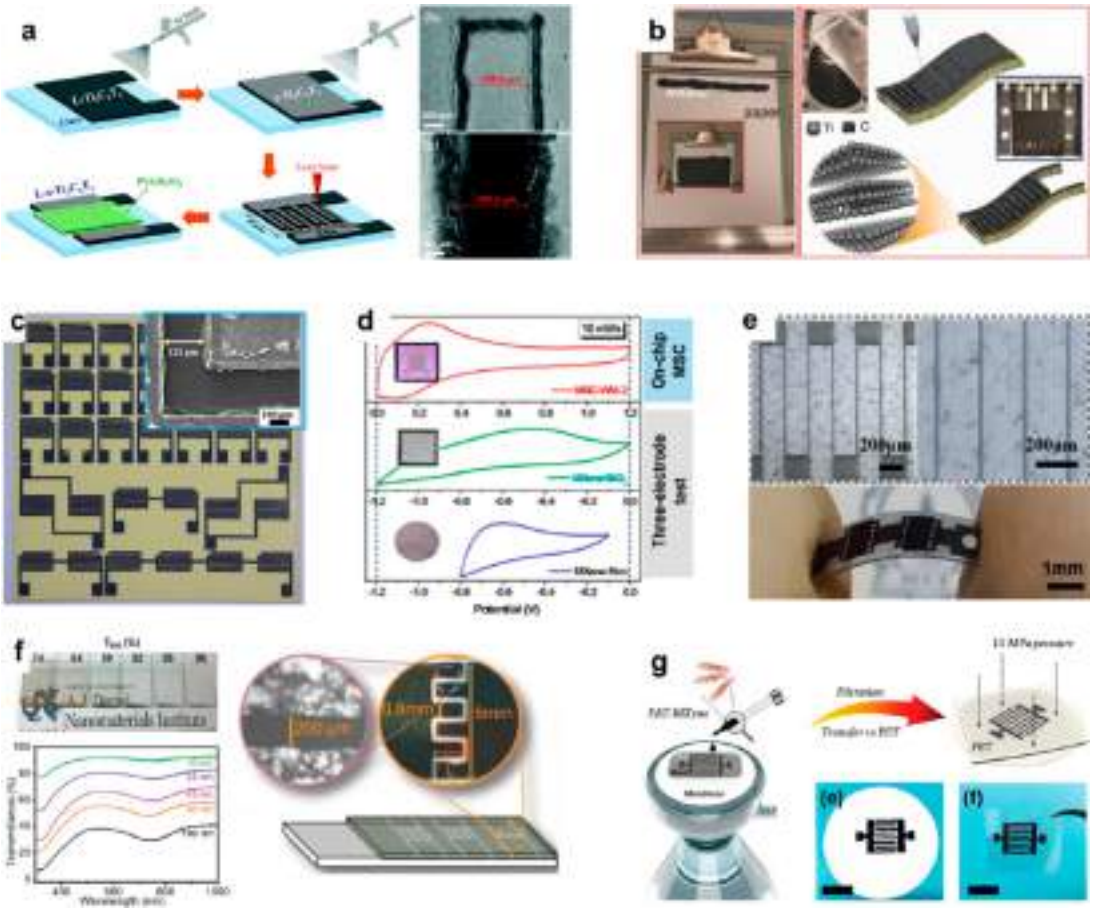

Figure 8. MXene MSCs based on pure MXene ink. (a) Fabrication of all-$Ti_3C_2T_x$ MXene MSCs through spray-coating and laser scribing, and corresponding SEM images of interdigital electrode. Reprinted with permission from ref [88]. Copyright 2016 RSC. (b) Fabrication of MXene-on-paper MSCs through spray-coating and laser patterning. Reprinted with permission from ref [146]. Copyright 2016 John Wiley and Sons. (c) Paper-based MXene MSCs fabricated on a large scale by UV-cooled laser. Reprinted with permission from ref [70]. Copyright 2020 Elsevier. (d) MXene-SiO_2 interdigital structure from cold laser processing effectively enhances the voltage window of MXene MSCs. Reprinted with permission from ref [93]. Copyright 2022 American Chemical Society. (e) Femtosecond laser etching further improves the resolution of MXene MSCs and obtains ultranarrow gaps (10 μm). Reprinted with permission from ref [24]. Copyright 2020 John Wiley and Sons. (f) Transparent MXene MSCs via automated scalpel patterning. Optically transparent Ti_3C_2 MXene films are prepared by dip coating and exhibit excellent transmission in different thicknesses. Reprinted with permission from ref [148]. Copyright 2018 John Wiley and Sons. (g) All-MXene MSC manufactured by mask-assisted filtration. Reprinted with permission from ref [151]. Copyright 2020 John Wiley and Sons.

reduces the cost of mass-producing MXene MSCs, and has positive implications for scalability and sustainable production of MXene-based wearable smart electronics.

3.2. MXene MSCs Based On MXene Composites. The aforementioned research studies are based on pure MXene as the electrode material for MSCs. Due to its high conductivity and volumetric capacitance, MXene MSCs exhibits superior electrochemical performance.[39,85] However, to further enhance the energy storage performance of MXene MSCs, intercalation confinement engineering has been proposed as a promising processing strategy for MXene, as it can effectively enlarge the interlayer spacing and regulate the interface structure of MXene composites.[49,119,120,152] Doping with heteroatoms has been proven to be an effective method for improving the electrochemical properties of carbon materials by controlling the number of charge carriers and increasing material conductivity.[153] This approach can also be applied to MXene materials, as heteroatom doping can alter the composition and structure of MXene, thereby significantly improving its electrochemical capacitance.[114,154] Yu et al. developed wrinkled N-doped MXene ink for printing microscale energy storage devices (Figure 10a), which improved the electrochemical performance of MXene through enhanced conductivity and redox activity.[139] Using screen printing, the MXene-N MSC achieved a specific capacitance of 70.1 mF cm^{-2} and impressive mechanical strength. Additionally, Lukatskaya et al. discovered that various cations, such as Na^+, K^+, NH^{4+}, Mg^{2+}, and Al^{3+}, can be intercalated into MXene layers through electrochemical methods, resulting in a volumetric capacitance of over 300 F cm^{-3}.[51] Building upon this research, Zheng et al. developed a flexible ionogel MXene MSC with high voltage and energy by ionic liquid preintercalated.[33] Remarkably, the device can operate at up to 3 V, while its areal and volumetric energy densities can reach as high as 13.9 μWh cm^{-2} and 43.7 mWh cm^{-3}, respectively. Overall, heteroatom doping and ion intercalation techniques allow effective tuning of the interlayer spacing and conductivity of MXene, resulting in significant improvements in the electrochemical performance of MXene MSCs.

https://doi.org/10.1021/acsnano.3c10246
ACS Nano 2024, 18, 4651−4682

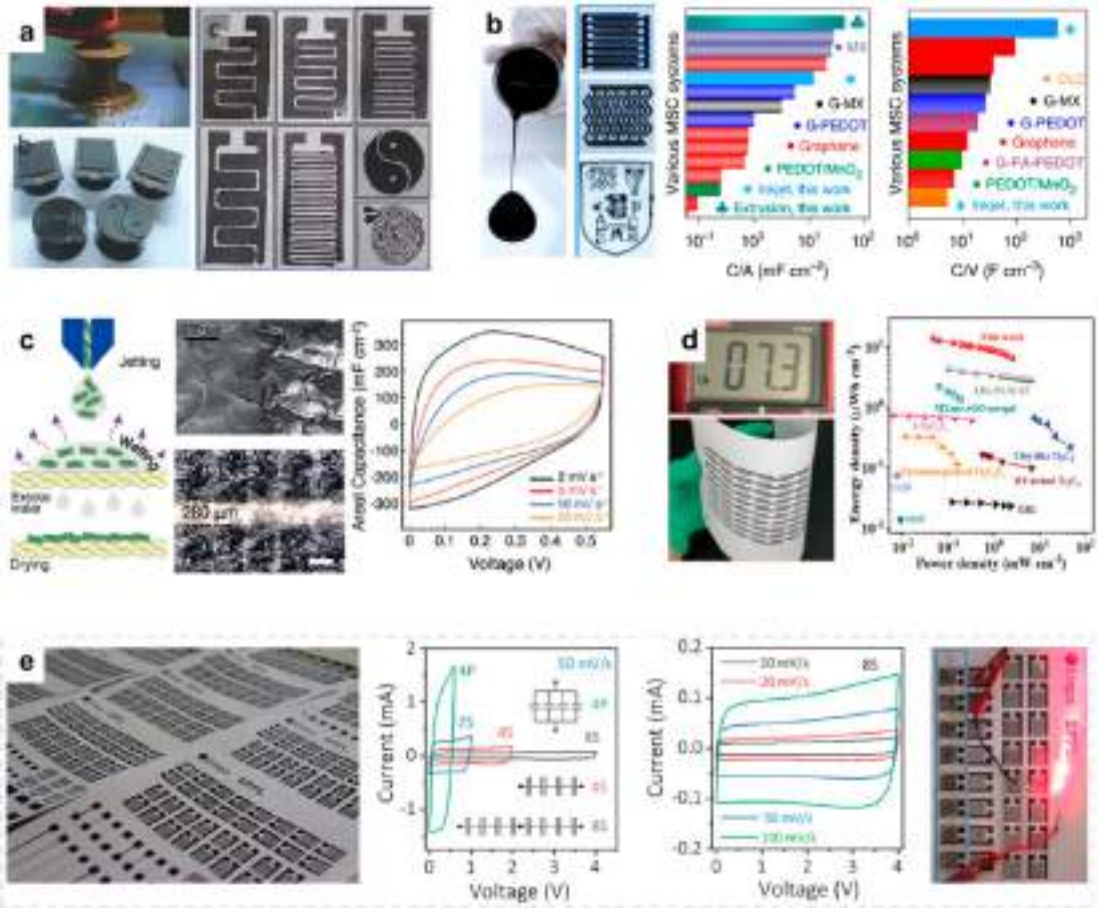

Figure 9. Printing MXene MSCs based on pure MXene ink. (a) Flexible coplanar MSCs stamped with MXene ink showing low resolution. Reprinted with permission from ref [74]. Copyright 2018 John Wiley and Sons. (b) All-MXene MSCs by inkjet printing and extrusion printing using NMP ink. The inkjet printed MXene MSCs exhibit a volumetric capacitance of 562 F cm^{-3}, while the extrusion-printed MSCs obtain the highest areal capacitance of 43 mF cm^{-2}. Reprinted with permission under a Creative Commons CC BY License from ref [42]. Copyright 2019 Springer Nature. (c) Thermal inkjet printing of MXene MSCs on textiles with additive-free aqueous MXene inks. By controlling the $Ti_3C_2T_x$ flake size, optimized $Ti_3C_2T_x$-printed MSCs display a high areal capacitance of 294 mF cm^{-2}. Reprinted with permission from ref [66]. Copyright 2021 John Wiley and Sons. (d) High-viscosity MXene ink (with an apparent viscosity of 3548 Pa·s) for screen printing, exhibiting an ultrahigh areal capacitance of 1.1 F cm^{-2} and an energy density of 13.8 μWh cm^{-2}. Reprinted with permission from ref [57]. Copyright 2021 John Wiley and Sons. (e) Turning trash into treasure strategy to prepare MXene sediment ink for screen printing. These MSCs provide a high areal capacitance of 158 mF cm^{-2} along with excellent series-parallel performance. Reprinted with permission from ref [142]. Copyright 2020 John Wiley and Sons.

Meanwhile, the use of the insertion process to synthesize MXene-based composite materials is also a common approach for effectively improving the performance of MXene MSCs.[47,67,117,155,156] These composites are typically made by combining MXene layers with other materials, such as carbon-based substances,[47,157] black phosphorus,[48] metal oxides/sulfides,[141,155,156] and organic polymers.[46,158] For instance, carbon nanotubes (CNTs) and graphene are popular options for creating MXene composites because they act as spacers between MXene layers, which prevents restacking and enables rapid ion diffusion. This makes them ideal for energy storage applications requiring fast charging and discharging processes. To illustrate, Eunji Kim et al. utilized focused ion beam (FIB) technology to manufacture coplanar MXene/CNT MSCs with a gap of only 500 nm (Figure 10b).[73] By using CNTs as spacers between MXene layers, they created a fast pathway for ion diffusion, achieving a specific capacitance of around 317 mF cm^{-2}, as well as outstanding rate capability. Specifically, the electrode retained 32.8% of its capacity at a scan rate of 100 V s^{-1}. Similarly, Li et al. developed flexible MSCs by combining MXene with electrochemically exfoliated graphene, achieving a high volumetric capacitance of up to 216 F cm^{-3} (Figure 10c).[157] Small MXene particles between graphene layers in this composite electrode served as conductive spacers, preventing irreversible $\pi-\pi$ stacking between graphene layers while also acting as ideal "buffers" for active materials and shuttling electrolytes.

Metal oxides/sulfides, such as MoS_2, RuO_2, MnO_2, and LDH, offer significantly higher energy storage capacity compared to double-layer capacitors, making them an important option for developing MXene composite materials.[141,155,159−161] For example, adding MoS_2 to MXene increases its specific capacitance by 60% and brings the energy density of MXene MSCs up to 15.5 mWh cm^{-3} (Figure 10d).[141] However, due to the semiconductor properties of molybdenum sulfide, it negatively affects the conductivity of microelectrodes, resulting in only 17.6% capacitance retention at a scanning rate of 50 mV s^{-1}. To address this issue, Li et al. developed a high-conductivity ink that combines RuO_2@MXene nanosheets with silver nanowires (AgNWs) to

https://doi.org/10.1021/acsnano.3c10246
ACS Nano 2024, 18, 4651−4682

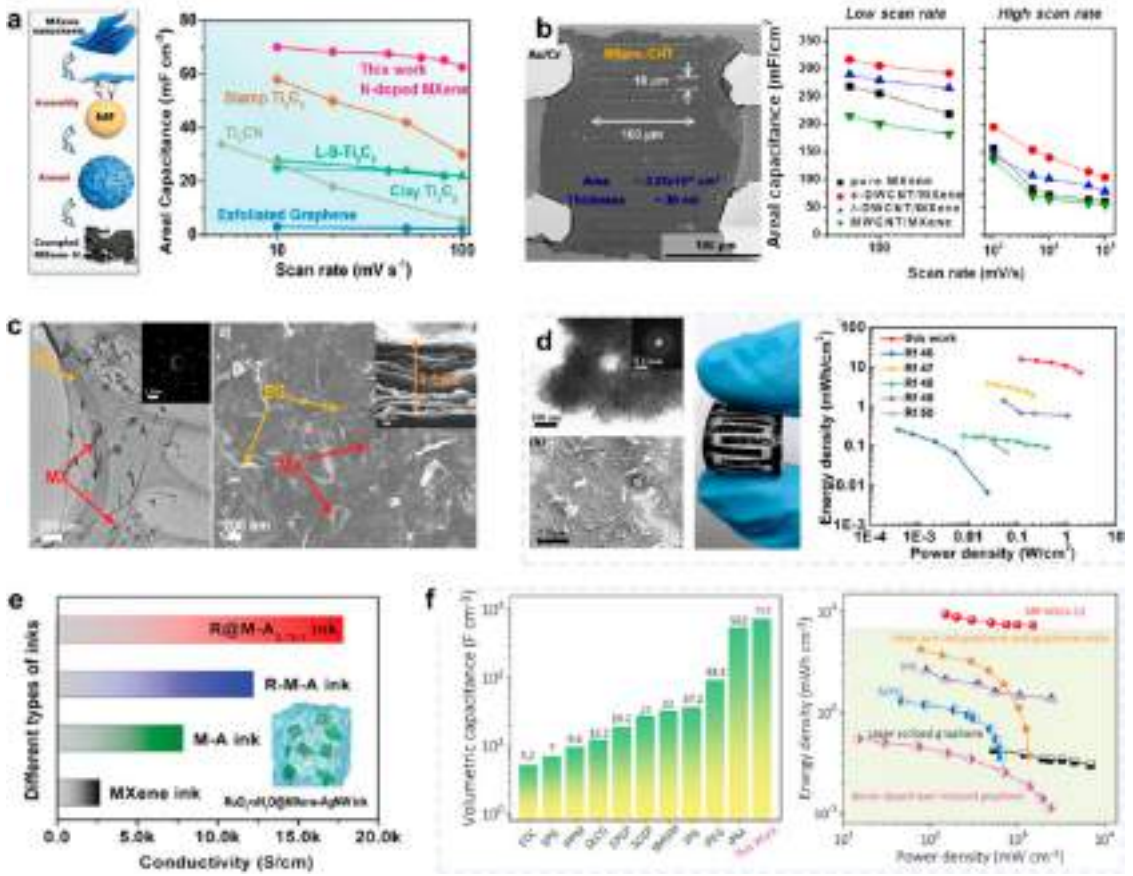

Figure 10. MXene MSCs based on MXene-composite inks. (a) N-doped MXene inks for screen printing and extrusion printing. The crumpled MXene-N nanosheets are synthesized by an MF templating method, and the corresponding printing MSC has an areal capacity of 70.1 mF cm^{-2}. Reprinted with permission from ref [139]. Copyright 2019 John Wiley and Sons. (b) MXene/CNT MSCs with a gap of 500 nm exhibit the specific capacitance of 317 mF cm^{-2} and a capacity retention of 32.8% at a scan rate of 100 V s^{-1}. Reprinted with permission from ref [73]. Copyright 2021 Elsevier. (c) Small MXene particles in MXene-graphene composite electrodes act as conductive spacers between graphene layers, preventing irreversible π–π stacking between graphene layers. Reprinted with permission from ref [157]. Copyright 2017 John Wiley and Sons. (d) Direct laser etching of MXene-MoS_2 films for MSCs, with an energy density of 15.5 mWh cm^{-3}. Reprinted with permission from ref [141]. Copyright 2019 John Wiley and Sons. (e) Hydrous RuO_2-decorated MXene coordinating with silver nanowire inks for screen printing. Reprinted with permission from ref [155]. Copyright 2019 John Wiley and Sons. (f) Inkjet-printed MSCs with aqueous MXene/PH1000 hybrid ink exhibits a volumetric capacitance of 754 F cm^{-3} and an energy density of 9.4 mWh cm^{-3}. Reprinted with permission from ref [46]. Copyright 2021 John Wiley and Sons.

manufacture high-performance fully printed MSCs (Figure 10e).[155] This approach not only utilizes the high pseudocapacitance properties of RuO_2 nanoparticles but also prevents MXene nanosheets from restacking through RuO_2 intercalation, ensuring fast ion transport channels. Additionally, AgNWs provide a highly conductive network structure that achieves fast charge transfer. Based on RuO_2@MXene/AgNWs, the microdevices have a high volumetric capacitance of 864.2 F cm^{-3}, 35.2% capacitance retention (at 2000 mV s^{-1}), and a high power density of 48.5 W cm^{-3}. This also highlights the unique advantages of metal oxide (sulfide)/MXene composite electrodes in producing high-performance micro-supercapacitors.

Organic polymers possess excellent flexibility, mechanical strength, and high pseudocapacitance, making MXene/polymer composite materials ideal electrodes for constructing miniaturized supercapacitors, especially those that are flexible, stretchable, and self-healing.[46,67,141,158] For instance, Wu's research group designed an aqueous MXene/PH1000 hybrid ink for inkjet printing MXene MSCs (Figure 10f).[46] The highly conductive PH1000 effectively prevents the restacking of MXene nanosheets, facilitating the rapid diffusion of electrons and ions throughout the microelectrode, along with additional pseudocapacitance. As a result, the microdevices achieve an ultrahigh volumetric capacitance of 754 F cm^{-3} and a high energy density of 9.4 mWh cm^{-3}. Furthermore, the MXene/bacterial cellulose (BC) composite paper displays a high increase in mechanical strength, with a tensile strength of up to 70.0 MPa (with a fracture strain of approximately 15.5%), as well as high areal capacitance.[67] The resulting MSCs exhibited a high areal capacitance of 111.5 mF cm^{-2} and excellent stretchability (with a high strain of 100%). Due to the abundance of conductive polymers,[162] MXene/polymer composite materials can be designed with versatility, providing great potential for achieving exceptional electrochemical performance and mechanical stability.

The unique 2D structure of MXene can provide an excellent environment for chemical reactions, while its high metallic conductivity facilitates efficient electron transfer when combined with other materials. As a result, an increasing number of MXene composite electrodes have been developed for energy storage applications, demonstrating a range of

https://doi.org/10.1021/acsnano.3c10246
ACS Nano 2024, 18, 4651−4682

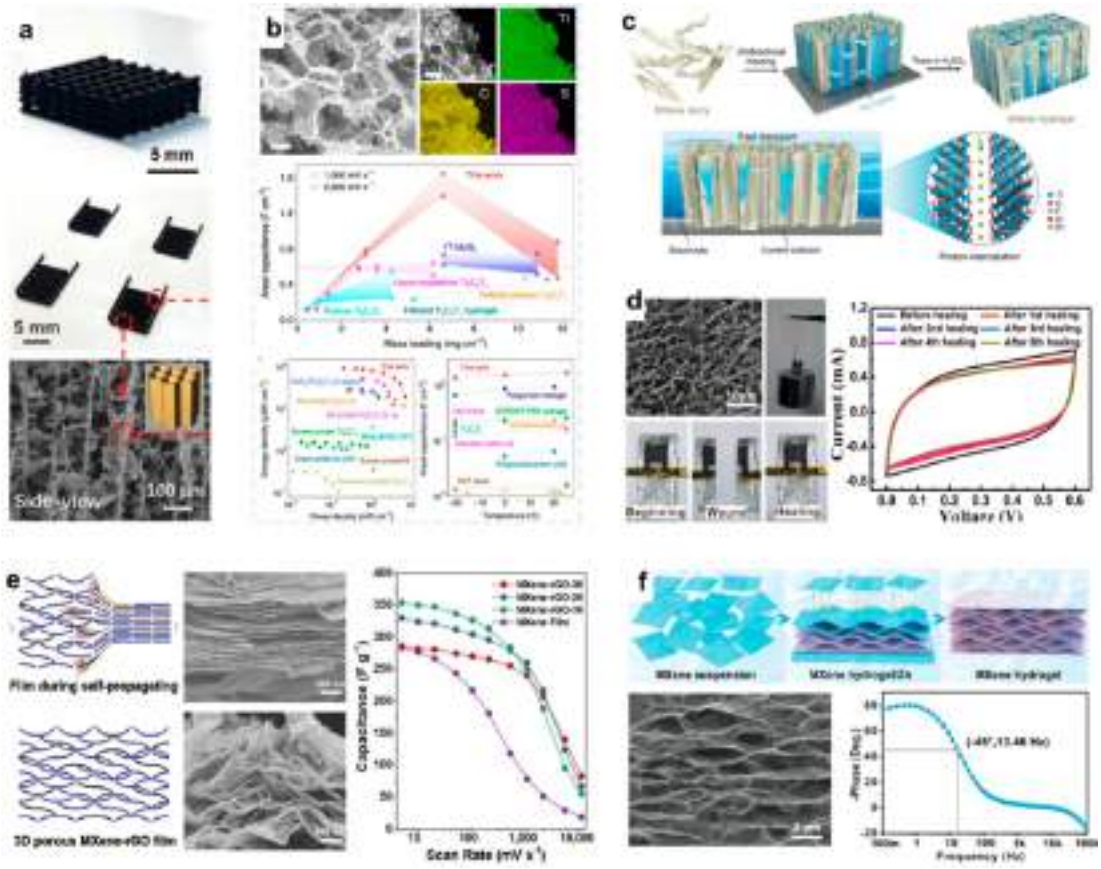

Figure 11. MXene MSCs based on 3D MXene structure. (a) 3D printed MXene-AgNW-MnONW-C60 MSCs. Reprinted with permission from ref [179]. Copyright 2020 John Wiley and Sons. (b) 4D printing technology to build MXene hydrogels, including Nb_2CT_x, $Ti_3C_2T_x$, and $Mo_2Ti_2C_3T_x$. Cross-linked MXene hydrogels with high mechanical strength were obtained by 3D printing and thermally stimulated self-assembly processes using PEDOT:PSS as a cross-linker. $Ti_3C_2T_x$ hydrogel MSCs offer ultrahigh areal capacitance and high energy/power density. Reprinted with permission under a Creative Commons CC BY License from ref [171]. Copyright 2022 Springer Nature. (c) Process diagram of unidirectional frozen MXene slurry forming ice templates to construct 3D open MXene structures. Reprinted with permission under a Creative Commons CC BY License from ref [169]. Copyright 2021 John Wiley and Sons. (d) Self-healable MXene−graphene composite aerogel for MSCs, showing good self-healing and electrochemical performance. Reprinted with permission from ref [167]. Copyright 2018 American Chemical Society. (e) Self-propagating fabricated 3D porous MXene-rGO for enhanced capacitance and rate performance of MSCs. Reprinted with permission from ref [178]. Copyright 2021 Elsevier. (f) Formation of 3D MXene films by simultaneous reduction and self-assembly of MXene sheets on the surface of zinc foil. Reprinted with permission from ref [174]. Copyright 2021 John Wiley and Sons.

unique properties that provide opportunities for the development of high-performance MXene-based micro-supercapacitors.

3.3. MXene MSCs Based on 3D Structure. As a typical 2D material, MXene nanosheets tend to undergo restacking during the thin film fabrication process due to the strong interlayer van der Waals forces and hydrogen bonding.[90,163] This decreases the accessibility of electrolyte ions to the active sites on the MXene surface and prolongs ion transport pathways.[164,165] To address this issue, two primary strategies are employed: (i) introducing interlayer spacers into MXene interlayers, such as hexadecyl trimethylammonium bromide (CTAB), carbon nanotubes (CNTs), graphene, *etc.*,[33,47,157,158,166] to enlarge the interlayer spacing of MXene layers and offset their self-stacking tendency; and (ii) transforming the 2D MXene into 3D structures through engineering methods such as 3D printing, template synthesis, electrostatic self-assembly, and mechanical shear, which avoids MXene restacking and increases the accessibility of ions to active sites.[53,68,90,167−170] Earlier we discussed different intercalation confinement engineering techniques. In this context, we mainly focus on the construction of MXene 3D structures and their potential applications in micro-supercapacitors.

In 2019, Yang et al. discovered that $Ti_3C_2T_x$ ink with a concentration of over 50 mg mL^{-1} could effortlessly flow through narrow nozzles and instantly recover its solid behavior during the 3D printing process, resulting in the formation of a 3D MXene network that maintained its filamentous shape after extrusion.[68] Morphological characterization also indicated that singly printed MXene filaments (with an average diameter of about 326 μm) formed stable 3D network structures without overlapping or internal collapse. Subsequently, Li et al. prepared a nanocomposite ink composed of $Ti_3C_2T_x$ MXene nanosheets, manganese dioxide nanowires (MnONWs), silver nanowires (AgNWs), and fullerene (C60), and employed high-resolution 3D printing technology to construct a thick and honeycomb-like porous structure (Figure 11a).[12] The 3D printed MSC achieved an excellent areal capacitance of 216.2 mF cm^{-2} and remained stable after 1000 stretch/release cycles.

https://doi.org/10.1021/acsnano.3c10246
ACS Nano 2024, 18, 4651−4682

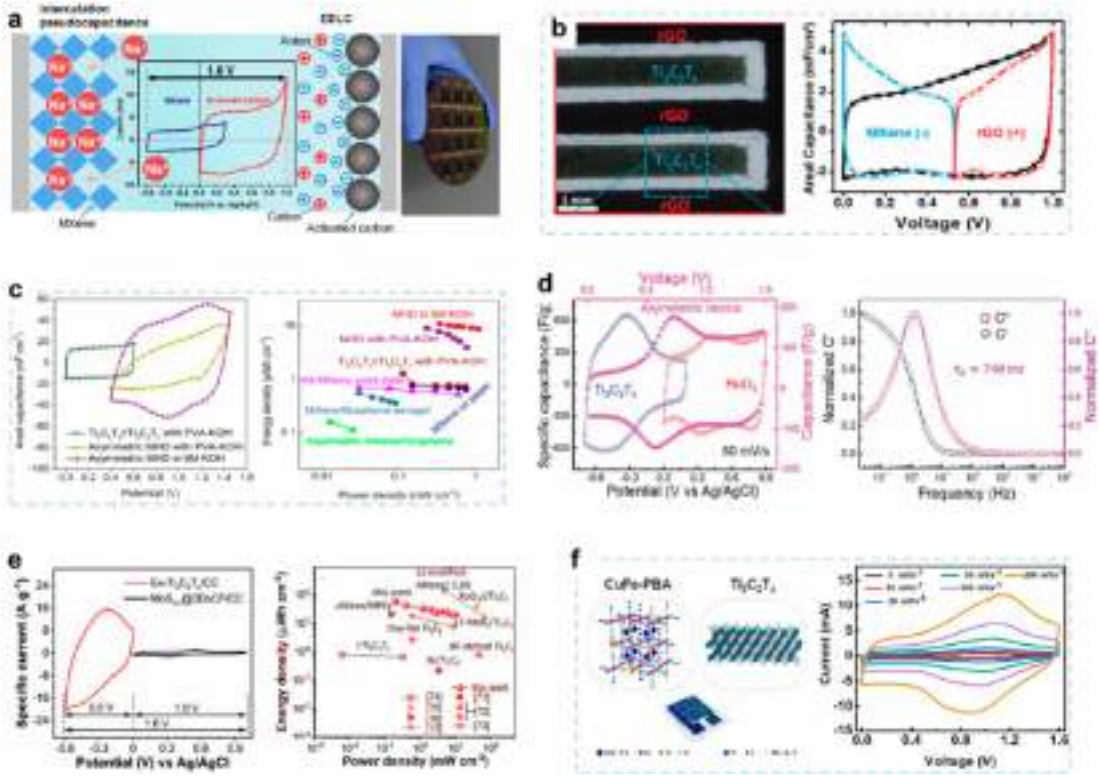

Figure 12. MXene MSCs with asymmetric configuration. (a) Asymmetric MSCs based on MXene negative electrode and activated carbon (AC) positive electrode. Reprinted with permission from ref [184]. Copyright 2020 Elsevier. (b) MXene and graphene constructed asymmetric devices. Reprinted with permission from ref [185]. Copyright 2018 John Wiley and Sons. (c) Two-step screen printing process to fabricate flexible coplanar asymmetric microhybrid devices (MHDs), with $Ti_3C_2T_x$ MXene serving as the negative electrode and Co-Al-LDH serving as the positive electrode. The MHD exhibits a high voltage of 1.45 V and an improved energy density of 10.80 μWh cm^{-2}. Reprinted with permission from ref [143]. Copyright 2018 Elsevier. (d) All pseudocapacitance asymmetric devices combining MXene with RuO_2 cathode, with a voltage window of 1.5 V and a relaxation time constant τ_0 of 740 ms. Reprinted with permission from ref [186]. Copyright 2018 John Wiley and Sons. (e) Transition metal chalcogenide (MoS_{3-x}) coated 3D printed nanocarbon framework (MoS_{3-x}@3DnCF) serving as the positive electrode. The voltage window of the asymmetric device is broadened to 1.6 V, and the energy density reaches 56.94 μWh cm^{-2}. Reprinted with permission from ref [187]. Copyright 2021 John Wiley and Sons. (f) Prussian blue analogue (PBA) as the cathode material for MXene asymmetric MSCs, showing impressive performance, including a wide operating voltage of 1.6 V, high specific capacitance of 198 mF cm^{-2}, and energy density of 34 μWh cm^{-2}. Reprinted with permission under a Creative Commons CC BY License from ref [69]. Copyright 2022 American Chemical Society.

Furthermore, Ke Li et al. proposed a universal 4D printing technology for manufacturing MXene hydrogels, which is applicable to MXenes such as Nb_2CT_x, $Ti_3C_2T_x$, and $Mo_2Ti_2C_3T_x$ (Figure 11b).[171] This 4D printing technology utilized conductive polymer poly(3,4-ethylenedioxythiophene):poly(styrenesulfonate) (PEDOT:PSS) as a cross-linking agent and obtained cross-linked MXene hydrogels with high mechanical strength through a thermo-stimulated self-assembly process. The $Ti_3C_2T_x$ hydrogel MSCs provided aultrahigh areal capacitance of 3.32 F cm^{-2}, high energy/power density (92.88 μWh cm^{-2} and 6.96 mW cm^{-2}), and rate performance independent of mass loading/thickness. While 3D printing technology offers some advantages in constructing 3D MXene electrode structures, it does not yet offer advantages in terms of large-scale production.[90]

Template synthesis is one of the most direct and effective methods for manufacturing 3D porous structures.[172,173] Polystyrene (PS) and poly(methyl methacrylate) (PMMA) spheres are widely used templates for 3D graphene.[174] Likewise, they are also appropriate for building 3D porous MXenes.[165] As a result of interactions between surface hydroxyl groups, MXene nanosheets will spontaneously wrap around the surface of PS spheres, and then a 3D porous MXene framework can be obtained by removing the PS spheres in an argon atmosphere at 450 °C. Furthermore, due to the hydrophilicity of MXene nanosheets, large-pore MXene can be produced by freeze-drying with ice crystals as a template.[169,175] Huang et al. formed an ice template by unidirectionally freezing MXene hydrogels and constructed a 3D MXene structure by thawing in sulfuric acid electrolyte.[169] This method can be extended to fabricated all-MXene micro-supercapacitors with an ultrahigh surface capacitance of 2.0 F cm^{-2} and a high energy density of 0.1 mWh cm^{-2} (Figure 11c). In fact, this ice template assembly method can endow MXene with a macroscopic 3D porous structure, which improves its electrochemical performance. However, its mechanical properties are often unsatisfactory, making it unsuitable as a highly flexible electrode.

In addition, by introducing a gelator to disturb the balance between electrostatic repulsion and van der Waals interactions, 2D MXene nanosheets in solution can be interconnected and assembled into 3D porous structures.[168,176] For instance, graphene oxide (GO), a typical gelator, can be uniformly mixed with MXene nanosheets in water to form a 3D MXene/rGO composite material (Figure 11d).[177] The MSCs based on

https://doi.org/10.1021/acsnano.3c10246
ACS Nano 2024, 18, 4651−4682

3D MXene-rGO aerogel exhibit a large areal capacitance of 34.6 mF cm^{-2} and an excellent self-healing ability (81.7% capacitance retention after the fifth self-healing) and effectively resist damage under mechanical deformation. Similarly, Miao et al. produced a flexible 3D porous MXene/GO through a self-propagating reduction technique.[178] The self-propagating process released a significant amount of gas instantly within a short period of time (1.25 s), resulting in the formation of a 3D porous framework that enhanced the capacitance and rate performance of the film electrode (Figure 11e). Additionally, Zhao et al. lowered the electrostatic repulsion between MXene sheets by the high reduction of Zn and produced 3D MXene films via simultaneous reduction and self-assembly of MXene sheets on the surface of Zn foil (Figure 11f).[174] Subsequently, by patterning the Zn layer, MXene can spontaneously form 3D interdigital electrodes on the substrate.

Compared to 2D structures, 3D MXene structures typically offer several advantages: (1) Effective inhibition of nanosheet restacking allows for the maintenance of the large specific surface area of MXene nanosheets in 3D structures, exposing numerous electrochemically active sites to the electrolyte and enabling sufficient electrochemical reactions. (2) The abundant channels within the 3D structure facilitate rapid diffusion of electrolyte ions, and the excellent conductivity of MXene enables quick transportation of charge carriers within the porous framework. (3) The rich surface functional groups enable integration with various organic or inorganic materials, creating opportunities for the construction of functional 3D MXene composite structures. Therefore, 3D MXene structures provide a feasible route for the development of high-performance micro-supercapacitors. However, attention still needs to be paid to the stability and mechanical strength of the 3D MXene structure, such as whether the device can recover after extrusion and whether the performance will be affected.

3.4. Asymmetric MXene MSCs with High Operating Voltage. Despite MXene MSCs exhibiting high areal capacitance and power density, most symmetric MXene MSCs have a limited voltage window of 0.6−0.8 V due to the inherent properties of MXene material, which greatly limits their energy density.[31,34,75,180] Therefore, the design of an MXene-based asymmetric structure is important to improve the operating voltage and energy density of MXene MSCs.

Researchers have explored various approaches to construct MXene-based asymmetric micro-supercapacitors.[181−183] Xie et al. designed on-chip asymmetric micro-supercapacitors based on $Ti_3C_2T_x$ MXene and activated carbon on a silicon substrate, which exhibited an areal capacitance of 7.8 mF cm^{-2} in a neutral electrolyte (PVA/Na_2SO_4), with an operating voltage up to 1.6 V (Figure 12a).[184] Similarly, Couly et al. utilized customized masking and spray techniques to produce an asymmetric MXene micro-supercapacitor on a flexible transparent substrate, where $Ti_3C_2T_x$ served as the negative electrode and rGO served as the positive electrode (Figure 12b).[185] The MXene-based asymmetric MSCs can operate at 1 V and maintain 97% capacity retention after 10,000 cycles, but their energy density is only 8.7 mWh cm^{-3}. Although the voltage window of the asymmetric device constructed by combining carbon materials with MXene has been effectively enhanced, its areal capacitance and energy density (<9 mF cm^{-2}, <10 mWh cm^{-3}) have not yet reached the expected levels. This is mainly caused by the limited bilayer capacitance of carbon materials, which makes it difficult to fully utilize the pseudocapacitance performance of MXene and pulls down the areal performance of the whole device. Therefore, it is necessary to find other alternative materials that can maintain the high electrochemical capacity of the MSCs matched with MXene.

To achieve high capacitance while maintaining a high voltage window, pseudocapacitive materials such as metal oxides/sulfides/hydroxides and conductive polymers may be a more ideal choice for constructing asymmetric devices.[55,156,186−189] Xu et al. proposed a simple, cost-effective, and scalable two-step screen printing process to fabricate a flexible coplanar asymmetric microhybrid device (MHD), with $Ti_3C_2T_x$ serving as the negative electrode and Co-Al-LDH (layered double hydroxides) serving as the positive electrode.[143] This screen-printed asymmetric MHD exhibited a wide voltage window (1.45 V), excellent cycling stability (92% capacitance retention after 10,000 cycles), improved energy density (10.80 μWh cm^{-2}), and good mechanical flexibility (Figure 12c). Moreover, this two-step screen-printing method for manufacturing coplanar asymmetric micro-supercapacitors on flexible substrates has important implications for the mass production of MXene-based asymmetric MSCs. RuO_2, MnO_2, and MoS_3 have voltage windows mostly above 0 V and high pseudocapacitance, making them ideal candidates for pairing with MXene (−0.6 to 0 V). For example, an asymmetric device consisting of MXene as the negative electrode and ruthenium oxide (RuO_2) as the positive electrode can operate within a voltage window of 1.5 V, with a relaxation time constant τ_0 of 740 ms, corresponding to excellent rate performance, and an energy density of 37 μWh cm^{-2} (Figure 12d).[186] Similarly, by using a transition metal chalcogenide (MoS_{3-x}) coated 3D printed nanocarbon framework (MoS_{3-x}@3DnCF) as the positive electrode, the voltage window of the asymmetric device is broadened to 1.6 V and the energy density reaches 56.94 μWh cm^{-2} (Figure 12e).[187]

Recently, Prussian blue analogues (PBAs) have been applied as positive electrode materials in MXene asymmetric micro-supercapacitors due to their open and highly stable frameworks which allow for higher loading of active materials, larger contact surface area, and faster ion diffusion within the crystal.[69] The MSCs utilizing CuFe-PBA as the positive electrode and $Ti_3C_2T_x$ as the negative electrode exhibited impressive performance, including a wide operating voltage of 1.6 V, high specific capacitance of 198 mF cm^{-2}, and energy density of 34 μWh cm^{-2}. This effective electrode matching between transition metal analogues of Prussian blue and MXene provides more possibilities for constructing MXene-based asymmetric devices.

On the other hand, metal-ion hybrid supercapacitors consisting of a cathode of battery-type and an anode of capacitor-type have drawn significant attention from researchers due to their ability to achieve high power and energy density simultaneously.[193−199] In 2015, Wang et al. demonstrated the use of Ti_2C MXene as the negative electrode for Na-ion capacitors, achieving a high specific power of 1.4 kW kg^{-1} and energy density of 260 Wh kg^{-1}.[200] However, for sodium-ion capacitors, Ti_2C is not the optimal MXene material. Subsequently, Dall'Agnese et al. applied V_2C MXene as the positive electrode for Na-ion capacitors, achieving a maximum cell voltage of 3.5 V and a capacity of 50 mAh g^{-1}.[105] They also demonstrated the fast intercalation/deintercalation process of Na-ion. These results validate the potential applications of two-dimensional MXene in metal-ion hybrid micro-supercapacitors. For instance, Zheng et al.

https://doi.org/10.1021/acsnano.3c10246
ACS Nano 2024, 18, 4651−4682

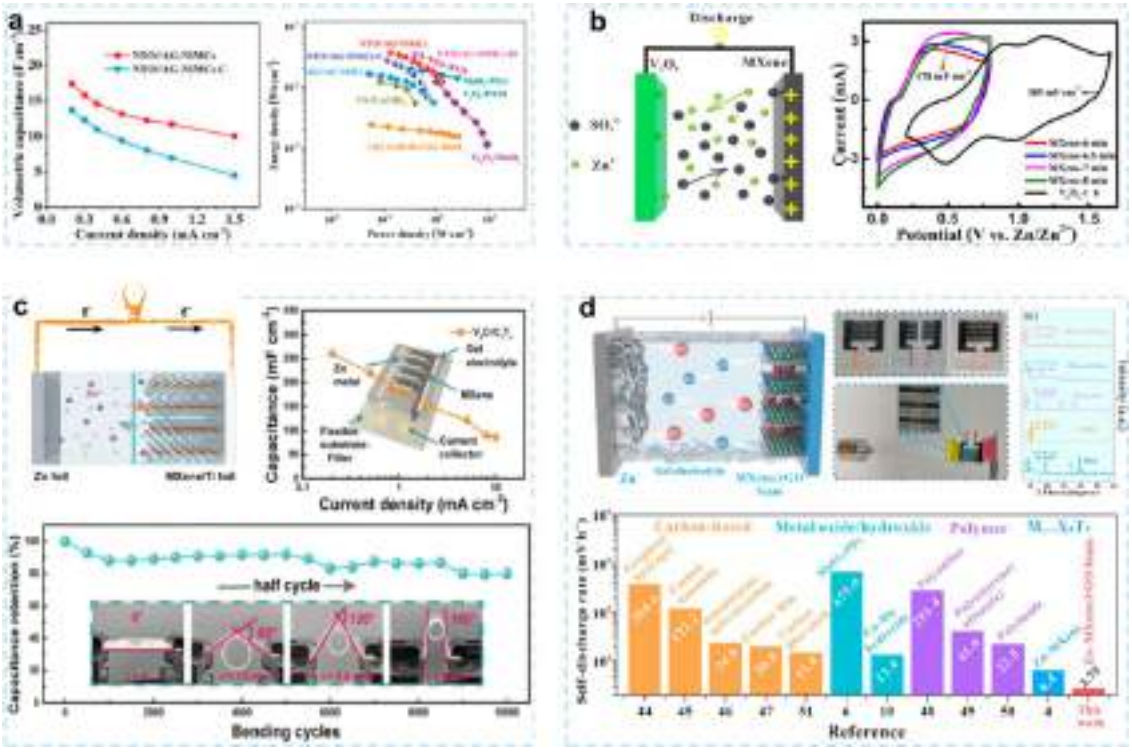

Figure 13. MXene-based metal-ion hybrid MSCs. (a) Sodium ion microcapacitor formed by Ti_3C_2 MXene derived urchin-like sodium titanate (NTO) as the anode and nanoporous active graphene (AG) as the cathode, achieving a high energy density of 37.1 mWh cm^{-3} and power density of 1.2 W cm^{-3}. Reprinted with permission under a Creative Commons CC BY License from ref [190]. Copyright 2019 John Wiley and Sons. (b) Zn-ion hybrid MSCs based on an MXene anode and V_2O_5 cathode with high areal capacitance of 129 mF cm^{-2}. Reprinted with permission from ref [191]. Copyright 2022 Elsevier. (c) Solid solution reinforced $V_3CrC_3T_x$ as anode for Zn-ion MSCs, which showing improved capacitance (1680.2 mF cm^{-2}), high energy density (51.12 mWh cm^{-2}) and good cycling stability (50,000 cycles retains 70.2% of the initial value). Reprinted with permission from ref [192]. Copyright 2022 RSC. (d) 3D MXene/rGO foam fabricated by hydrazine vapor-induced reduction for Zn-ion MSCs. The MXene/rGO//Zn zinc-ion MSC exhibits a large areal capacitance of 83.96 mF cm^{-2}, low self-discharge rate of 2.75 mV h^{-1} and good self-healing ability. Reprinted with permission from ref [56]. Copyright 2022 Elsevier.

employed the simultaneous oxidation and alkalinization of Ti_3C_2 MXene to synthesize urchin-like sodium titanate (NTO) for the anode and combined it with a nanoporous active graphene (AG) cathode to form a sodium ion microcapacitor (NTO//AG-NIMC).[190] The device achieved a high energy density of 37.1 mWh cm^{-3} and an excellent power density of 1.2 W cm^{-3} (Figure 13a).[190] The nonflammable ion gel electrolytes also provide the solid-state device with excellent flexibility and high-temperature resistance of up to 80 °C.

Compared with Li/Na-ion hybrid capacitors, zinc ion capacitors usually employ water-based electrolytes, which have the advantages of low cost, high electrode potential, environmental friendliness, and good safety, making them the most popular research field for building MXene-based hybrid ion supercapacitors.[64,121,191,192,201,202] In 2022, Li et al. designed a zinc-ion hybrid micro-supercapacitor (ZIHMSC) using $Ti_3C_2T_x$ MXene as the capacitor-type anode and V_2O_5 as the battery-type cathode (Figure 13b).[191] This device exhibited excellent electrochemical performance, including a high voltage window (1.65 V), high areal capacitance (129 mF cm^{-2}), and high energy density (48.9 μWh cm^{-2}). Similarly, Wang et al. used solid solution reinforced $V_3CrC_3T_x$ as the anode material for their zinc-ion micro-supercapacitor (Figure 13c).[192] By partially replacing Cr atoms with V atoms in $V_4C_3T_x$, they were able to increase the interlayer spacing of MXene, improve Zn-ion adsorption and promote ion diffusion, thus improving the capacitance (1680.2 mF cm^{-2}), discharge potential (from 1.25 to 1.30 V), energy density (51.12 mWh cm^{-2}) and cycling stability (50,000 cycles retains 70.2% of the initial value). This also illustrates the enhancing effect of double M or multiple M MXenes on the electrochemical performance of MXene-based ZIHMSCs.

Moreover, designing 3D MXene structures has been proven as an effective approach for enhancing the performance of ion hybrid micro-supercapacitor.[56,140,199,203,204] Zhang et al. fabricated MXene/rGO foam by hydrazine vapor-induced reduction, which had a controllable pore size and porosity of up to 77.9% (Figure 13d).[56] This 3D MXene/rGO foam formed a continuous ion pathway, ensuring sufficient electrolyte permeation, accelerating electrochemical reaction kinetics, and significantly improving Zn-ion storage performance, including rate performance and cycling stability. The MXene/rGO//Zn zinc-ion micro-supercapacitor exhibited a large area-specific capacitance of 83.96 mF cm^{-2}, good self-discharge resistance (self-discharge rate of 2.75 mV h^{-1}) and self-healing ability, making it suitable for providing energy for self-powered integrated pressure sensing systems.[56] However, due to the limitations of water-based electrolytes, the operating voltage of the above-mentioned zinc-ion hybrid MSC is relatively low (<2 V), limiting the further increase of energy density.

Despite the effective expansion of the operating voltage and improvement in energy density of MXene MSCs achieved through the design of asymmetric structures, there are still

https://doi.org/10.1021/acsnano.3c10246
ACS Nano 2024, 18, 4651−4682

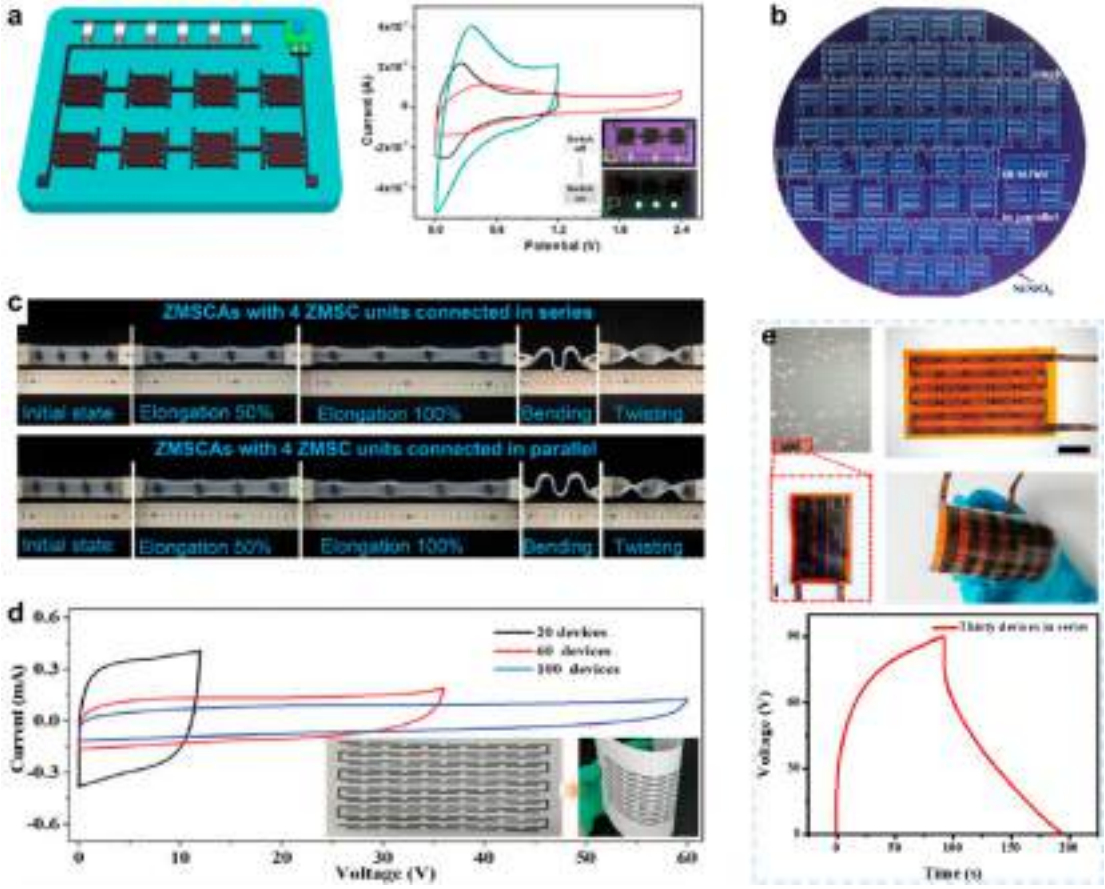

Figure 14. Series and parallel integration of MXene MSCs. (a, b) High-conductivity MXene serves as a conductive path between MXene MSCs in series and parallel. Reprinted with permission from ref [70]. Copyright 2020 Elsevier. Reprinted with permission from ref [93]. Copyright 2022 American Chemical Society. (c) Liquid metal bridge/island (LMBI) interconnect structures are used for series-parallel connection of stretchable Zn-ion MSCs, thus maintaining the electrochemical stability and mechanical robustness of the microdevice under different deformations. Reprinted with permission from ref [30]. Copyright 2021 Elsevier. (d) Screen-printing of 100 tandem linear MXene MSCs to reach an operating voltage of 60 V. Reprinted with permission from ref [57]. Copyright 2021 John Wiley and Sons. (e) Series connection of 30 MSCs based on ionic liquid wrapped MXene film to achieve 90 V output voltage. Reprinted with permission from ref [59]. Copyright 2023 Springer Nature.

many challenges that remain. These include criteria for selecting electrode materials that are compatible with MXene, balancing high energy and high power, and addressing stability issues in ion hybrid micro-supercapacitors. Due to the complexity of in-plane asymmetric structures, large-scale manufacturing remains a major obstacle to the industrial development of MXene asymmetric MSCs, and this is where subsequent researchers need to pay more attention.

4. INTEGRATED SYSTEM WITH MXENE MSCS

With the development of high-performance materials and miniaturization of electronic devices, people are eager to integrate micro-supercapacitors into microdevices with various functions to achieve integrated multifunctional systems.[86,205,206] These micro-integrated systems can be self-powered through intermittent energy harvesting units such as solar cells and nanogenerators, be stored by MXene MSCs, and respond to external stimuli such as voltage, mechanical deformation, temperature, and light.[127,207−210] It is worth noting that the AC output generated by these units may not directly charge the MSC and requires a rectification unit to convert AC to DC for obtaining a constant voltage or current signal.[57,60] Currently, the focus of MXene MSCs is primarily on manufacturing technology and electrode material optimization, with less attention paid to integration. However, the multifunctional energy integration of MXene-based micro-supercapacitors is also a key driving force for promoting the industrialization. Integration compatibility mainly includes process compatibility, power matching, function matching, *etc.*, for example, the integrated processing on silicon substrate, the voltage/current provided by the capacitor needed for the back-end device, and the functions needed for the system to be integrated.

4.1. Self-Powered Integrated Systems. To meet the diverse requirements of various application scenarios, it is necessary to connect MXene MSCs in series or parallel to achieve higher output voltages or greater energy storage capacity.[206,209] As shown in Figures 14a−b, high-conductivity MXene is often served as a conductive path between MXene MSCs in series and parallel.[70,93] This improves compatibility between microdevices and eliminates the increase in contact resistance that can be caused by other current collectors. MXene as a conductive path also avoids the requirement for external wire connections, thus increasing the area density of the integrated system and facilitating the integrated processing. Also, it is important to ensure that the electrolytes of each

https://doi.org/10.1021/acsnano.3c10246
ACS Nano 2024, 18, 4651−4682

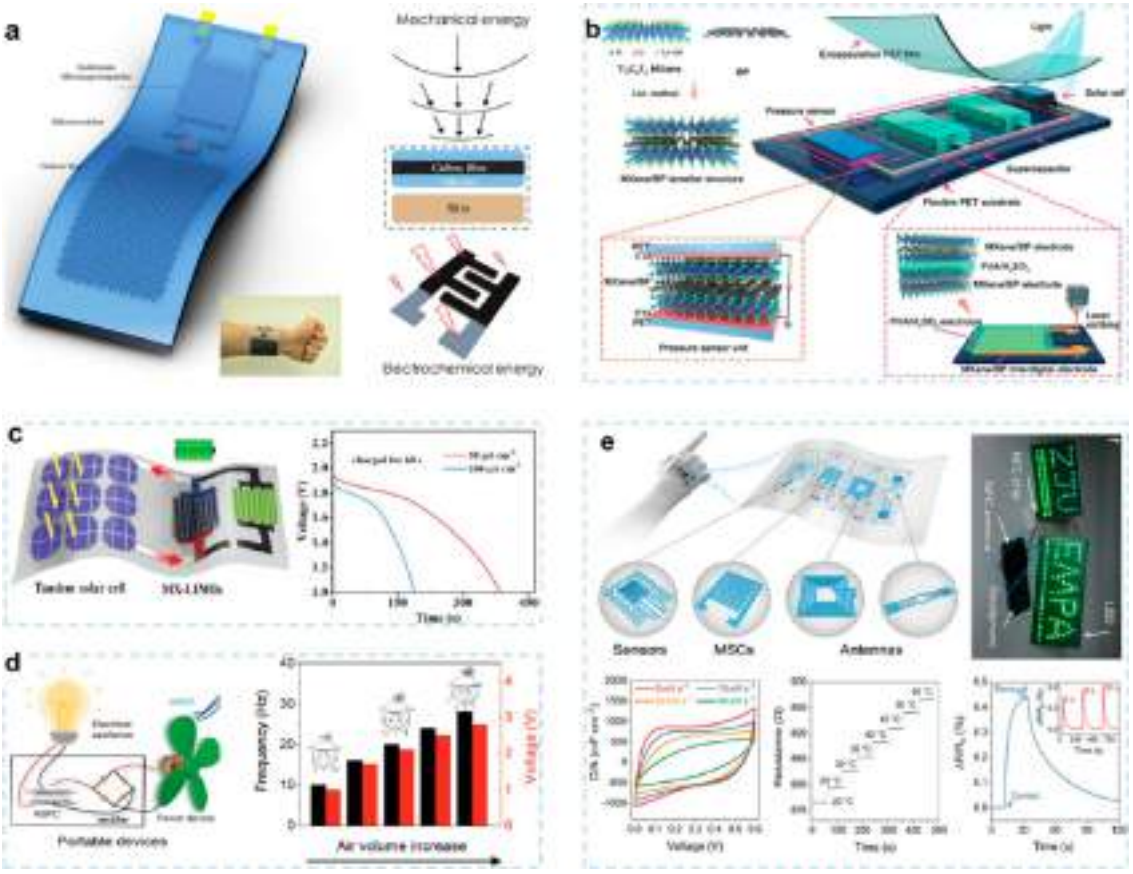

Figure 15. Integration of MXene MSCs with energy harvesting devices. (a) MXene MSCs integrated with triboelectric nanogenerator for a wearable self-powered system. Reprinted with permission from ref [213]. Copyright 2018 Elsevier. (b) Integration of solar cells, direct laser-writing MSCs and flexible pressure sensors to produce a self-powered smart sensor system based on MXene/black phosphorus (BP). Reprinted with permission from ref [48]. Copyright 2021 John Wiley and Sons. (c) Tandem solar cells, MXene-LIMB and MXene hydrogel pressure sensors integrated by screen-printing technology to create a flexible self-powered integrated system. The Si-SC charging circuit reaches an output voltage of 2.2 V in 60 s, and MXene-LIMB can discharge at a constant current of 50 and 100 μA cm^{-2} for 390 and 180 s. Reprinted with permission from ref [57]. Copyright 2021 John Wiley and Sons. (d) Wind power drives asymmetric MSCs consisting of VMG and PEDOT. The integrated system can convert AC wind signals into DC signals and store the collected energy in MSCs. Reprinted with permission from ref [61]. Copyright 2022 John Wiley and Sons. (e) Room-temperature direct printing of MXene inks for wireless charging, energy storage and sensing in one flexible integrated system. The sensing module exhibits positive temperature coefficient behavior, enabling it to quickly respond to temperature changes. Reprinted with permission under a Creative Commons CC BY License from ref [60]. Copyright 2022 Springer Nature.

device in the MXene MSC array are isolated from each other to avoid any effect on the actual voltage that can be achieved through series connection.[93] And for stretchable devices, the liquid metal bridge/island (LMBI) interconnection structure enables a separation of mechanical and electrochemical properties, resulting in the maintenance of electrochemical stability and mechanical robustness of microdevices under different deformations, as shown in Figure 14c.[30] Moreover, for microelectronic device integration systems with higher voltage requirements, high voltages can be obtained by connecting more MXene MSCs in series.[46,59,202] An example is the 60 V operating voltage achieved by screen-printing 100 connecting MXene MSCs (Figure 14d).[57] And Zhu et al. fabricated an MSC array consisting of 30 MSC units connected in series on a polyimide tape, which can achieve a high output voltage of 90 V, as illustrated in Figure 14e.[59] In the integration of high-density MXene MSCs, the homogeneity of the device proved to be critical to the stability of the output voltage, highlighting the advantages of solution-based printing methods in building integrated functional systems.

Currently, the main energy harvesting devices that can be integrated with MXene MSCs are nanogenerators, solar cells, and wireless charging (Figure 15).[46,48,60,61,211−213] Frictional electric supercapacitors are a type of self-powered device that can efficiently store electrical energy by converting mechanical energy from the surrounding environment to meet the potential needs of micro and wearable electronics. For instance, Jiang et al. integrated an MXene-based micro-supercapacitor with a skin-touching frictional triboelectric nanogenerator (TENG) to develop a self-charging device (Figure 15a).[213] But even at a motion frequency of 5 Hz, it still takes about 30 min to charge the supercapacitor to 0.6 V. In fact, although nanogenerators can convert biomechanical motion into electrochemical energy and store it, its lower energy conversion efficiency still needs to be further verified for practical applications.

Solar cells and wind power are commonly used energy supply methods for MXene integrated systems.[46,48,57,61] Zhang et al. integrated flexible pressure sensors with laser-writing MSCs and solar cells to design a self-powered intelligent sensor

https://doi.org/10.1021/acsnano.3c10246
ACS Nano 2024, 18, 4651−4682

Table 3. Summary of Key Performance and Integration Applications of MXene-Based MSCs[a]

Solution processing method	Ink composition	Electrochemical performance	Applications	Ref
Direct laser machining	MXene/BP hybrid ink	Potential window: 0.8 V Capacitance: 896.8 F cm^{-3} Energy density: 15.9 μWh cm^{-2}	Self-powered smart sensor system	48
Screen printing	MXene-LTO and MXene-LFP; 100 mg mL^{-1}	Potential window: 0.6 V Capacitance: 1108 mF cm^{-2} Energy density: 13.8 μWh cm^{-2}	Self-powered pressure sensing system	57
Extrusion printing	MXene aqueous inks (60 mg mL^{-1})	Potential window: 0.6 V Capacitance: 900 mF cm^{-2} Energy density: 9.7 μWh cm^{-2}	Wireless sensing electronics	60
Screen printing	$Ti_3C_2T_x$/NMP; Co-Al-LDH/NMP	Potential window: 1.45 V Capacitance: 28.5 mF cm^{-2} Energy density: 8.84 μWh cm^{-2}	Force sensor	143
Inkjet printing	MXene/PH1000; 30 mg mL^{-1}	Potential window: 0.6 V Capacitance: 754 F cm^{-3} Energy density: 9.4 mWh cm^{-3}	Temperature monitor	133
Spraying method	$Ti_3C_2T_x$–LiCl	Potential window: 1.3 V Capacitance: 802.3 F cm^{-3} Energy density: 188 μWh cm^{-3}	Pressure sensor	64
Laser engraving	MXene and GO aqueous solution	Potential window: 1.35 V Capacitance: 83.96 mF cm^{-2} Energy density: 21.3 μWh cm^{-2}	Pressure sensing system	56
Laser scribing	MXene aqueous inks	Potential window: 1.2 V Capacitance: 84.07 mF cm^{-2} Energy density: 16.8 μWh cm^{-2}	Photodetector	63
Mask-assisted filtration	Mn ions-introduced $Ti_3C_2T_x$ suspension	Potential window: 1.0 V Capacitance: 87 mF cm^{-2} Energy density: 11.8 mWh cm^{-3}	Electromagnetic interference shielding	96
Electrochemical polymerization	MXene; PEDOT aqueous solution	Potential window: 0.6 V Areal capacitance: 2.7 mF cm^{-2} Energy density: 8.7 mWh cm^{-3}	Electrochromic	216
Spray coating	MXene aqueous solution	Potential window: 0.6 V Capacitance: 0.5 mF cm^{-2} Relaxation time constant: 0.45 ms	AC-line filtering	214
Vacuum filtration	MXene aqueous solution	Potential window: 1.0 V Capacitance: 8 mF cm^{-2} Capacity maintenance of 75% at 120 Hz	Filter/oscillator	207

[a]Note: BP, black phosphorus; LTO, lithium titanate; LFP, lithium iron phosphate; Co-Al-LDH, Co-Al layered double hydroxide; NMP, *N*-methyl-2-pyrrolidone; GO, graphene oxide; PEDOT, poly(3,4-ethylenedioxythiophene).

system based on MXene/black phosphorus (BP) (Figure 15b).[48] The solar cell can increase the open-circuit potential of the micro-supercapacitor to 1.61 V within 76 s. This self-powered intelligent sensor system can be used for real-time human pulse wave measurement, showing high detection sensitivity (77.61 kPa^{-1}) and fast response/recovery time (10.9/12.9 ms). Similarly, Zheng et al. employed screen-printing technology to seamlessly integrate tandem solar cells, MXene-LIMB, and MXene hydrogel pressure sensors to build a fully flexible self-powered integrated system on a single substrate.[57] The Si-SC charging circuit reaches an output voltage of 2.2 V in 60 s, and MXene-LIMB can discharge at a constant current of 50 and 100 μA cm^{-2} for 390 and 180 s, respectively (Figure 15c). Figure 15d shows an integrated system powered by wind.[61] The integrated system can convert AC wind signals into DC signals and store the collected energy in MSCs. The capacitor section is an asymmetric structure composed of VMG (vertically oriented MXene and reduced graphene oxide composite) and PEDOT, with a voltage of 1.4 V and areal energy density of 805 mF V^2 cm^{-2}, and exhibits excellent filtering performance. However, these two types of energy collection devices have relatively high environmental requirements and limited applicable scenarios. They also suffer from the problem of low energy conversion efficiency

Additionally, wireless charging provides a low-wear, low-risk, and convenient energy supply method.[14,60,63] In 2022, Shao et al. utilized additive-free aqueous MXene ink to enable the direct printing of flexible wireless electronic products at room temperature, thus efficiently manufacturing flexible systems for energy collection, wireless communication, and sensing (Figure 15e).[60] The self-powered wireless system employs the electromagnetic conversion process to charge MXene MSCs, resulting in an energy conversion efficiency of approximately 70%. The sensing module exhibits positive temperature coefficient behavior (with a sensitivity of about 0.066% $°C^{-1}$), enabling it to quickly respond to temperature changes. Additionally, Duan et al. developed a fully integrated system using MXene on a small area of only 1.78 cm^2 via a one-step laser scribing method.[63] The system incorporates an integrated wireless charging coil, micro-supercapacitor, and

https://doi.org/10.1021/acsnano.3c10246
ACS Nano 2024, 18, 4651−4682

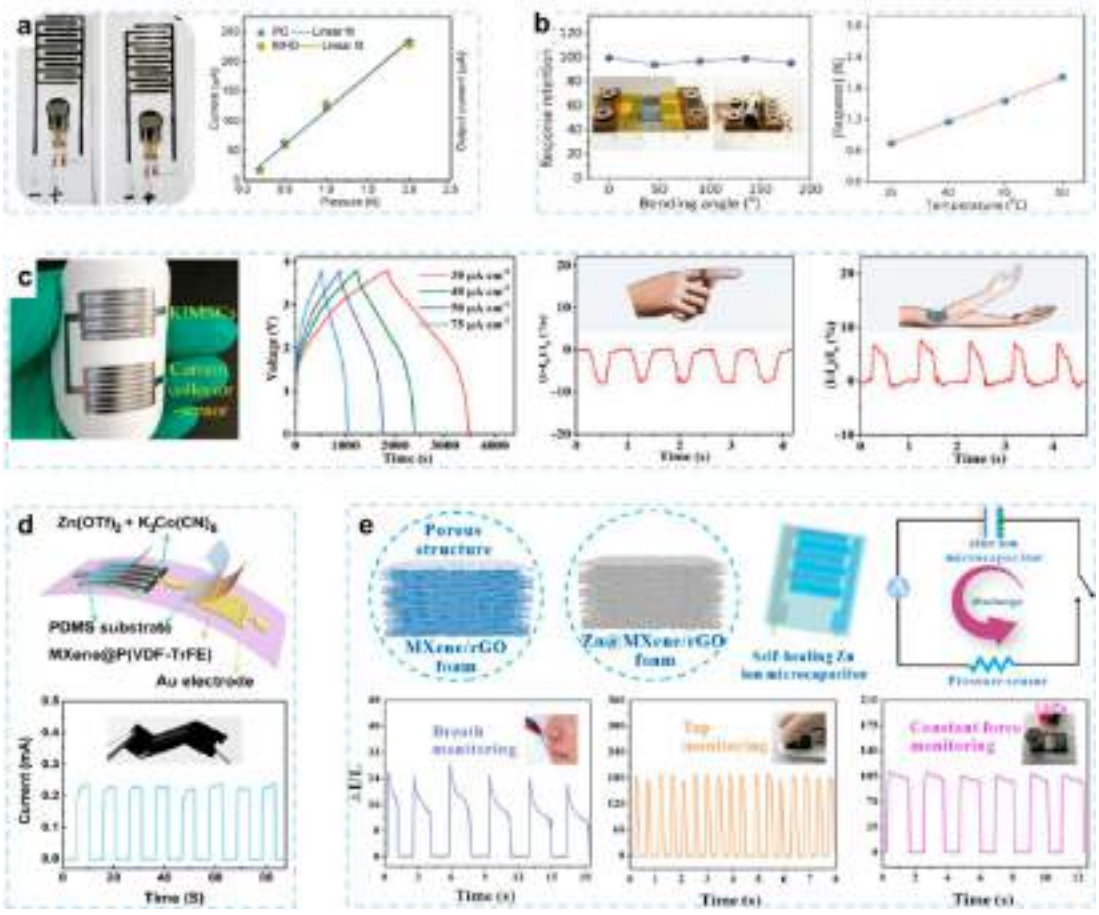

Figure 16. Integration of MXene MSCs with microsensors. (a) Screen-printed asymmetric MSCs based on MXene and layered double hydroxide electrodes to power force sensors. The response current of the sensor is proportional to the force applied to the active surface area. Reprinted with permission from ref [143]. Copyright 2018 Elsevier. (b) Direct inkjet-printing of MP-MSC and thermal sensors utilizing aqueous MXene/PH1000 (MP) inks. The self-powered sensing system shows excellent flexibility, and the current response increases linearly with temperature. Reprinted with permission from ref [46]. Copyright 2021 John Wiley and Sons. (c) Potassium-ion micro-supercapacitors (KIMSCs) based on an MXene-derived potassium titanate (KTO) nanorod anode and porous activated graphene (AG) cathode to power the wearable pressure sensor system. This integrated sensor system demonstrated considerable sensitivity in detecting body movements such as finger joints and elbows, as well as bending monitoring. Reprinted with permission from ref [210]. Copyright 2021 John Wiley and Sons. (d) In-plane integration of MXene-based Zn-ion MSCs with $Ti_3C_2T_x$−DMF@P(VDF−TrFE) pressure sensor. The MSCs provided stable energy for the pressure sensor, achieving a fast and stable response to different mass loads. Reprinted with permission from ref [64]. Copyright 2023 RSC. (e) Zn-ion microcapacitor (ZIMC) and pressure sensor simultaneously constructed with 3D porous MXene/rGO foam. The integrated system exhibited excellent performance in detecting small deformations and human physiology. Reprinted with permission from ref [56]. Copyright 2022 Elsevier.

optoelectronic detector, all composed of $Ti_3C_2T_x$ MXene and connected by highly conductive MXene wires without the need for additional welding or assembly operations.

The majority of these energy harvesting devices above collect intermittent AC signals and need to be integrated with rectifier units for stable charging of MSC. Circuit optimizations are often necessary to improve the overall energy collection and conversion efficiency of the integrated system. In summary, the integration of MXene-based micro energy storage devices with energy harvesters is an interesting and meaningful direction. However, at present, integration of the two is still in the laboratory stage, and the manufacture of truly practical self-powered systems is still in its early stages.

4.2. Integration of MXene MSCs with Other Functional Devices. Currently, the integration of MXene MSCs is mainly reflected in microsensing, filtering, photoelectric detection, and electromagnetic shielding.[14,62,137,214,215] Different applications require different performance levels from the MXene MSCs module, including voltage, current, power, and energy, among others, as shown in Table 3.

Portable and wearable sensors are widely applied in monitoring personal health and environment, and integrating them with MSCs can eliminate the need for external power sources, reduce overall volume, and improve flexibility, which is currently the primary development trend.[217,218] With this motivation, MXene MSCs have been extensively used to integrate with miniaturized sensor systems, including gas sensors, strain sensors, temperature sensors, and photodetectors.[137,143,208,210,215] Figure 16a illustrates one of the simplest systems for integrating MXene MSCs with miniaturized force sensors.[143] The asymmetric MXene MSCs can provide a voltage of 1.4 V and maintain it at 1.0 V after 1000 s, which is sufficient to drive the force sensor as a power source. The response current of the sensor is proportional to the force applied to the active surface area, proving the feasibility of using an asymmetric device as an alternative energy unit to

https://doi.org/10.1021/acsnano.3c10246
ACS Nano 2024, 18, 4651−4682

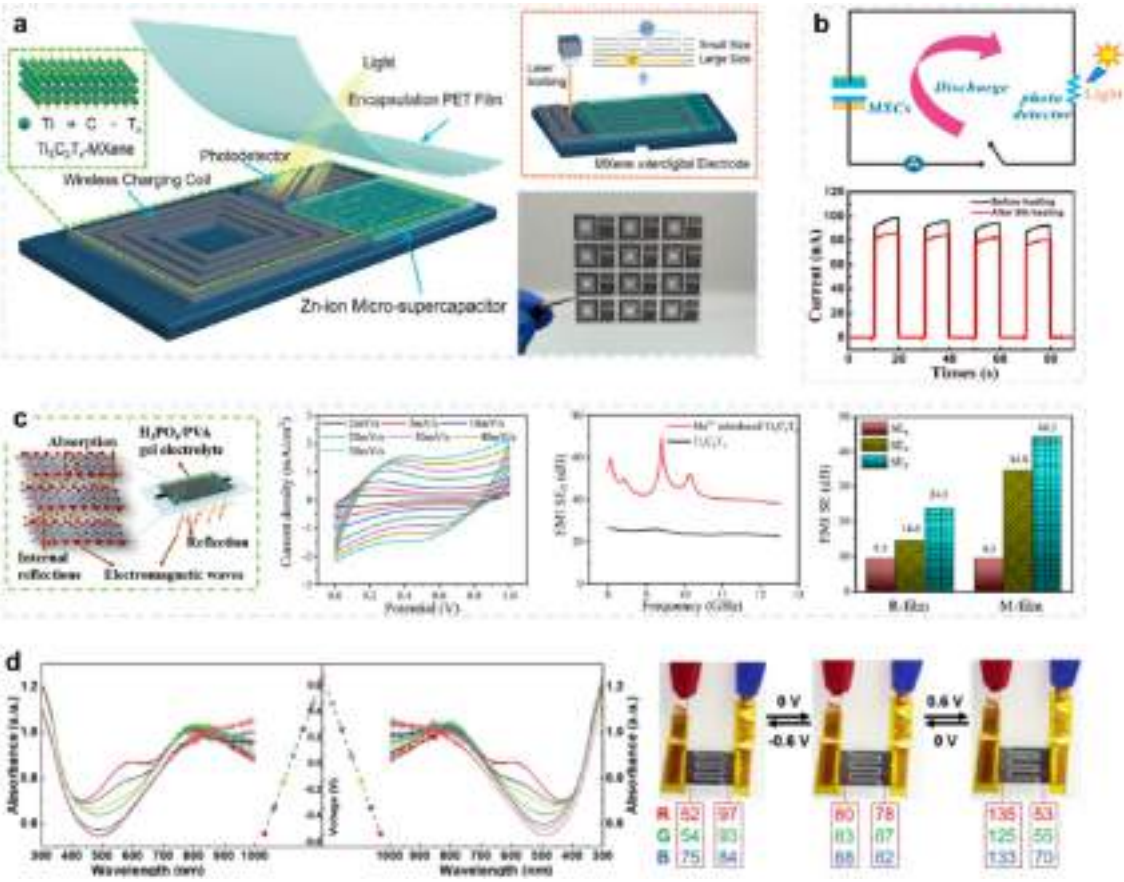

Figure 17. Integration of MXene MSCs with other functional devices. (a) Schematic and physical photos of all-MXene-based integrated system, including wireless charging coil, MSCs and photodetector. Reprinted with permission from ref [63]. Copyright 2023 John Wiley and Sons. (b) Integration of MSCs based on 3D MXene-rGO composite aerogels with photodetector. This 3D MSC has an areal capacitance of 34.6 mF cm^{-2} and can still drive the photodetector stably after the fifth self-healing. Reprinted with permission from ref [167]. Copyright 2018 American Chemical Society. (c) Flexible MXene MSC with electromagnetic interference (EMI) shielding. The multifunctional MSC exhibits a high surface capacitance of 87 mF cm^{-2}, an energy density of 11.8 mWh cm^{-3}, and an outstanding shielding effect of 44 dB. Reprinted with permission from ref [120]. Copyright 2020 Elsevier. (d) MXene-PEDOT electrochromic MSCs. The devices demonstrate significant electrochromic behavior with bleaching and coloring times of 6.4 and 5.5 s, respectively, over the voltage range of −0.6 to 0.6 V. Reprinted with permission from ref [216]. Copyright 2019 Elsevier.

drive force sensors. Similarly, Ma et al. designed an aqueous MXene/poly(3,4-ethylenedioxythiophene):poly-(styrenesulfonate) (MP) ink, for direct inkjet printing of MP-MSCs and thermosensitive sensors (TSs).[46] A TS shows stable response and mechanical durability under infrared irradiation, and the current response linearly increases with temperature, reaching a maximum response value of ∼2.0% at 50 °C (Figure 16b).

Metal-ion hybrid capacitors based on MXene are a reliable option for constructing integrated sensing systems due to their ability to operate at higher voltage windows compared to aqueous electrolyte devices.[191,201] For example, Zheng et al. constructed potassium ion micro-supercapacitors (KIMSCs) by applying MXene-derived potassium titanate (KTO) nanorod anodes and porous active graphene (AG) cathodes to power a sensitive integrated pressure sensing system (Figure 16c).[210] This integrated sensor system demonstrated considerable sensitivity in detecting body movements such as finger joints and elbows, as well as bending monitoring. Also, the pressure sensor made of a graphene-conductive hydrogel even showed the ability to self-heal quickly. In a similar study, Liu et al. designed the in-plane integration of an MXene-based Zn-ion micro-supercapacitor with a $Ti_3C_2T_x$−DMF@P(VDF−TrFE) pressure sensor (Figure 16d).[64] By adding $K_3Co(CN)_6$ to the $Zn(CF_3SO_3)_2$ electrolyte, the rate performance and cycling stability of Zn-ion hybrid MSCs were considerably improved. The stable energy source provided stable energy for the pressure sensor, achieving a fast and stable response to different mass loads.

In the integrated system described above, different materials were adopted for the MSC and sensors, requiring separate processing before integration. In fact, MXene's metallic conductivity, tunable layer spacing and controlled surface chemistry have shown great potential for applications such as pressure and humidity sensors, promoting the simultaneous fabrication of MXene MSCs and MXene sensors.[65,215] In 2020, Wei et al. designed an RGO/CNFs/Ti_3C_2 composite paper after the conch shell structure, which can be used for both pressure/temperature/light multisensing units and flexible micro-supercapacitor (MSC) electrodes.[208] This integrated device achieved appropriate electrochemical capacitance (148.25 F cm^{-3}) and reliable response to stimuli. It can identify users and monitor vital signs by detecting different signal stimuli, such as motion, pulse, sound, and signatures. Furthermore, Zhang et al. employed 3D porous MXene/rGO foam to simultaneously construct the multifunctional Zn-ion

https://doi.org/10.1021/acsnano.3c10246
ACS Nano 2024, 18, 4651−4682

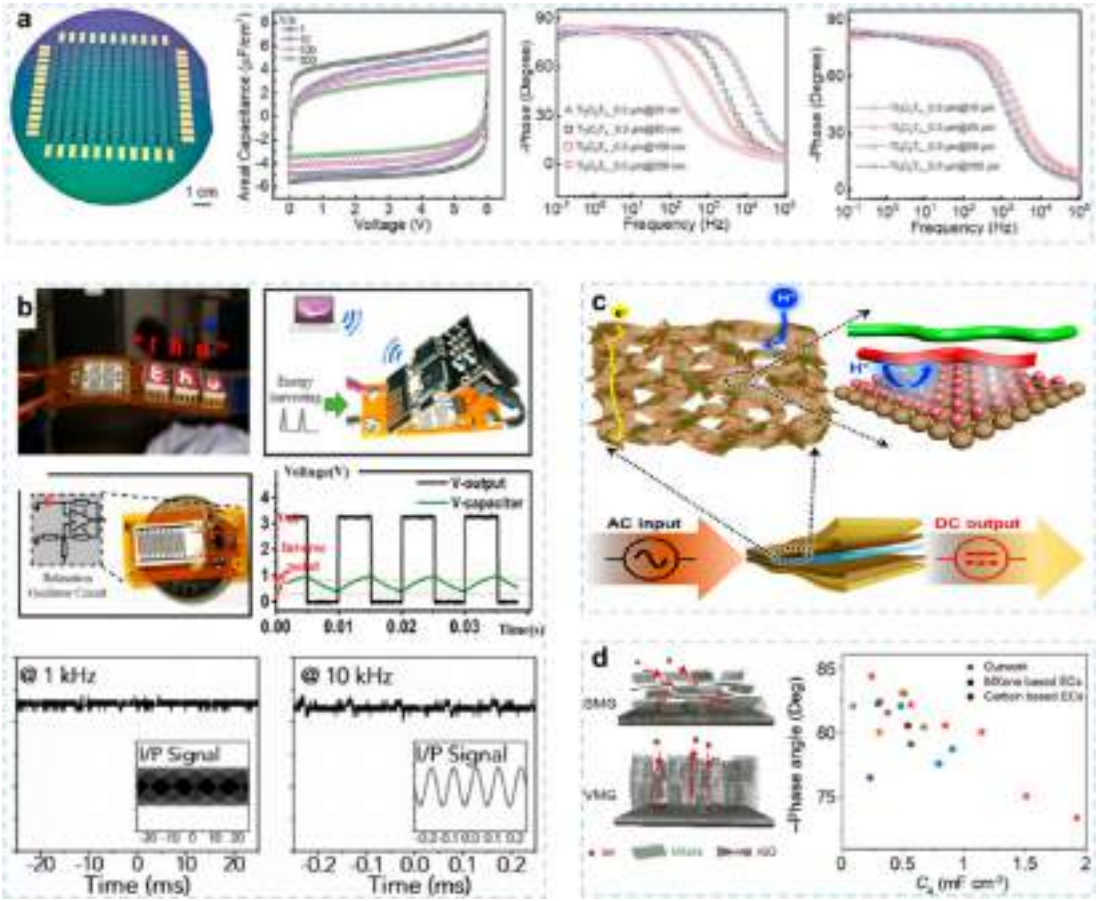

Figure 18. MXene MSCs for AC filtering applications. (a) Wafer-scale micro-supercapacitors offer superior frequency filtering performance by controlling the lateral size of MXene flakes. MXene MSCs exhibit a high volumetric capacitance (30 F cm^{-3} at 120 Hz), high-rate performance (300 V s^{-1}), and relaxation time constant (τ_0) lower than conventional electrolytic capacitors (from 0.45 to 0.8 ms). Reprinted with permission from ref [214]. Copyright 2019 John Wiley and Sons. (b) MXene/MWCNT-based high-frequency MSCs for filter/oscillator. The MSCs display a high areal capacitance of 6 mF cm^{-2} at 120 Hz, providing excellent performance in both low-pass filter circuits and relaxation oscillator circuits. Reprinted with permission from ref [207]. Copyright 2019 Elsevier. (c) Porous MXene/PEDOT:PSS hybrids for flexible AC filtering symmetric electrochemical capacitors. Reprinted with permission from ref [158]. Copyright 2019 Elsevier. (d) Vertical-oriented MXene and reduced graphene oxide composite (VMG) electrodes by electrochemical codeposition for AC filtering. The MSCs maintain a phase angle of 80° at 120 Hz. Reprinted with permission from ref [61]. Copyright 2022 John Wiley and Sons.

microcapacitor (ZIMC) and pressure sensor. This integrated pressure sensing system exhibited excellent performance in detecting small deformations and human physiology, as shown in Figure 16e.[56]

In addition, there has been relevant research on the integration of MXene MSCs with photodetectors.[62,219,220] Duan et al. designed an all-MXene based integrated system, including the wireless charging coil, MSC, and photodetector (Figure 17a). The MXene MSC can maintain a voltage above 0.8 V for more than 4000 s after full charging, which is sufficient to drive the photodetector for an extended period.[63] The performance of the integrated system was comparable to the 0.95 V external power supply driven system and could achieve a rapid response to 808 nm light stimulation. Zhang et al. also achieved similar integration results using 3D MXene MSCs (Figure 17b).[167] They proposed a simple ice-templating method to manufacture 3D MXene-rGO composite aerogels and further prepared a self-healing 3D MSC based on this. The MSC has an areal capacitance of 34.6 mF cm^{-2} and maintains 81.7% of its specific capacitance after the fifth self-healing process, which can stably drive photodetectors.

In addition to applications integrating with sensors, the high electromagnetic (EM) wave reflectivity and low mid-infrared emissivity resulting from the high conductivity make MXene MSCs perform well in the field of electromagnetic shielding and electrochromic fields.[62,120,216,221] Feng et al. designed a flexible MXene MSC with an electromagnetic interference (EMI) shielding function based on Mn ion-intercalated $Ti_3C_2T_x$ MXene (Figure 17c).[120] The incorporation of transition metal Mn^{2+} ions effectively enhances the energy storage and EM waves absorption in EMI shielding. This multifunctional MSC exhibits a high surface capacitance of 87 mF cm^{-2}, an energy density of 11.8 mWh cm^{-3}, and an outstanding shielding effect of 44 dB. For electrochromic, Yury Gogotsi's group developed a titanium carbide-poly(3,4-ethylenedioxythiophene) (PEDOT) heterostructure by electrochemical deposition and combined it with an automated scalpel technique to obtain MXene-PEDOT electrochromic MSCs (Figure 17d).[216] The hybrid MSC exhibited a 5-fold increase in areal capacitance (from 455 to 2.4 mF cm^{-2}) and higher rate capabilities. More importantly, the PEDOT/$Ti_3C_2T_x$ MSCs demonstrate significant electrochromic behavior with bleaching and coloring times of 6.4 and 5.5 s,

https://doi.org/10.1021/acsnano.3c10246
ACS Nano 2024, 18, 4651−4682

respectively, over the voltage range of −0.6 to 0.6 V, showing great potential for visual energy storage.

Besides, for wearable electronics, integrating printed MSCs may suffer from mechanical damage that can cause electrochemical performance degradation or even collapse.[167,222] Therefore, self-healing MXene MSCs are an effective strategy to address such issues, which is an important research direction mentioned previously.

4.3. MXene MSCs for AC Filtering Applications. The open structure of an in-plane interdigital electrode provides MSCs with fast ion transport capability, which makes them viable miniaturization alternatives for large electrolytic capacitors in alternating current (AC) line circuit filtering applications.[223,224] In filtering applications, especially in full wave rectification (120 Hz AC) waveforms, the RC time constant of the capacitor should be less than 8.3 ms, which means that the phase angle and frequency response of the capacitor should remain close to −90° up to 120 Hz frequency.[61,207,225] Due to the unique 2D morphology of MXene that forms ion channels between layers, its metallic conductivity (8,000−10,000 S cm^{-1}), and rapid surface redox reactions, MXene MSCs often exhibit exceptional rate and power performance, which are critical for AC line circuit filtering.[27]

In 2019, Jiang et al. achieved wafer-scale micro-supercapacitors with superior frequency filtering performance by controlling the lateral size of MXene flakes (Figure 18a).[214] The on-chip MXene MSCs exhibit high volumetric capacitance (30 F cm^{-3} at 120 Hz), high-rate performance (300 V s^{-1}), and a relaxation time constant (τ_0) lower than conventional electrolytic capacitors (from 0.45 to 0.8 ms), enabling them to filter the 120 Hz ripple produced by 60 Hz AC line electricity. Similarly, Xu et al. utilized multiwalled carbon nanotubes (MWCNTs) as interlayer supports for MXene, providing fast ion transport pathways (Figure 18b).[207] This MSC exhibits a high areal capacitance of 6 mF cm^{-2} at 120 Hz, much higher than commercial tantalum capacitors, and maintains a nearly rectangular CV curve at rates as high as 300 and 500 V/s^{-1}. Moreover, the equivalent series resistance of the device is only 0.3 Ω, providing excellent performance in both low-pass filter circuits and relaxation oscillator circuits.

3D porous and vertically aligned MXene structures have also been used to build power devices for AC filtering, effectively balancing the charge storage and transport characteristics of MXene. For instance, Gund et al. synthesized porous MXene/PEDOT:PSS hybrids ($Ti_3C_2T_x$/poly(3,4-ethylenedioxythiophene):polystyrenesulfonate) for large-scale flexible alternating current filtering symmetric electrochemical capacitors (Figure 18c).[158] The interconnected porous channels promote fast ion and charge transfer, endowing it with high-rate and power characteristics. The capacitor can achieve up to 10,000 Hz ripple voltage filtering and over 30,000 cycles of durability. Subsequently, Zhang et al. treated MXene/PEDOT:PSS coatings with tartaric acid, which exhibited similar AC filtering performance with a relaxation time constant of only 1.3 ms.[152] Additionally, Wen et al. prepared vertical-oriented MXene and reduced graphene oxide composite (VMG) electrodes by electrochemical codeposition, which can maintain a phase angle of 80° at 120 Hz, an energy density of 805 μF V^2 cm^{-2}, and stable DC signals at different frequencies (Figure 18d).[61]

5. SUMMARY AND PERSPECTIVES

Since being initially synthesized in 2011, MXenes offer attractive electronic, electrochemical, optical and mechanical properties and show great potential in the fields of energy storage, sensors, catalysis, water purification, and electromagnetic shielding.[226−231] The intercalation pseudocapacitance mechanism of an MXene has enabled it to outperform in supercapacitors, but it was not until 2016 that it became widely applied to micro-supercapacitors, and current publications on printed and patterned coated MXene MSCs are showing exponential growth.[85,88,146] On the one hand, the extensive exploration of MXene solution processing has developed a variety of methods for patterning MXene MSCs.[8] On the other hand, MXene has been successfully hybridized with other electrochemically active materials such as inorganic nonmetallic materials, metal oxides/sulfides, and organic polymers for the construction of high-performance composite electrodes.[232] From the perspective of electrode design, the diversity of MXene species and structures can bring endless possibilities, which is advantageous to achieve the construction of MXene MSCs having energy density comparable to that of thin film Li-ion batteries while maintaining high power density. In addition, MXene MSCs should be highly integrated and compatible with other on-chip electronic devices to meet the demands of multifunctional wearable electronics. To achieve these goals, the existing problems and future directions are as follows:

(1) Although over 30 types of MXene have been successfully synthesized, only one type of MXene ($Ti_3C_2T_x$) has been developed for patterning micro-supercapacitors. However, the intrinsic characteristics of $Ti_3C_2T_x$ limit its operating voltage, resulting in a limited voltage window of 0.6 V for printed MXene MSCs, which hinders its energy density improvement and broader applications. The exploitation of other MXene inks and the tuning of the surface end points of $Ti_3C_2T_x$ may further advance the development of MXene MSCs.

(2) $Ti_3C_2T_x$ can be easily dispersed in various polar solvents, and the colloidal rheology can be tuned by adjusting the concentration, MXene layers, and nanosheet size to accommodate various patterning processing techniques. Although there have been many reports on the rheology of MXene-containing colloids to demonstrate their application in solution process processing, the physical principles behind their behavior remain poorly understood. More dedicated rheological studies are required to analyze and model its rheology mechanism, in order to guide the selective processing of MXene MSC.

(3) High mass production and long-term stability of MXene inks is also an essential issue for industrialization. Despite many efforts to improve the stability and oxidation resistance of MXene inks, their shelf life remains only a few months, far from the requirements of industrialization.[134,233,234] In addition, the supercritical method proposed by Yang's group has increased the production batch of MXene from the gram level to the kilogram level,[110] and although further exploration of subsequent layering and dispersion methods is required, it also provides a viable pathway for the industrial application of MXene.

(4) The unique two-dimensional structure of MXenes can provide a favorable environment for chemical reactions, and the compounding with other electrode materials can bring breakthroughs in certain properties, such as voltage and energy

https://doi.org/10.1021/acsnano.3c10246
ACS Nano 2024, 18, 4651−4682

density. The application of current rapidly developing machine learning and artificial intelligence techniques to the design of MXene composites could be considered, which would certainly be an attractive direction for scientific research.

(5) Although some reports have demonstrated MXene MSCs with excellent performance, most efforts have been limited to laboratory scale while commercial production remains elusive. To achieve this goal, all stages of the printing process chain, including etching, layering, ink rheology and printing/coating processes, need to be optimized. More exploration of manufacturing MXene MSCs at scale, while ensuring low cost and high performance, is necessary to achieve a match for commercialization.

(6) Finally, the next-generation MXene-based MSCs are expected to have functions other than energy storage. To date, micro-integrated systems with self-charging, self-healing, sensing, electrochromic, electromagnetic shielding, and filtering functions have been successfully developed. In addition to the exploration of MXene MSCs for performance improvement, manufacturing cost reduction, ease of integration and miniaturization, both device components and manufacturing processes should be optimized to ensure their compatibility with other on-chip electronic devices, including processing, performance, functionality.

AUTHOR INFORMATION

Corresponding Author

Weiqing Yang − *Research Institute of Frontier Science and Key Laboratory of Advanced Technologies of Materials (Ministry of Education), School of Materials Science and Engineering, Southwest Jiaotong University, Chengdu 610031, China;* orcid.org/0000-0001-8828-9862; Email: wqyang@swjtu.edu.cn

Author

Haichao Huang − *Research Institute of Frontier Science and Key Laboratory of Advanced Technologies of Materials (Ministry of Education), School of Materials Science and Engineering, Southwest Jiaotong University, Chengdu 610031, China*

Complete contact information is available at: https://pubs.acs.org/10.1021/acsnano.3c10246

Author Contributions

W.Q.Y. initialized and supervised the whole project. H.C.H. mainly performed the literature collection and summarization. The manuscript was completed by all authors. All authors approved the final version of the manuscript.

Notes

The authors declare no competing financial interest.

ACKNOWLEDGMENTS

This work was financially supported by the National Natural Science Foundation of China (No. 51972277) and the Sichuan Science and Technology Program (Nos. 20ZDYF2478, 20ZDYF2833 and 21ZDYF3951).

VOCABULARY

Micro-supercapacitor: The basic structure consists of positive and negative electrodes separated by an ionic conductor electrolyte. There are three main types of micro-supercapacitor structures: thin film electrodes (<10 μm thick) with a sandwich structure, planar electrode arrays with micrometer dimensions in at least two dimensions, or fiber-based electrodes with a core−shell structure.

MXene: The general formula is $M_{n+1}X_nT_x$, where M is a transition metal (e.g., Ti, Nb, Mo, Zr, Cr, *etc.*), X is carbon and/or nitrogen, and T represents a surface functional group.

Asymmetric micro-supercapacitors: They are assembled using two different electrode materials with complementary windows of operating potential, with the aim of increasing the cell voltage and energy density.

Symmetric micro-supercapacitors: They are assembled using two similar electrode materials.

Electromagnetic shielding: The shielding body through reflection or absorption to interfere with the signal source, to prevent electronic equipment from being affected by external electromagnetic fields; usually requires the shielding body to have good conductive continuity.

REFERENCES

(1) Wang, R.; Luo, S.; Xiao, C.; Chen, Z.; Li, H.; Asif, M.; Chan, V.; Liao, K.; Sun, Y. Mxene-Carbon Nanotubes Layer-by-Layer Assembly Based On-Chip Micro-Supercapacitor with Improved Capacitive Performance. *Electrochim. Acta* **2021**, *386*, No. 138420.

(2) Wang, F.; Wu, X.; Yuan, X.; Liu, Z.; Zhang, Y.; Fu, L.; Zhu, Y.; Zhou, Q.; Wu, Y.; Huang, W. Latest Advances in Supercapacitors: from New Electrode Materials to Novel Device Designs. *Chem. Soc. Rev.* **2017**, *46* (22), 6816−6854.

(3) Augustyn, V.; Simon, P.; Dunn, B. Pseudocapacitive Oxide Materials for High-Rate Electrochemical Energy Storage. *Energy Environ. Sci.* **2014**, *7* (5), 1597−1614.

(4) Liu, L.; Niu, Z.; Chen, J. Design and Integration of Flexible Planar Micro-Supercapacitors. *Nano Res.* **2017**, *10* (5), 1524−1544.

(5) Jiang, X.; Li, W.; Hai, T.; Yue, R.; Chen, Z.; Lao, C.; Ge, Y.; Xie, G.; Wen, Q.; Zhang, H. Inkjet-printed MXene Micro-Scale Devices for Integrated Broadband Ultrafast Photonics. *npj 2D Mater. Appl.* **2019**, *3* (1), No. 34.

(6) Lethien, C.; Le Bideau, J.; Brousse, T. Challenges and Prospects of 3D Micro-Supercapacitors for Powering the Internet of Things. *Energy Environ. Sci.* **2019**, *12* (1), 96−115.

(7) Zhu, Y.; Ma, J.; Das, P.; Wang, S.; Wu, Z. S. High-Voltage MXene-Based Supercapacitors: Present Status and Future Perspectives. *Small Methods* **2023**, *7*, No. 2201609.

(8) Zhu, Y.; Wang, S.; Ma, J.; Das, P.; Zheng, S.; Wu, Z.-S. Recent status and future perspectives of 2D MXene for micro-supercapacitors and micro-batteries. *Energy Storage Mater.* **2022**, *51*, 500−526.

(9) Hawes, G. F.; Rehman, S.; Rangom, Y.; Pope, M. A. Advanced Manufacturing Approaches for Electrochemical Energy Storage Devices. *Int. Mater. Rev.* **2023**, *68* (3), 323−364.

(10) Gaikwad, A. M.; Arias, A. C.; Steingart, D. A. Recent Progress on Printed Flexible Batteries: Mechanical Challenges, Printing Technologies, and Future Prospects. *Energy Technol.* **2015**, *3* (4), 305−328.

(11) Kyerematen, N. A.; Brousse, T.; Pech, D. Microsupercapacitors as Miniaturized Energy-Storage Components for On-Chip Electronics. *Nat. Nanotechnol.* **2017**, *12* (1), 7−15.

(12) Jiang, Q.; Lei, Y.; Liang, H.; Xi, K.; Xia, C.; Alshareef, H. N. Review of MXene Electrochemical Microsupercapacitors. *Energy Storage Mater.* **2020**, *27*, 78−95.

(13) Shi, X.; Wu, Z.-S.; Bao, X. Recent Advancements and Perspective of High-Performance Printed Power Sources with Multiple Form Factors. *Electrochem. Energy Rev.* **2020**, *3* (3), 581−612.

(14) Wu, Y.; Hu, H.; Yuan, C.; Song, J.; Wu, M. Electrons/ions Dual Transport Channels Design: Concurrently Tuning Interlayer Conductivity and Space within Re-Stacked Few-Layered MXenes

Film Electrodes for High-Areal-Capacitance Stretchable Micro-Supercapacitor-Arrays. *Nano Energy* **2020**, *74*, No. 104812.
(15) Li, L.; Hu, C.; Liu, W.; Shen, G. Progress and Perspectives in Designing Flexible Microsupercapacitors. *Micromachines-Basel* **2021**, *12* (11), 1305.
(16) Peng, X.; Peng, L.; Wu, C.; Xie, Y. Two Dimensional Nanomaterials for Flexible Supercapacitors. *Chem. Soc. Rev.* **2014**, *43* (10), 3303−3323.
(17) Gao, C.; Chen, K.; Wang, Y.; Zhao, Y.; Qu, L. 2D Graphene-Based Macroscopic Assemblies for Micro-Supercapacitors. *ChemSusChem* **2020**, *13* (6), 1255−1274.
(18) Wen, D.; Ying, G.; Liu, L.; Li, Y.; Sun, C.; Hu, C.; Zhao, Y.; Ji, Z.; Zhang, J.; Wang, X. Direct Inkjet Printing of Flexible MXene/graphene Composite Films for Supercapacitor Electrodes. *J. Alloy. Compd* **2022**, *900*, No. 163436.
(19) Jiang, T.; Wang, Y.; Chen, G. Z. Electrochemistry of Titanium Carbide MXenes in Supercapacitor. *Small Methods* **2023**, *7*, No. 2201724.
(20) Bonaccorso, F.; Bartolotta, A.; Coleman, J. N.; Backes, C. 2D-Crystal-Based Functional Inks. *Adv. Mater.* **2016**, *28* (29), 6136−6166.
(21) Zazoum, B.; Bachri, A.; Nayfeh, J. Functional 2D MXene Inks for Wearable Electronics. *Materials* **2021**, *14* (21), 6603.
(22) Azadmanjiri, J.; Thuniki, N. R.; Guzzetta, F.; Sofer, Z. Liquid Metals-Assisted Synthesis of Scalable 2D Nanomaterials: Prospective Sediment Inks for Screen-Printed Energy Storage Applications. *Adv. Funct. Mater.* **2021**, *31* (17), No. 2010320.
(23) VahidMohammadi, A.; Rosen, J.; Gogotsi, Y. The World of Two-Dimensional Carbides and Nitrides (MXenes). *Science* **2021**, *372* (6547), 1165.
(24) Li, Q.; Wang, Q.; Li, L.; Yang, L.; Wang, Y.; Wang, X.; Fang, H. T. Femtosecond Laser-Etched MXene Microsupercapacitors with Double-Side Configuration *via* Arbitrary On- and Through-Substrate Connections. *Adv. Energy Mater.* **2020**, *10* (24), No. 2000470.
(25) Naguib, M.; Mochalin, V. N.; Barsoum, M. W.; Gogotsi, Y. 25th Anniversary Article: MXenes: a New Family of Two-Dimensional Materials. *Adv. Mater.* **2014**, *26* (7), 992−1005.
(26) Das, P.; Wu, Z.-S. MXene for Energy Storage: Present Status and Future Perspectives. *J. Phys. Energy* **2020**, *2* (3), No. 032004.
(27) Sohan, A.; Banoth, P.; Aleksandrova, M.; Nirmala Grace, A.; Kollu, P. Review on MXene Synthesis, Properties, and Recent Research Exploring Electrode Architecture for Supercapacitor Applications. *International Journal of Energy Research* **2021**, *45* (14), 19746−19771.
(28) Li, X. L.; Huang, Z. D.; Shuck, C. E.; Liang, G. J.; Gogotsi, Y.; Zhi, C. Y. MXene Chemistry, Electrochemistry and Energy Storage Applications. *Nat. Rev. Chem.* **2022**, *6* (6), 389−404.
(29) Thakur, N.; Kumar, P.; Sati, D. C.; Neffati, R.; Sharma, P. Recent advances in Two-Dimensional MXenes for Power and Smart Energy Systems. *J. Energy Storage* **2022**, *50*, No. 104604.
(30) Cao, Z.; Fu, J.; Wu, M.; Hua, T.; Hu, H. Synchronously Manipulating Zn^{2+} Transfer and Hydrogen/Oxygen Evolution Kinetics in MXene Host Electrodes Toward Symmetric Zn-ions Micro-Supercapacitor with Enhanced Areal Energy Density. *Energy Storage Mater.* **2021**, *40*, 10−21.
(31) Lukatskaya, M. R.; Bak, S.-M.; Yu, X.; Yang, X.-Q.; Barsoum, M. W.; Gogotsi, Y. Probing the Mechanism of High Capacitance in 2D Titanium Carbide Using *In Situ* X-Ray Absorption Spectroscopy. *Adv. Energy Mater.* **2015**, *5* (15), No. 1500589.
(32) Lukatskaya, M. R.; Kota, S.; Lin, Z.; Zhao, M.-Q.; Shpigel, N.; Levi, M. D.; Halim, J.; Taberna, P.-L.; Barsoum, M. W.; Simon, P.; Gogotsi, Y. Ultra-high-rate Pseudocapacitive Energy Storage In Two-Dimensional Transition Metal Carbides. *Nature Energy* **2017**, *2* (8), No. 17105.
(33) Zheng, S.; Zhang, C.; Zhou, F.; Dong, Y.; Shi, X.; Nicolosi, V.; Wu, Z.-S.; Bao, X. Ionic Liquid Pre-Intercalated MXene films for ionogel-based flexible micro-supercapacitors with High Volumetric Energy Density. *J. Mater. Chem. A* **2019**, *7* (16), 9478−9485.
(34) Li, K.; Wang, X.; Li, S.; Urbankowski, P.; Li, J.; Xu, Y.; Gogotsi, Y. An Ultrafast Conducting Polymer@MXene Positive Electrode with High Volumetric Capacitance for Advanced Asymmetric Supercapacitors. *Small* **2020**, *16* (4), No. 1906851.
(35) Wu, Y.; Fu, J.; He, N.; Liu, J.; Hua, T.; Qin, C.; Hu, H. Surface terminals reconstruction: The Way to Widen the Output Voltage of MXene-based Aqueous Symmetrical Micro-Supercapacitors. *Nano Res.* **2023**, *16*, 6780.
(36) Sarycheva, A.; Gogotsi, Y. Raman Spectroscopy Analysis of the Structure and Surface Chemistry of $Ti_3C_2T_x$ MXene. *Chem. Mater.* **2020**, *32* (8), 3480−3488.
(37) Greaves, M.; Mende, M.; Wang, J.; Yang, W.; Barg, S. Investigating the Rheology of 2D Titanium Carbide (MXene) Dispersions for Colloidal Processing: Progress and challenges. *J. Mater. Res.* **2021**, *36* (22), 4578−4600.
(38) Maleski, K.; Mochalin, V. N.; Gogotsi, Y. Dispersions of Two-Dimensional Titanium Carbide MXene in Organic Solvents. *Chem. Mater.* **2017**, *29* (4), 1632−1640.
(39) Azadmanjiri, J.; Reddy, T. N.; Khezri, B.; Děkanovský, L.; Parameswaran, A. K.; Pal, B.; Ashtiani, S.; Wei, S.; Sofer, Z. Prospective Advances in MXene Inks: Screen Printable Sediments for Flexible Micro-Supercapacitor Applications. *J. Mater. Chem. A* **2022**, *10* (9), 4533−4557.
(40) Liang, J.; Jiang, C.; Wu, W. Printed flexible supercapacitor: Ink Formulation, Printable Electrode Materials and Applications. *Appl. Phys. Rev.* **2021**, *8* (2), No. 021319.
(41) Derby, B. Inkjet Printing of Functional and Structural Materials: Fluid Property Requirements, Feature Stability, and Resolution. *Annu. Rev. Mater. Res.* **2010**, *40* (1), 395−414.
(42) Zhang, C. J.; McKeon, L.; Kremer, M. P.; Park, S. H.; Ronan, O.; Seral-Ascaso, A.; Barwich, S.; Coileain, C. O.; McEvoy, N.; Nerl, H. C.; Anasori, B.; Coleman, J. N.; Gogotsi, Y.; Nicolosi, V. Additive-free MXene Inks and Direct Printing of Micro-Supercapacitors. *Nat. Commun.* **2019**, *10* (1), 1795.
(43) Sajedi-Moghaddam, A.; Rahmanian, E.; Naseri, N. Inkjet-Printing Technology for Supercapacitor Application: Current State and Perspectives. *ACS Appl. Mater. Interfaces* **2020**, *12* (31), 34487−34504.
(44) Hu, G.; Kang, J.; Ng, L. W. T.; Zhu, X.; Howe, R. C. T.; Jones, C. G.; Hersam, M. C.; Hasan, T. Functional Inks and Printing of Two-Dimensional Materials. *Chem. Soc. Rev.* **2018**, *47* (9), 3265−3300.
(45) Abdolhosseinzadeh, S.; Jiang, X.; Zhang, H.; Qiu, J.; Zhang, C. Perspectives on Solution Processing of Two-Dimensional MXenes. *Mater. Today* **2021**, *48*, 214−240.
(46) Ma, J.; Zheng, S.; Cao, Y.; Zhu, Y.; Das, P.; Wang, H.; Liu, Y.; Wang, J.; Chi, L.; Liu, S.; Wu, Z. S. Aqueous MXene/PH1000 Hybrid Inks for Inkjet-Printing Micro-Supercapacitors with Unprecedented Volumetric Capacitance and Modular Self-Powered Microelectronics. *Adv. Energy Mater.* **2021**, *11* (23), No. 2100746.
(47) Wang, R.; Luo, S.; Xiao, C.; Chen, Z.; Li, H.; Asif, M.; Chan, V.; Liao, K.; Sun, Y. MXene-Carbon Nanotubes Layer-By-Layer Assembly based On-Chip Micro-Supercapacitor with Improved Capacitive Performance. *Electrochim. Acta* **2021**, *386*, No. 138420.
(48) Zhang, Y.; Wang, L.; Zhao, L.; Wang, K.; Zheng, Y.; Yuan, Z.; Wang, D.; Fu, X.; Shen, G.; Han, W. Flexible Self-Powered Integrated Sensing System with 3D Periodic Ordered Black Phosphorus@MXene Thin-Films. *Adv. Mater.* **2021**, *33* (22), No. 2007890.
(49) Mashtalir, O.; Naguib, M.; Mochalin, V. N.; Dall'Agnese, Y.; Heon, M.; Barsoum, M. W.; Gogotsi, Y. Intercalation and Delamination of Layered Carbides and Carbonitrides. *Nat. Commun.* **2013**, *4*, 1716.
(50) Kajiyama, S.; Szabova, L.; Sodeyama, K.; Iinuma, H.; Morita, R.; Gotoh, K.; Tateyama, Y.; Okubo, M.; Yamada, A. Sodium-Ion Intercalation Mechanism in MXene Nanosheets. *ACS Nano* **2016**, *10* (3), 3334−3341.
(51) Lukatskaya, M. R.; Mashtalir, O.; Ren, C. E.; Dall'Agnese, Y.; Rozier, P.; Taberna, P. L.; Naguib, M.; Simon, P.; Barsoum, M. W.; Gogotsi, Y. Cation Intercalation and High Volumetric Capacitance of

https://doi.org/10.1021/acsnano.3c10246
ACS Nano 2024, 18, 4651−4682

Two-Dimensional Titanium Carbide. *Science* **2013**, *341* (6153), 1502−1505.
(52) Fang, Y. Z.; Hu, R.; Zhu, K.; Ye, K.; Yan, J.; Wang, G.; Cao, D. Aggregation-Resistant 3D $Ti_3C_2T_x$ MXene with Enhanced Kinetics for Potassium Ion Hybrid Capacitors. *Adv. Funct. Mater.* **2020**, *30* (50), No. 2005663.
(53) Shang, T.; Lin, Z.; Qi, C.; Liu, X.; Li, P.; Tao, Y.; Wu, Z.; Li, D.; Simon, P.; Yang, Q. H. 3D Macroscopic Architectures from Self-Assembled MXene Hydrogels. *Adv. Funct. Mater.* **2019**, *29* (33), No. 1903960.
(54) Orangi, J.; Hamade, F.; Davis, V. A.; Beidaghi, M. 3D Printing of Additive-Free 2D $Ti_3C_2T_x$ (MXene) Ink for Fabrication of Micro-Supercapacitors with Ultra-High Energy Densities. *ACS Nano* **2020**, *14* (1), 640−650.
(55) An, N.; Guo, Z.; Guo, C.; Wei, M.; Sun, D.; He, Y.; Li, W.; Zhou, L.; Hu, Z.; Dong, X. A Novel COF/MXene Film Electrode with Fast Redox Kinetics for High-Performance Flexible Supercapacitor. *Chem. Eng. J.* **2023**, *458*, No. 141434.
(56) Zhang, H.; Wei, Z.; Wu, J.; Cheng, F.; Ma, Y.; Liu, W.; Cheng, Y.; Lin, Y.; Liu, N.; Gao, Y.; Yue, Y. Interlayer-spacing-regulated MXene/rGO Foam for Multi-functional Zinc-ion Microcapacitors. *Energy Storage Mater.* **2022**, *50*, 444−453.
(57) Zheng, S.; Wang, H.; Das, P.; Zhang, Y.; Cao, Y.; Ma, J.; Liu, S. F.; Wu, Z. S. Multitasking MXene Inks Enable High-Performance Printable Microelectrochemical Energy Storage Devices for All-Flexible Self-Powered Integrated Systems. *Adv. Mater.* **2021**, *33* (10), No. 2005449.
(58) Cao, Z.; Hu, H.; Ho, D. Micro-Redoxcapacitor: A Hybrid Architecture Out of the Notorious Energy-Power Density Dilemma. *Adv. Funct. Mater.* **2022**, *32* (19), No. 2111805.
(59) Ren, C.-Y.; Qiu, S.-Y.; Zhai, J.-R.; Zhang, K.-Q.; Lu, J.-X.; Gao, J.; Wang, C.; Zhang, Y.-C.; Zhu, X.-D. Ionic Liquid-Wrapped MXene Film with Bowl-Like Structures for Highly Integrated Micro-supercapacitor Array with Ultrahigh Output Voltage. *Nano Res.* **2023**, *16*, 4926.
(60) Shao, Y.; Wei, L.; Wu, X.; Jiang, C.; Yao, Y.; Peng, B.; Chen, H.; Huangfu, J.; Ying, Y.; Zhang, C. J.; Ping, J. Room-Temperature High-Precision Printing of Flexible Wireless Electronics based on MXene inks. *Nat. Commun.* **2022**, *13* (1), 3223.
(61) Wen, Y.; Chen, H.; Wu, M.; Li, C. Vertically Oriented MXene Bridging the Frequency Response and Capacity Density Gap for AC-Filtering Pseudocapacitors. *Adv. Funct. Mater.* **2022**, *32* (21), No. 2111613.
(62) Zhang, X.; Yang, Y.; Xue, P.; Valenzuela, C.; Chen, Y.; Yang, X.; Wang, L.; Feng, W. Three-Dimensional Electrochromic Soft Photonic Crystals Based on MXene-Integrated Blue Phase Liquid Crystals for Bioinspired Visible and Infrared Camouflage. *Angew. Chem., Int. Ed. Engl.* **2022**, *61* (42), No. 202211030.
(63) Duan, Z.; Hu, C.; Liu, W.; Liu, J.; Chu, Z.; Yang, W.; Li, L.; Shen, G. An All-MXene-Based Flexible, Seamless System with Integrated Wireless Charging Coil, Micro-Supercapacitor, and Photodetector. *Adv. Mater. Technol.* **2023**, *8*, No. 2300157.
(64) Liu, W.; Li, L.; Shen, G. A $Ti_3C_2T_x$ MXene Cathode and Redox-Active Electrolyte based Flexible Zn-ion Microsupercapacitor for Integrated Pressure Sensing Application. *Nanoscale* **2023**, *15* (6), 2624−2632.
(65) Zheng, X.; Zhang, S.; Zhou, M.; Lu, H.; Guo, S.; Zhang, Y.; Li, C.; Tan, S. C. MXene Functionalized, Highly Breathable and Sensitive Pressure Sensors with Multi-Layered Porous Structure. *Adv. Funct. Mater.* **2023**, *33*, No. 2214880.
(66) Uzun, S.; Schelling, M.; Hantanasirisakul, K.; Mathis, T. S.; Askeland, R.; Dion, G.; Gogotsi, Y. Additive-Free Aqueous MXene Inks for Thermal Inkjet Printing on Textiles. *Small* **2021**, *17* (1), No. 2006376.
(67) Jiao, S.; Zhou, A.; Wu, M.; Hu, H. Kirigami Patterning of MXene/Bacterial Cellulose Composite Paper for All-Solid-State Stretchable Micro-Supercapacitor Arrays. *Adv. Sci.* **2019**, *6* (12), No. 1900529.
(68) Yang, W.; Yang, J.; Byun, J. J.; Moissinac, F. P.; Xu, J.; Haigh, S. J.; Domingos, M.; Bissett, M. A.; Dryfe, R. A. W.; Barg, S. 3D Printing of Freestanding MXene Architectures for Current-Collector-Free Supercapacitors. *Adv. Mater.* **2019**, *31* (37), No. 1902725.
(69) Lei, Y.; Zhao, W.; Zhu, Y.; Buttner, U.; Dong, X.; Alshareef, H. N. Three-Dimensional $Ti_3C_2T_x$ MXene-Prussian Blue Hybrid Micro-supercapacitors by Water Lift-Off Lithography. *ACS Nano* **2022**, *16* (2), 1974−1985.
(70) Huang, H.; He, J.; Wang, Z.; Zhang, H.; Jin, L.; Chen, N.; Xie, Y.; Chu, X.; Gu, B.; Deng, W.; Yang, W. Scalable, and Low-Cost Treating-Cutting-Coating Manufacture Platform for MXene-based On-Chip Micro-Supercapacitors. *Nano Energy* **2020**, *69*, No. 104431.
(71) Hu, H.; Bai, Z.; Niu, B.; Wu, M.; Hua, T. Binder-free Bonding Of Modularized MXene Thin Films into Thick Film Electrodes for On-Chip Micro-Supercapacitors with Enhanced Areal Performance Metrics. *J. Mater. Chem. A* **2018**, *6* (30), 14876−14884.
(72) Huang, H.; Su, H.; Zhang, H.; Xu, L.; Chu, X.; Hu, C.; Liu, H.; Chen, N.; Liu, F.; Deng, W.; Gu, B.; Zhang, H.; Yang, W. Extraordinary Areal and Volumetric Performance of Flexible Solid-State Micro-Supercapacitors Based on Highly Conductive Free-standing $Ti_3C_2T_x$ Films. *Adv. Electron. Mater.* **2018**, *4* (8), No. 1800179.
(73) Kim, E.; Lee, B.-J.; Maleski, K.; Chae, Y.; Lee, Y.; Gogotsi, Y.; Ahn, C. W. Microsupercapacitor with a 500 nm Gap between MXene/CNT Electrodes. *Nano Energy* **2021**, *81*, No. 105616.
(74) Zhang, C. J.; Kremer, M. P.; Seral-Ascaso, A.; Park, S.-H.; McEvoy, N.; Anasori, B.; Gogotsi, Y.; Nicolosi, V. Stamping of Flexible, Coplanar Micro-Supercapacitors Using MXene Inks. *Adv. Funct. Mater.* **2018**, *28* (9), No. 1705506.
(75) Kim, E.; Song, J.; Song, T.-E.; Kim, H.; Kim, Y.-J.; Oh, Y.-W.; Jung, S.; Kang, I.-S.; Gogotsi, Y.; Han, H.; Ahn, C. W.; Lee, Y. Scalable Fabrication of MXene-based Flexible Micro-Supercapacitor with Outstanding Volumetric Capacitance. *Chem. Eng. J.* **2022**, *450*, No. 138456.
(76) Bonaccorso, F.; Colombo, L.; Yu, G.; Stoller, M.; Tozzini, V.; Ferrari, A. C.; Ruoff, R. S.; Pellegrini, V. Graphene, Related Two-Dimensional Crystals, and Hybrid Systems for Energy Conversion and Storage. *Science* **2015**, *347* (6217), No. 1246501.
(77) Zhang, H.; Zhang, X.; Sun, X.; Zhang, D.; Lin, H.; Wang, C.; Wang, H.; Ma, Y. Large-scale Production of Nanographene Sheets with a Controlled Mesoporous Architecture as High-Performance Electrochemical Electrode Materials. *ChemSusChem* **2013**, *6* (6), 1084−1090.
(78) Kim, B. C.; Hong, J.-Y.; Wallace, G. G.; Park, H. S. Recent Progress in Flexible Electrochemical Capacitors: Electrode Materials, Device Configuration, and Functions. *Adv. Energy Mater.* **2015**, *5* (22), 1500959.
(79) Tian, X. Direct Ink Writing of 2D Material-Based Supercapacitors. *2D Materials* **2022**, *9* (1), No. 012001.
(80) Huang, T.-T.; Wu, W. Scalable Nanomanufacturing of Inkjet-Printed Wearable Energy Storage Devices. *J. Mater. Chem. A* **2019**, *7* (41), 23280−23300.
(81) Xu, S.; Wei, G.; Li, J.; Ji, Y.; Klyui, N.; Izotov, V.; Han, W. Binder-free $Ti_3C_2T_x$ MXene Electrode Film for Supercapacitor Produced by Electrophoretic Deposition Method. *Chem. Eng. J.* **2017**, *317*, 1026−1036.
(82) Weingarth, D.; Cericola, D.; Mornaghini, F. C. F.; Hucke, T.; Kötz, R. Carbon Additives for Electrical Double Layer Capacitor Electrodes. *J. Power Sources* **2014**, *266*, 475−480.
(83) Akuzum, B.; Maleski, K.; Anasori, B.; Lelyukh, P.; Alvarez, N. J.; Kumbur, E. C.; Gogotsi, Y. Rheological Characteristics of 2D Titanium Carbide (MXene) Dispersions: A Guide for Processing MXenes. *ACS Nano* **2018**, *12* (3), 2685−2694.
(84) Li, H.; Liang, J. Recent Development of Printed Micro-Supercapacitors: Printable Materials, Printing Technologies, and Perspectives. *Adv. Mater.* **2020**, *32* (3), No. 1805864.
(85) Zhang, Y. Z.; Wang, Y.; Jiang, Q.; El-Demellawi, J. K.; Kim, H.; Alshareef, H. N. MXene Printing and Patterned Coating for Device Applications. *Adv. Mater.* **2020**, *32* (21), No. 1908486.

https://doi.org/10.1021/acsnano.3c10246
ACS Nano 2024, 18, 4651−4682

(86) Wang, J.; Li, F.; Zhu, F.; Schmidt, O. G. Recent Progress in Micro-Supercapacitor Design, Integration, and Functionalization. *Small Methods* **2019**, *3*, No. 1800367.
(87) Song, L.; Jin, X.; Dai, C.; Han, Y.; Zhang, J.; Zhang, Z.; Qu, L. Multifunctional Devices based on Planar Microsupercapacitors: Progress And Challenges. *Sci. China Mater.* **2022**, *65* (12), 3202−3228.
(88) Peng, Y.-Y.; Akuzum, B.; Kurra, N.; Zhao, M.-Q.; Alhabeb, M.; Anasori, B.; Kumbur, E. C.; Alshareef, H. N.; Ger, M.-D.; Gogotsi, Y. All-MXene (2D Titanium Carbide) Solid-State Microsupercapacitors for On-Chip Energy Storage. *Energy Environ. Sci.* **2016**, *9* (9), 2847−2854.
(89) Kamyshny, A.; Magdassi, S. Conductive Nanomaterials for 2D and 3D Printed Flexible Electronics. *Chem. Soc. Rev.* **2019**, *48* (6), 1712−1740.
(90) Li, K.; Liang, M.; Wang, H.; Wang, X.; Huang, Y.; Coelho, J.; Pinilla, S.; Zhang, Y.; Qi, F.; Nicolosi, V.; Xu, Y. 3D MXene Architectures for Efficient Energy Storage and Conversion. *Adv. Funct. Mater.* **2020**, *30* (47), No. 2000842.
(91) Li, P.; Shi, W.; Liu, W.; Chen, Y.; Xu, X.; Ye, S.; Yin, R.; Zhang, L.; Xu, L.; Cao, X. Fabrication of High-Performance MXene-based All-Solid-State Flexible Microsupercapacitor based on a Facile Scratch Method. *Nanotechnology* **2018**, *29* (44), No. 445401.
(92) Trantidou, T.; Elani, Y.; Parsons, E.; Ces, O. Hydrophilic Surface Modification of PDMS for Droplet Microfluidics Using A Simple, Quick, and Robust Method *via* PVA Deposition. *Microsyst. Nanoeng.* **2017**, *3*, 16091.
(93) Huang, H.; Chu, X.; Xie, Y.; Zhang, B.; Wang, Z.; Duan, Z.; Chen, N.; Xu, Z.; Zhang, H.; Yang, W. $Ti_3C_2T_x$ MXene-Based Micro-Supercapacitors with Ultrahigh Volumetric Energy Density for All-in-One Si-Electronics. *ACS Nano* **2022**, *16* (3), 3776−3784.
(94) Huang, H.; He, J.; Wang, Z.; Zhang, H.; Jin, L.; Chen, N.; Xie, Y.; Chu, X.; Gu, B.; Deng, W.; Yang, W. Scalable, and Low-Cost Treating-Cutting-Coating Manufacture Platform for MXene-based On-Chip Micro-Supercapacitors. *Nano Energy* **2020**, *69*, No. 104431.
(95) Deegan, R. D.; Bakajin, O.; Dupont, T. F.; Huber, G.; Nagel, S. R.; Witten, T. A. Publisher Correction: Capillary Flow as the Cause of Ring Stains from Dried Liquid Drops. *Nature* **1997**, *389*, 827−829.
(96) Feng, X.; Ning, J.; Wang, B.; Guo, H.; Xia, M.; Wang, D.; Zhang, J.; Wu, Z.-S.; Hao, Y. Functional Integrated Electromagnetic Interference Shielding in Flexible Micro-Supercapacitors by Cation-Intercalation Typed $Ti_3C_2T_x$ MXene. *Nano Energy* **2020**, *72*, No. 104741.
(97) An, N.; Li, W.; Shao, Z.; Zhou, L.; He, Y.; Sun, D.; Dong, X.; Hu, Z. Graphene Oxide Coated Polyaminoanthraquinone@MXene based Flexible Film Electrode for High-Performance Supercapacitor. *J. Energy Storage* **2023**, *57*, No. 106180.
(98) Mao, K.; Shi, J.; Zhang, Q.; Hou, Y.; Wen, L.; Liu, Z.; Long, F.; Niu, K.; Liu, N.; Long, F.; Gao, Y. High-capacitance MXene Anode based on Zn-ion Pre-Intercalation Strategy for Degradable Micro Zn-ion Hybrid Supercapacitors. *Nano Energy* **2022**, *103*, No. 107791.
(99) Chen, N.; Yang, W.; Zhang, C. Perspectives on Preparation of Two-Dimensional MXenes. *Sci. Technol. Adv. Mater.* **2021**, *22* (1), 917−930.
(100) Naguib, M.; Gogotsi, Y. Synthesis of Two-Dimensional Materials by Selective Extraction. *Acc. Chem. Res.* **2015**, *48* (1), 128−135.
(101) Halim, J.; Kota, S.; Lukatskaya, M. R.; Naguib, M.; Zhao, M.-Q.; Moon, E. J.; Pitock, J.; Nanda, J.; May, S. J.; Gogotsi, Y.; Barsoum, M. W. Synthesis and Characterization of 2D Molybdenum Carbide (MXene). *Adv. Funct. Mater.* **2016**, *26* (18), 3118−3127.
(102) Lipatov, A.; Alhabeb, M.; Lukatskaya, M. R.; Boson, A.; Gogotsi, Y.; Sinitskii, A. Effect of Synthesis on Quality, Electronic Properties and Environmental Stability of Individual Monolayer Ti3C2MXene Flakes. *Adv. Electron. Mater.* **2016**, *2* (12), No. 1600255.
(103) Alhabeb, M.; Maleski, K.; Anasori, B.; Lelyukh, P.; Clark, L.; Sin, S.; Gogotsi, Y. Guidelines for Synthesis and Processing of Two-Dimensional Titanium Carbide ($Ti_3C_2T_x$ MXene). *Chem. Mater.* **2017**, *29* (18), 7633−7644.
(104) Naguib, M.; Mashtalir, O.; Carle, J.; Presser, V.; Lu, J.; Hultman, L.; Gogotsi, Y.; Barsoum, M. W. Two-Dimensional Transition Metal Carbides. *ACS Nano* **2012**, *6* (2), 1322−1331.
(105) Dall'Agnese, Y.; Taberna, P. L.; Gogotsi, Y.; Simon, P. Two-Dimensional Vanadium Carbide (MXene) as Positive Electrode for Sodium-Ion Capacitors. *J. Phys. Chem. Lett.* **2015**, *6* (12), 2305−2309.
(106) Ghidiu, M.; Lukatskaya, M. R.; Zhao, M. Q.; Gogotsi, Y.; Barsoum, M. W. Conductive Two-Dimensional Titanium Carbide 'Clay' with High Volumetric Capacitance. *Nature* **2014**, *516* (7529), 78−81.
(107) Li, T.; Yao, L.; Liu, Q.; Gu, J.; Luo, R.; Li, J.; Yan, X.; Wang, W.; Liu, P.; Chen, B.; Zhang, W.; Abbas, W.; Naz, R.; Zhang, D. Fluorine-Free Synthesis of High-Purity $Ti_3C_2T_x$ (T = OH, O) *via* Alkali Treatment. *Angew. Chem., Int. Ed. Engl.* **2018**, *57* (21), 6115−6119.
(108) Li, M.; Lu, J.; Luo, K.; Li, Y.; Chang, K.; Chen, K.; Zhou, J.; Rosen, J.; Hultman, L.; Eklund, P.; Persson, P. O. A.; Du, S.; Chai, Z.; Huang, Z.; Huang, Q. Element Replacement Approach by Reaction with Lewis Acidic Molten Salts to Synthesize Nanolaminated MAX Phases and MXenes. *J. Am. Chem. Soc.* **2019**, *141* (11), 4730−4737.
(109) Li, Y.; Shao, H.; Lin, Z.; Lu, J.; Liu, L.; Duployer, B.; Persson, P. O. A.; Eklund, P.; Hultman, L.; Li, M.; Chen, K.; Zha, X. H.; Du, S.; Rozier, P.; Chai, Z.; Raymundo-Pinero, E.; Taberna, P. L.; Simon, P.; Huang, Q. A General Lewis Acidic Etching Route for Preparing MXenes with Enhanced Electrochemical Performance in Non-Aqueous Electrolyte. *Nat. Mater.* **2020**, *19* (8), 894−899.
(110) Chen, N.; Duan, Z.; Cai, W.; Wang, Y.; Pu, B.; Huang, H.; Xie, Y.; Tang, Q.; Zhang, H.; Yang, W. Supercritical Etching Method for the Large-Scale Manufacturing of MXenes. *Nano Energy* **2023**, *107*, No. 108147.
(111) Anasori, B.; Lukatskaya, M. R.; Gogotsi, Y. 2D Metal Carbides and Nitrides (MXenes) for Energy Storage. *Nat. Rev. Mater.* **2017**, *2* (2), 16098.
(112) Xu, C.; Wang, L.; Liu, Z.; Chen, L.; Guo, J.; Kang, N.; Ma, X. L.; Cheng, H. M.; Ren, W. Large-Area High-Quality 2D Ultrathin Mo_2C Superconducting Crystals. *Nat. Mater.* **2015**, *14* (11), 1135−1141.
(113) Alhabeb, M.; Maleski, K.; Mathis, T. S.; Sarycheva, A.; Hatter, C. B.; Uzun, S.; Levitt, A.; Gogotsi, Y. Selective Etching of Silicon from Ti_3SiC_2(MAX) To Obtain 2D Titanium Carbide (MXene). *Angew. Chem., Int. Ed. Engl.* **2018**, *57* (19), 5444−5448.
(114) Hu, M.; Cheng, R.; Li, Z.; Hu, T.; Zhang, H.; Shi, C.; Yang, J.; Cui, C.; Zhang, C.; Wang, H.; Fan, B.; Wang, X.; Yang, Q. H. Interlayer Engineering of $Ti_3C_2T_x$ MXenes Towards High Capacitance Supercapacitors. *Nanoscale* **2020**, *12* (2), 763−771.
(115) Kamysbayev, V.; Filatov, A. S.; Hu, H.; Rui, X.; Lagunas, F.; Wang, D.; Klie, R. F.; Talapin, D. V. Covalent Surface Modifications and Superconductivity of Two-Dimensional Metal Carbide MXenes. *Science* **2020**, *369*, 979−983.
(116) Maleski, K.; Ren, C. E.; Zhao, M. Q.; Anasori, B.; Gogotsi, Y. Size-Dependent Physical and Electrochemical Properties of Two-Dimensional MXene Flakes. *ACS Appl. Mater. Interfaces* **2018**, *10* (29), 24491−24498.
(117) Haider, W. A.; Tahir, M.; He, L.; Mirza, H. A.; Zhu, R.; Han, Y.; Mai, L. Structural Engineering and Coupling of Two-Dimensional Transition Metal Compounds for Micro-Supercapacitor Electrodes. *ACS. Cent. Sci.* **2020**, *6* (11), 1901−1915.
(118) Luo, J.; Zhang, W.; Yuan, H.; Jin, C.; Zhang, L.; Huang, H.; Liang, C.; Xia, Y.; Zhang, J.; Gan, Y.; Tao, X. Pillared Structure Design of MXene with Ultralarge Interlayer Spacing for High-Performance Lithium-Ion Capacitors. *ACS Nano* **2017**, *11* (3), 2459−2469.
(119) Liang, K.; Matsumoto, R. A.; Zhao, W.; Osti, N. C.; Popov, I.; Thapaliya, B. P.; Fleischmann, S.; Misra, S.; Prenger, K.; Tyagi, M.; Mamontov, E.; Augustyn, V.; Unocic, R. R.; Sokolov, A. P.; Dai, S.; Cummings, P. T.; Naguib, M. Engineering the Interlayer Spacing by Pre-Intercalation for High Performance Supercapacitor MXene

https://doi.org/10.1021/acsnano.3c10246
ACS Nano 2024, 18, 4651−4682

Electrodes in Room Temperature Ionic Liquid. *Adv. Funct. Mater.* **2021**, *31* (33), No. 2104007.
(120) Feng, X.; Ning, J.; Wang, B.; Guo, H.; Xia, M.; Wang, D.; Zhang, J.; Wu, Z.-S.; Hao, Y. Functional Integrated Electromagnetic Interference Shielding in Flexible Micro-Supercapacitors by Cation-Intercalation Typed $Ti_3C_2T_x$ MXene. *Nano Energy* **2020**, *72*, No. 104741.
(121) Mao, K.; Shi, J.; Zhang, Q.; Hou, Y.; Wen, L.; Liu, Z.; Long, F.; Niu, K.; Liu, N.; Long, F.; Gao, Y. High-capacitance MXene Anode based on Zn-ion Pre-Intercalation Strategy for Degradable Micro Zn-ion Hybrid Supercapacitors. *Nano Energy* **2022**, *103*, No. 107791.
(122) Li, J.; Yuan, X.; Lin, C.; Yang, Y.; Xu, L.; Du, X.; Xie, J.; Lin, J.; Sun, J. Achieving High Pseudocapacitance of 2D Titanium Carbide (MXene) by Cation Intercalation and Surface Modification. *Adv. Energy Mater.* **2017**, *7* (15), No. 1602725.
(123) Zhao, X.; Vashisth, A.; Prehn, E.; Sun, W.; Shah, S. A.; Habib, T.; Chen, Y.; Tan, Z.; Lutkenhaus, J. L.; Radovic, M.; Green, M. J. Antioxidants Unlock Shelf-Stable $Ti_3C_2T_x$ (MXene) Nanosheet Dispersions. *Matter* **2019**, *1* (2), 513−526.
(124) Zhang, Q.; Lai, H.; Fan, R.; Ji, P.; Fu, X.; Li, H. High Concentration of $Ti_3C_2T_x$ MXene in Organic Solvent. *ACS Nano* **2021**, *15* (3), 5249−5262.
(125) Zhao, X.; Cao, H.; Coleman, B. J.; Tan, Z.; Echols, I. J.; Pentzer, E. B.; Lutkenhaus, J. L.; Radovic, M.; Green, M. J. The Role of Antioxidant Structure in Mitigating Oxidation in $Ti_3C_2T_x$ and Ti_2CT_x MXenes. *Adv. Mater. Interfaces.* **2022**, *9* (20), No. 2200480.
(126) Zhang, J.; Uzun, S.; Seyedin, S.; Lynch, P. A.; Akuzum, B.; Wang, Z.; Qin, S.; Alhabeb, M.; Shuck, C. E.; Lei, W.; Kumbur, E. C.; Yang, W.; Wang, X.; Dion, G.; Razal, J. M.; Gogotsi, Y. Additive-Free MXene Liquid Crystals and Fibers. *ACS. Cent. Sci.* **2020**, *6* (2), 254−265.
(127) Gao, Q.; Feng, M.; Li, E.; Liu, C.; Shen, C.; Liu, X. Mechanical, Thermal, and Rheological Properties of $Ti_3C_2T_x$ MXene/Thermoplastic Polyurethane Nanocomposites. *Macromol. Mater.Eng.* **2020**, *305* (10), No. 2000343.
(128) Guzmán, E.; Tajuelo, J.; Pastor, J. M.; Rubio, M. Á.; Ortega, F.; Rubio, R. G. Shear Rheology of Fluid Interfaces: Closing the Gap between Macro- and Micro-Rheology. *Curr. Opin. Colloid In.* **2018**, *37*, 33−48.
(129) Naficy, S.; Jalili, R.; Aboutalebi, S. H.; Gorkin, R. A., III; Konstantinov, K.; Innis, P. C.; Spinks, G. M.; Poulin, P.; Wallace, G. G. Graphene Oxide Dispersions: Tuning Rheology to Enable Fabrication. *Mater. Horiz.* **2014**, *1* (3), 326−331.
(130) Usman, K. A. S.; Zhang, J.; Qin, S.; Yao, Y.; Lynch, P. A.; Mota-Santiago, P.; Naebe, M.; Henderson, L. C.; Hegh, D.; Razal, J. M. Inducing Liquid Crystallinity in Dilute MXene Dispersions for Facile Processing of Multifunctional Fibers. *J. Mater. Chem. A* **2022**, *10* (9), 4770−4781.
(131) Quain, E.; Mathis, T. S.; Kurra, N.; Maleski, K.; Van Aken, K. L.; Alhabeb, M.; Alshareef, H. N.; Gogotsi, Y. Direct Writing of Additive-Free MXene-in-Water Ink for Electronics and Energy Storage. *Adv. Mater. Technol.* **2019**, *4* (1), No. 1800256.
(132) Uzun, S.; Schelling, M.; Hantanasirisakul, K.; Mathis, T. S.; Askeland, R.; Dion, G.; Gogotsi, Y. Additive-Free Aqueous MXene Inks for Thermal Inkjet Printing on Textiles. *Small* **2021**, *17* (1), No. 2006376.
(133) Ma, J.; Zheng, S.; Cao, Y.; Zhu, Y.; Das, P.; Wang, H.; Liu, Y.; Wang, J.; Chi, L.; Liu, S.; Wu, Z. S. Aqueous MXene/PH1000 Hybrid Inks for Inkjet-Printing Micro-Supercapacitors with Unprecedented Volumetric Capacitance and Modular Self-Powered Microelectronics. *Adv. Energy Mater.* **2021**, *11* (23), No. 2100746.
(134) Wu, C.-W.; Unnikrishnan, B.; Chen, I. W. P.; Harroun, S. G.; Chang, H.-T.; Huang, C.-C. Excellent Oxidation Resistive MXene Aqueous Ink for Micro-Supercapacitor Application. *Energy Storage Mater.* **2020**, *25*, 563−571.
(135) Vural, M.; Pena-Francesch, A.; Bars-Pomes, J.; Jung, H.; Gudapati, H.; Hatter, C. B.; Allen, B. D.; Anasori, B.; Ozbolat, I. T.; Gogotsi, Y.; Demirel, M. C. Inkjet Printing of Self-Assembled 2D Titanium Carbide and Protein Electrodes for Stimuli-Responsive Electromagnetic Shielding. *Adv. Funct. Mater.* **2018**, *28* (32), No. 1801972.
(136) Fan, Z.; Wei, C.; Yu, L.; Xia, Z.; Cai, J.; Tian, Z.; Zou, G.; Dou, S. X.; Sun, J. 3D Printing of Porous Nitrogen-Doped Ti_3C_2 MXene Scaffolds for High-Performance Sodium-Ion Hybrid Capacitors. *ACS Nano* **2020**, *14* (1), 867−876.
(137) Li, X.; Sun, R.; Pan, J.; Shi, Z.; Lv, J.; An, Z.; He, Y.; Chen, Q.; Han, R. P. S.; Zhang, F.; Lu, Y.; Liang, H.; Liu, Q. All-MXene-Printed RF Resonators as Wireless Plant Wearable Sensors for *In Situ* Ethylene Detection. *Small* **2023**, *19* (24), No. 2207889.
(138) Hu, M.; Hu, T.; Li, Z.; Yang, Y.; Cheng, R.; Yang, J.; Cui, C.; Wang, X. Surface Functional Groups and Interlayer Water Determine the Electrochemical Capacitance of $Ti_3C_2T_x$ MXene. *ACS Nano* **2018**, *12* (4), 3578−3586.
(139) Yu, L.; Fan, Z.; Shao, Y.; Tian, Z.; Sun, J.; Liu, Z. Versatile N-Doped MXene Ink for Printed Electrochemical Energy Storage Application. *Adv. Energy Mater.* **2019**, *9* (34), No. 1901839.
(140) Fan, Z.; Jin, J.; Li, C.; Cai, J.; Wei, C.; Shao, Y.; Zou, G.; Sun, J. 3D-Printed Zn-Ion Hybrid Capacitor Enabled by Universal Divalent Cation-Gelated Additive-Free Ti_3C_2 MXene Ink. *ACS Nano* **2021**, *15* (2), 3098−3107.
(141) Chen, X.; Wang, S.; Shi, J.; Du, X.; Cheng, Q.; Xue, R.; Wang, Q.; Wang, M.; Ruan, L.; Zeng, W. Direct Laser Etching Free-Standing MXene-MoS_2 Film for Highly Flexible Micro-Supercapacitor. *Adv. Mater. Interfaces* **2019**, *6* (22), No. 1901160.
(142) Abdolhosseinzadeh, S.; Schneider, R.; Verma, A.; Heier, J.; Nuesch, F.; Zhang, C. J. Turning Trash into Treasure: Additive Free MXene Sediment Inks for Screen-Printed Micro-Supercapacitors. *Adv. Mater.* **2020**, *32* (17), No. 2000716.
(143) Xu, S.; Dall'Agnese, Y.; Wei, G.; Zhang, C.; Gogotsi, Y.; Han, W. Screen-Printable Microscale Hybrid Device based on MXene and Layered Double Hydroxide Electrodes for Powering Force Sensors. *Nano Energy* **2018**, *50*, 479−488.
(144) El-Kady, M. F.; Strong, V.; Dubin, S.; Kaner, R. B. Laser Scribing of High-Performance and Flexible Graphene-Based Electrochemical Capacitors. *Science* **2012**, *335* (6074), 1326−1330.
(145) Wen, F.; Hao, C.; Xiang, J.; Wang, L.; Hou, H.; Su, Z.; Hu, W.; Liu, Z. Enhanced Laser Scribed Flexible Graphene-Based Micro-Supercapacitor Performance with Reduction of Carbon Nanotubes Diameter. *Carbon* **2014**, *75*, 236−243.
(146) Kurra, N.; Ahmed, B.; Gogotsi, Y.; Alshareef, H. N. MXene-on-Paper Coplanar Microsupercapacitors. *Adv. Energy Mater.* **2016**, *6* (24), No. 1601372.
(147) Huang, H.; Chu, X.; Su, H.; Zhang, H.; Xie, Y.; Deng, W.; Chen, N.; Liu, F.; Zhang, H.; Gu, B.; Deng, W.; Yang, W. Massively Manufactured Paper-Based All-Solid-State Flexible Micro-Supercapacitors with Sprayable MXene Conductive Inks. *J. Power Sources* **2019**, *415*, 1−7.
(148) Salles, P.; Quain, E.; Kurra, N.; Sarycheva, A.; Gogotsi, Y. Automated Scalpel Patterning of Solution Processed Thin Films for Fabrication of Transparent MXene Microsupercapacitors. *Small* **2018**, *14* (44), No. 1802864.
(149) Li, Z.; Song, J.; Hu, H.; Yuan, C.; Wu, M.; Ho, D. Rolled-up Island-Bridge (RIB): A New and General Electrode Configuration Design for A Wire-Shaped Stretchable Micro-Supercapacitor Array. *J. Mater. Chem. A* **2021**, *9* (5), 2899−2911.
(150) Wu, Y.; Wu, M.; Ho, D.; Hu, H. Biaxial Stretching Array Based on High-Energy-Efficient MXene-Based Al-Ion Micro-supercapacitor Island and Editable Stretchable Bridge. *ACS Appl. Mater. Interfaces* **2022**, *14* (50), 55770−55779.
(151) Huang, X.; Wu, P. A Facile, High-Yield, and Freeze-and-Thaw-Assisted Approach to Fabricate MXene with Plentiful Wrinkles and Its Application in On-Chip Micro-Supercapacitors. *Adv. Funct. Mater.* **2020**, *30* (12), No. 1910048.
(152) Zhang, M.; Héraly, F.; Yi, M.; Yuan, J. Multitasking Tartaric-Acid-Enabled, Highly Conductive, and Stable MXene/Conducting Polymer Composite for Ultrafast Supercapacitor. *Cell Rep. Phys. Sci.* **2021**, *2* (6), No. 100449.

https://doi.org/10.1021/acsnano.3c10246
ACS Nano 2024, 18, 4651−4682

(153) Paraknowitsch, J. P.; Thomas, A. Doping Carbons Beyond Nitrogen: An Overview of Advanced Heteroatom Doped Carbons with Boron, Sulphur and Phosphorus for Energy Applications. *Energy Environ. Sci.* **2013**, *6* (10), 2839−2855.
(154) Bao, W.; Liu, L.; Wang, C.; Choi, S.; Wang, D.; Wang, G. Facile Synthesis of Crumpled Nitrogen-Doped MXene Nanosheets as a New Sulfur Host for Lithium-Sulfur Batteries. *Adv. Energy Mater.* **2018**, *8* (13), No. 1702485.
(155) Li, H.; Li, X.; Liang, J.; Chen, Y. Hydrous RuO_2-Decorated MXene Coordinating with Silver Nanowire Inks Enabling Fully Printed Micro-Supercapacitors with Extraordinary Volumetric Performance. *Adv. Energy Mater.* **2019**, *9* (15), No. 1803987.
(156) Zhang, L.; Yang, G.; Chen, Z.; Liu, D.; Wang, J.; Qian, Y.; Chen, C.; Liu, Y.; Wang, L.; Razal, J.; Lei, W. MXene Coupled with Molybdenum Dioxide Nanoparticles as 2D-0D Pseudocapacitive Electrode for High Performance Flexible Asymmetric Micro-Supercapacitors. *J. Materiomics* **2020**, *6* (1), 138−144.
(157) Li, H.; Hou, Y.; Wang, F.; Lohe, M. R.; Zhuang, X.; Niu, L.; Feng, X. Flexible All-Solid-State Supercapacitors with High Volumetric Capacitances Boosted by Solution Processable MXene and Electrochemically Exfoliated Graphene. *Adv. Energy Mater.* **2017**, *7* (4), No. 1601847.
(158) Gund, G. S.; Park, J. H.; Harpalsinh, R.; Kota, M.; Shin, J. H.; Kim, T.-i.; Gogotsi, Y.; Park, H. S. MXene/Polymer Hybrid Materials for Flexible AC-Filtering Electrochemical Capacitors. *Joule* **2019**, *3* (1), 164−176.
(159) Liu, Y. T.; Zhang, P.; Sun, N.; Anasori, B.; Zhu, Q. Z.; Liu, H.; Gogotsi, Y.; Xu, B. Self-Assembly of Transition Metal Oxide Nanostructures on MXene Nanosheets for Fast and Stable Lithium Storage. *Adv. Mater.* **2018**, *30* (23), No. 1707334.
(160) Feng, X.; Ning, J.; Xia, M.; Guo, H.; Zhou, Y.; Wang, D.; Zhang, J.; Hao, Y. A High Operating Voltage Micro-Supercapacitor based on the Interlamellar Modulation Type $Ti_3C_2T_x$ MXene. *Nanotechnology* **2021**, *32* (3), No. 035402.
(161) Wang, W.; Jiang, D.; Chen, X.; Xie, K.; Jiang, Y.; Wang, Y. A Sandwich-Like Nano-Micro LDH-MXene-LDH for High-Performance Supercapacitors. *Appl. Surf. Sci.* **2020**, *515*, No. 145982.
(162) Snook, G. A.; Kao, P.; Best, A. S. Conducting-Polymer-Based Supercapacitor Devices and Electrodes. *J. Power Sources* **2011**, *196* (1), 1−12.
(163) Xia, Y.; Mathis, T. S.; Zhao, M. Q.; Anasori, B.; Dang, A.; Zhou, Z.; Cho, H.; Gogotsi, Y.; Yang, S. Thickness-Independent Capacitance of Vertically Aligned Liquid-Crystalline MXenes. *Nature* **2018**, *557* (7705), 409−412.
(164) Sun, N.; Guan, Z.; Zhu, Q.; Anasori, B.; Gogotsi, Y.; Xu, B. Enhanced Ionic Accessibility of Flexible MXene Electrodes Produced by Natural Sedimentation. *Nanomicro. Lett.* **2020**, *12* (1), 89.
(165) Yao, M.; Chen, Y.; Wang, Z.; Shao, C.; Dong, J.; Zhang, Q.; Zhang, L.; Zhao, X. Boosting Gravimetric and Volumetric Energy Density *via* engineering macroporous MXene Films for Supercapacitors. *Chem. Eng. J.* **2020**, *395*, No. 124057.
(166) Cheng, W.; Fu, J.; Hu, H.; Ho, D. Interlayer Structure Engineering of MXene-Based Capacitor-Type Electrode for Hybrid Micro-Supercapacitor toward Battery-Level Energy Density. *Adv. Sci.* **2021**, *8* (16), No. 2100775.
(167) Yue, Y.; Liu, N.; Ma, Y.; Wang, S.; Liu, W.; Luo, C.; Zhang, H.; Cheng, F.; Rao, J.; Hu, X.; Su, J.; Gao, Y. Highly Self-Healable 3D Microsupercapacitor with MXene-Graphene Composite Aerogel. *ACS Nano* **2018**, *12* (5), 4224−4232.
(168) Deng, Y.; Shang, T.; Wu, Z.; Tao, Y.; Luo, C.; Liang, J.; Han, D.; Lyu, R.; Qi, C.; Lv, W.; Kang, F.; Yang, Q. H. Fast Gelation of $Ti_3C_2T_x$ MXene Initiated by Metal Ions. *Adv. Mater.* **2019**, *31* (43), No. 1902432.
(169) Huang, X.; Huang, J.; Yang, D.; Wu, P. A Multi-Scale Structural Engineering Strategy for High-Performance MXene Hydrogel Supercapacitor Electrode. *Adv. Sci.* **2021**, *8* (18), No. 2101664.
(170) Chu, X.; Wang, Y.; Cai, L.; Huang, H.; Xu, Z.; Xie, Y.; Yan, C.; Wang, Q.; Zhang, H.; Li, H.; Yang, W. Boosting the Energy Density of Aqueous MXene-based Supercapacitor by Integrating 3D Conducting Polymer Hydrogel Cathode. *SusMat* **2022**, *2* (3), 379−390.
(171) Li, K.; Zhao, J.; Zhussupbekova, A.; Shuck, C. E.; Hughes, L.; Dong, Y.; Barwich, S.; Vaesen, S.; Shvets, I. V.; Mobius, M.; Schmitt, W.; Gogotsi, Y.; Nicolosi, V. 4D Printing of MXene Hydrogels for High-Efficiency Pseudocapacitive Energy Storage. *Nat. Commun.* **2022**, *13* (1), 6884.
(172) Dutta, S.; Bhaumik, A.; Wu, K. C. W. Hierarchically Porous Carbon Derived from Polymers and Biomass: Effect of Interconnected Pores on Energy Applications. *Energy Environ. Sci.* **2014**, *7* (11), 3574−3592.
(173) Xu, Z.; Deng, W.; Wang, X. 3D Hierarchical Carbon-Rich Micro-/Nanomaterials for Energy Storage and Catalysis. *Electrochemical Energy Rev.* **2021**, *4* (2), 269−335.
(174) Zhao, Z.; Wang, S.; Wan, F.; Tie, Z.; Niu, Z. Scalable 3D Self-Assembly of MXene Films for Flexible Sandwich and Microsized Supercapacitors. *Adv. Funct. Mater.* **2021**, *31* (23), No. 2101302.
(175) Zhang, P.; Zhu, Q.; Soomro, R. A.; He, S.; Sun, N.; Qiao, N.; Xu, B. *In Situ* Ice Template Approach to Fabricate 3D Flexible MXene Film-Based Electrode for High Performance Supercapacitors. *Adv. Funct. Mater.* **2020**, *30* (47), No. 2000922.
(176) Wang, G.; Jiang, N.; Zhang, Z.; Wang, G.; Cheng, K. Free-standing 3D Porous Energy Hydrogels Enabled by Ion-Induced Gelation Strategy for High-performance Supercapacitors. *Appl. Surf. Sci.* **2022**, *604*, No. 154636.
(177) Yang, X.; Wang, Q.; Zhu, K.; Ye, K.; Wang, G.; Cao, D.; Yan, J. 3D Porous Oxidation-Resistant MXene/Graphene Architectures Induced by *In Situ* Zinc Template toward High-Performance Supercapacitors. *Adv. Funct. Mater.* **2021**, *31* (20), No. 2101087.
(178) Miao, J.; Zhu, Q.; Li, K.; Zhang, P.; Zhao, Q.; Xu, B. Self-Propagating Fabrication of 3D Porous MXene-rGO Film Electrode for High-Performance Supercapacitors. *J. Energy Chem.* **2021**, *52*, 243−250.
(179) Li, X.; Li, H.; Fan, X.; Shi, X.; Liang, J. 3D-Printed Stretchable Micro-Supercapacitor with Remarkable Areal Performance. *Adv. Energy Mater.* **2020**, *10* (14), No. 1903794.
(180) Das, P.; Shi, X.; Fu, Q.; Wu, Z. S. Substrate-Free and Shapeless Planar Micro-Supercapacitors. *Adv. Funct. Mater.* **2020**, *30* (7), No. 1908758.
(181) Xie, X.; Zhao, M.-Q.; Anasori, B.; Maleski, K.; Ren, C. E.; Li, J.; Byles, B. W.; Pomerantseva, E.; Wang, G.; Gogotsi, Y. Porous Heterostructured MXene/Carbon Nanotube Composite Paper with High Volumetric Capacity for Sodium-Based Energy Storage Devices. *Nano Energy* **2016**, *26*, 513−523.
(182) Xia, Q. X.; Fu, J.; Yun, J. M.; Mane, R. S.; Kim, K. H. High Volumetric Energy Density Annealed-MXene-Nickel Oxide/MXene Asymmetric Supercapacitor. *RSC Adv.* **2017**, *7* (18), 11000−11011.
(183) Dang, A.; Sun, Y.; Fang, C.; Li, T.; Liu, X.; Xia, Y.; Ye, F.; Zada, A.; Khan, M. Rational Design of Ti_3C_2/Carbon Nanotubes/$MnCo_2S_4$ Electrodes for Symmetric Supercapacitors with High Energy Storage. *Appl. Surf. Sci.* **2022**, *581*, No. 152432.
(184) Xie, Y.; Zhang, H.; Huang, H.; Wang, Z.; Xu, Z.; Zhao, H.; Wang, Y.; Chen, N.; Yang, W. High-Voltage Asymmetric MXene-based On-Chip Micro-Supercapacitors. *Nano Energy* **2020**, *74*, No. 104928.
(185) Couly, C.; Alhabeb, M.; Van Aken, K. L.; Kurra, N.; Gomes, L.; Navarro-Suárez, A. M.; Anasori, B.; Alshareef, H. N.; Gogotsi, Y. Asymmetric Flexible MXene-Reduced Graphene Oxide Micro-Supercapacitor. *Adv. Electron. Mater.* **2018**, *4* (1), No. 1700339.
(186) Jiang, Q.; Kurra, N.; Alhabeb, M.; Gogotsi, Y.; Alshareef, H. N. All Pseudocapacitive MXene-RuO2Asymmetric Supercapacitors. *Adv. Energy Mater.* **2018**, *8* (13), 1703043.
(187) Ghosh, K.; Pumera, M. MXene and MoS_{3-x} Coated 3D-Printed Hybrid Electrode for Solid-State Asymmetric Supercapacitor. *Small Methods* **2021**, *5* (8), No. e2100451.
(188) Boota, M.; Gogotsi, Y. MXene—Conducting Polymer Asymmetric Pseudocapacitors. *Adv. Energy Mater.* **2019**, *9* (7), No. 1802917.

https://doi.org/10.1021/acsnano.3c10246
ACS Nano 2024, 18, 4651−4682

(189) Liu, S.; Zeng, T.; Zhang, Y.; Wan, Q.; Yang, N. Coupling $W_{18}O_{49}$/ $Ti_3C_2T_x$ MXene Pseudocapacitive Electrodes with Redox Electrolytes to Construct High-Performance Asymmetric Supercapacitors. *Small* **2022**, *18* (52), No. 2204829.
(190) Zheng, S.; Wang, S.; Dong, Y.; Zhou, F.; Qin, J.; Wang, X.; Su, F.; Sun, C.; Wu, Z. S.; Cheng, H. M.; Bao, X. All-Solid-State Planar Sodium-Ion Microcapacitors with Multidirectional Fast Ion Diffusion Pathways. *Adv. Sci.* **2019**, *6* (23), No. 1902147.
(191) Li, X.; Ma, Y.; Yue, Y.; Li, G.; Zhang, C.; Cao, M.; Xiong, Y.; Zou, J.; Zhou, Y.; Gao, Y. A Flexible Zn-ion Hybrid Micro-Supercapacitor based on MXene Anode and V_2O_5 Cathode with High Capacitance. *Chem. Eng. J.* **2022**, *428*, No. 130965.
(192) Wang, H.; Xue, Y.; Song, X.; Lei, S.; Yu, H.; Du, C.-F.; Ren, Z.; Guo, R.; Zhou, F. Solid Solution Reinforced $V_3CrC_3T_x$ MXene Cathodes for Zn-Ion Micro-Supercapacitors with High Areal Energy Density and Superior Flexibility. *J. Mater. Chem. A* **2022**, *10* (39), 20953−20963.
(193) Zuo, W.; Li, R.; Zhou, C.; Li, Y.; Xia, J.; Liu, J. Battery-Supercapacitor Hybrid Devices: Recent Progress and Future Prospects. *Adv. Sci.* **2017**, *4* (7), No. 1600539.
(194) Jin, J.; Geng, X.; Chen, Q.; Ren, T. L. A Better Zn-Ion Storage Device: Recent Progress for Zn-Ion Hybrid Supercapacitors. *Nano-micro. Lett.* **2022**, *14* (1), 64.
(195) Wu, G.; Sun, S.; Zhu, X.; Ma, Z.; Zhang, Y.; Bao, N. Microfluidic Fabrication of Hierarchical-Ordered ZIF-L(Zn)@ $Ti_3C_2T_x$ Core-Sheath Fibers for High-Performance Asymmetric Supercapacitors. *Angew. Chem., Int. Ed. Engl.* **2022**, *61* (8), No. 202115559.
(196) Xia, M.; Ning, J.; Feng, X.; Guo, H.; Wang, D.; Zhang, J.; Hao, Y. Ionization-Bombardment Assisted Deposition of MXene/SiC Heterostructure for Micro-Supercapacitor with Enhanced Sodium Storage. *Chem. Eng. J.* **2022**, *428*, No. 131114.
(197) Huang, T.; Gao, B.; Zhao, S.; Zhang, H.; Li, X.; Luo, X.; Cao, M.; Zhang, C.; Luo, S.; Yue, Y.; Ma, Y.; Gao, Y. All-MXenes Zinc Ion Hybrid Micro-Supercapacitor with Wide Voltage Window based on V_2CT_x Cathode and $Ti_3C_2T_x$ Anode. *Nano Energy* **2023**, *111*, No. 108383.
(198) Yu, P.; Cao, G.; Yi, S.; Zhang, X.; Li, C.; Sun, X.; Wang, K.; Ma, Y. Binder-free 2D Titanium Carbide (MXene)/Carbon Nanotube Composites for High-Performance Lithium-Ion Capacitors. *Nanoscale* **2018**, *10* (13), 5906−5913.
(199) Wang, L.; Zhang, X.; Xu, Y.; Li, C.; Liu, W.; Yi, S.; Wang, K.; Sun, X.; Wu, Z. S.; Ma, Y. Tetrabutylammonium-Intercalated 1T-MoS_2 Nanosheets with Expanded Interlayer Spacing Vertically Coupled on 2D Delaminated MXene for High-Performance Lithium-Ion Capacitors. *Adv. Funct. Mater.* **2021**, *31* (36), No. 2104286.
(200) Wang, X.; Kajiyama, S.; Iinuma, H.; Hosono, E.; Oro, S.; Moriguchi, I.; Okubo, M.; Yamada, A. Pseudocapacitance of MXene Nanosheets for High-Power Sodium-Ion Hybrid Capacitors. *Nat. Commun.* **2015**, *6*, 6544.
(201) Zhang, P.; Li, Y.; Wang, G.; Wang, F.; Yang, S.; Zhu, F.; Zhuang, X.; Schmidt, O. G.; Feng, X. Zn-Ion Hybrid Micro-Supercapacitors with Ultrahigh Areal Energy Density and Long-Term Durability. *Adv. Mater.* **2019**, *31* (3), No. 1806005.
(202) Li, L.; Liu, W.; Jiang, K.; Chen, D.; Qu, F.; Shen, G. In-Situ Annealed $Ti_3C_2T_x$ MXene Based All-Solid-State Flexible Zn-Ion Hybrid Micro Supercapacitor Array with Enhanced Stability. *Nanomicro. Lett.* **2021**, *13* (1), 100.
(203) Shi, B.; Li, L.; Chen, A.; Jen, T. C.; Liu, X.; Shen, G. Continuous Fabrication of $Ti_3C_2T_x$ MXene-Based Braided Coaxial Zinc-Ion Hybrid Supercapacitors with Improved Performance. *Nanomicro. Lett.* **2022**, *14* (1), 34.
(204) El-Kady, M. F.; Ihns, M.; Li, M.; Hwang, J. Y.; Mousavi, M. F.; Chaney, L.; Lech, A. T.; Kaner, R. B. Engineering Three-Dimensional Hybrid Supercapacitors and Microsupercapacitors for High-Performance Integrated Energy Storage. *Proc. Natl. Acad. Sci. U.S.A.* **2015**, *112* (14), 4233−4238.
(205) Guo, R.; Chen, J.; Yang, B.; Liu, L.; Su, L.; Shen, B.; Yan, X. In-Plane Micro-Supercapacitors for an Integrated Device on One Piece of Paper. *Adv. Funct. Mater.* **2017**, *27* (43), No. 1702394.
(206) Shen, C.; Xu, S.; Xie, Y.; Sanghadasa, M.; Wang, X.; Lin, L. A Review of On-Chip Micro Supercapacitors for Integrated Self-Powering Systems. *J. Microelectromech. S.* **2017**, *26* (5), 949−965.
(207) Xu, S.; Liu, W.; Hu, B.; Wang, X. Circuit-Integratable High-Frequency Micro Supercapacitors with Filter/Oscillator Demonstrations. *Nano Energy* **2019**, *58*, 803−810.
(208) Wei, J.; Teng, Y.; Meng, T.; Bu, X.; Du, H.; Li, D. A Multicomponent Interconnected Composite Paper for Triple-Mode Sensors and Flexible Micro-Supercapacitors. *J. Mater. Chem. A* **2020**, *8* (46), 24620−24634.
(209) Gao, C.; Huang, J.; Xiao, Y.; Zhang, G.; Dai, C.; Li, Z.; Zhao, Y.; Jiang, L.; Qu, L. A Seamlessly Integrated Device of Micro-Supercapacitor and Wireless Charging with Ultrahigh Energy Density and Capacitance. *Nat. Commun.* **2021**, *12* (1), 2647.
(210) Zheng, S.; Ma, J.; Fang, K.; Li, S.; Qin, J.; Li, Y.; Wang, J.; Zhang, L.; Zhou, F.; Liu, F.; Wang, K.; Wu, Z. S. High-Voltage Potassium Ion Micro-Supercapacitors with Extraordinary Volumetric Energy Density for Wearable Pressure Sensor System. *Adv. Energy Mater.* **2021**, *11* (17), No. 2003835.
(211) Xiao, X.; Li, T.; Yang, P.; Gao, Y.; Jin, H.; Ni, W.; Zhan, W.; Zhang, X.; Cao, Y.; Zhong, J.; Gong, L.; Yen, W. C.; Mai, W.; Chen, J.; Huo, K.; Chueh, Y. L.; Wang, Z. L.; Zhou, J. Fiber-based all-solid-state flexible supercapacitors for self-powered systems. *ACS Nano* **2012**, *6* (10), 9200−9206.
(212) Lei, J.; Xiong, Y.; Yu, F.; Ma, J. Flexible self-supporting CoFe-LDH/MXene Film as a Chloride Ions Storage Electrode in Capacitive Deionization. *Chem. Eng. J.* **2022**, *437*, No. 135381.
(213) Jiang, Q.; Wu, C.; Wang, Z.; Wang, A. C.; He, J.-H.; Wang, Z. L.; Alshareef, H. N. MXene Electrochemical Microsupercapacitor Integrated with Triboelectric Nanogenerator as a Wearable Self-Charging Power Unit. *Nano Energy* **2018**, *45*, 266−272.
(214) Jiang, Q.; Kurra, N.; Maleski, K.; Lei, Y.; Liang, H.; Zhang, Y.; Gogotsi, Y.; Alshareef, H. N. On-Chip MXene Microsupercapacitors for AC-Line Filtering Applications. *Adv. Energy Mater.* **2019**, *9*, No. 1901061.
(215) Chao, M.; Wang, Y.; Ma, D.; Wu, X.; Zhang, W.; Zhang, L.; Wan, P. Wearable MXene Nanocomposites-Based Strain Sensor with Tile-Like Stacked Hierarchical Microstructure for Broad-Range Ultrasensitive Sensing. *Nano Energy* **2020**, *78*, No. 105187.
(216) Li, J.; Levitt, A.; Kurra, N.; Juan, K.; Noriega, N.; Xiao, X.; Wang, X.; Wang, H.; Alshareef, H. N.; Gogotsi, Y. MXene-Conducting Polymer Electrochromic Microsupercapacitors. *Energy Storage Mater.* **2019**, *20*, 455−461.
(217) Yun, J.; Lim, Y.; Jang, G. N.; Kim, D.; Ha, J. S.; et al. Stretchable Patterned Graphene Gas Sensor Driven by Integrated Micro-Supercapacitor Array. *Nano Energy* **2016**, *19*, 401−414.
(218) Liu, J.; Jiang, X.; Zhang, R.; Zhang, Y.; Wu, L.; Lu, W.; Li, J.; Li, Y.; Zhang, H. MXene-Enabled Electrochemical Microfluidic Biosensor: Applications toward Multicomponent Continuous Monitoring in Whole Blood. *Adv. Funct. Mater.* **2019**, *29* (6), No. 1807326.
(219) Hantanasirisakul, K.; Alhabeb, M.; Lipatov, A.; Maleski, K.; Anasori, B.; Salles, P.; Ieosakulrat, C.; Pakawatpanurut, P.; Sinitskii, A.; May, S. J.; Gogotsi, Y. Effects of Synthesis and Processing on Optoelectronic Properties of Titanium Carbonitride MXene. *Chem. Mater.* **2019**, *31* (8), 2941−2951.
(220) Wu, Z.-S.; Parvez, K.; Feng, X.; Müllen, K. Photolithographic Fabrication of High-Performance All-Solid-State Graphene-Based Planar Micro-Supercapacitors with Different Interdigital Fingers. *J. Mater. Chem. A* **2014**, *2* (22), 8288−8293.
(221) Wu, W.; Fang, H.; Ma, H.; Wu, L.; Zhang, W.; Wang, H. Boosting Transport Kinetics of Ions and Electrons Simultaneously by $Ti_3C_2T_x$ (MXene) Addition for Enhanced Electrochromic Performance. *Nanomicro. Lett.* **2021**, *13* (1), 20.
(222) Wang, S.; Liu, N.; Su, J.; Li, L.; Long, F.; Zou, Z.; Jiang, X.; Gao, Y. Highly Stretchable and Self-Healable Supercapacitor with

https://doi.org/10.1021/acsnano.3c10246
ACS Nano 2024, 18, 4651−4682

Reduced Graphene Oxide Based Fiber Springs. *ACS Nano* **2017**, *11* (2), 2066−2074.
(223) Kurra, N.; Jenjeti, R. N. Micro-electrochemical capacitors: Progress and future status. *J. Energy Storage* **2022**, *55*, No. 105702.
(224) Yang, X.; Wang, Q.; Zhu, K.; Ye, K.; Wang, G.; Cao, D.; Yan, J. 3D Porous Oxidation-Resistant MXene/Graphene Architectures Induced by *In Situ* Zinc Template toward High-Performance Supercapacitors. *Adv. Funct. Mater.* **2021**, *31* (20), No. 2101087.
(225) Kurra, N.; Hota, M. K.; Alshareef, H. N. Conducting polymer micro-supercapacitors for Flexible Energy Storage and AC Line-Filtering. *Nano Energy* **2015**, *13*, 500−508.
(226) Aslam, M. K.; Niu, Y.; Xu, M. MXenes for Non-Lithium-Ion (Na, K, Ca, Mg, and Al) Batteries and Supercapacitors. *Adv. Energy Mater.* **2021**, *11* (2), No. 2000681.
(227) Gao, L.; Bao, W.; Kuklin, A. V.; Mei, S.; Zhang, H.; Agren, H. Hetero-MXenes: Theory, Synthesis, and Emerging Applications. *Adv. Mater.* **2021**, *33* (10), No. 2004129.
(228) Ma, C.; Ma, M. G.; Si, C.; Ji, X. X.; Wan, P. Flexible MXene-Based Composites for Wearable Devices. *Adv. Funct. Mater.* **2021**, *31* (22), No. 2009524.
(229) Pei, Y.; Zhang, X.; Hui, Z.; Zhou, J.; Huang, X.; Sun, G.; Huang, W. $Ti_3C_2T_x$ MXene for Sensing Applications: Recent Progress, Design Principles, and Future Perspectives. *ACS Nano* **2021**, *15* (3), 3996−4017.
(230) Zhong, Q.; Li, Y.; Zhang, G. Two-dimensional MXene-based and MXene-derived photocatalysts: Recent developments and perspectives. *Chem. Eng. J.* **2021**, *409*, No. 128099.
(231) Yu, S.; Tang, H.; Zhang, D.; Wang, S.; Qiu, M.; Song, G.; Fu, D.; Hu, B.; Wang, X. MXenes as Emerging Nanomaterials in Water Purification and Environmental Remediation. *Sci. Total Environ.* **2022**, *811*, No. 152280.
(232) Hong Ng, V. M.; Huang, H.; Zhou, K.; Lee, P. S.; Que, W.; Xu, J. Z.; Kong, L. B. Recent Progress in Layered Transition Metal Carbides and/or Nitrides (MXenes) and Their Composites: Synthesis and Applications. *J. Mater. Chem. A* **2017**, *5* (7), 3039−3068.
(233) Yang, X.; Yao, Y.; Wang, Q.; Zhu, K.; Ye, K.; Wang, G.; Cao, D.; Yan, J. 3D Macroporous Oxidation-Resistant $Ti_3C_2T_x$ MXene Hybrid Hydrogels for Enhanced Supercapacitive Performances with Ultralong Cycle Life. *Adv. Funct. Mater.* **2022**, *32* (10), No. 2109479.
(234) Cao, F.; Zhang, Y.; Wang, H.; Khan, K.; Tareen, A. K.; Qian, W.; Zhang, H.; Agren, H. Recent Advances in Oxidation Stable Chemistry of 2D MXenes. *Adv. Mater.* **2022**, *34* (13), No. 2107554.

https://doi.org/10.1021/acsnano.3c10246
ACS Nano 2024, 18, 4651−4682